University of Nottingham
UK | CHINA | MALAYSIA

Catalytic Palladium Nanoreactor Design for the Suzuki Cross Coupling Reaction

By

Charlotte L. Hayman

A thesis submitted to the University of Nottingham for the degree of
Master of Research
(Chemistry)

Prof. A. N. Khlobystov

September 2022

Acknowledgements

First and foremost, I would like to acknowledge and give my thanks and appreciation to Professor Andrei Khlobystov for providing me with this fantastic opportunity and for his ongoing support, guidance and supervision throughout this course in addition to also performing *in situ* TEM experiments to support my project.

My sincere thanks also go to Rhys Lodge for his support and guidance at the start of my project, patiently teaching and encouraging me in addition to performing *in situ* TEM experiments.

I would like to express my upmost gratitude to Will Cull and Tara Lemercier for helping me perform TGA and for their help, support and practical expertise and to Ben Weare, who I am also grateful for his proof reading and guidance. I would also like to thank Will, Ben and Brad Flinn for performing *in situ* TEM experiments

Thank you to Andreas Weilhard for helping me carry out hydrogenation experiments and to Luke Norman for performing magnetron sputtering for me.

Thank you to all members of Khlobystov group; Tom, Ian, Ethan and Madasamy for their advice, support and encouragement throughout the year.

Abbreviation	Definition
^{1}H NMR	Proton nuclear magnetic resonance
acac	acetylacetonate
$CDCl_3$	Deuterated chloroform
$CHCl_3$	Chloroform
CNT	Carbon nanotube
Cr_2O_3	Chromium oxide
CVD	Chemical vapour deposition
dba	dibenzylideneactone
DCT	dibenzo[a,e]cyclooctatetraene
DMF	Dimethylformamide
EDX	Energy dispersive analysis
FeNP	Iron nanoparticle
GNF	Graphitised carbon nanofibers
HRTEM	High resolution transmission electron microscope
ICP-OES	Inductively coupled plasma optical emission spectroscopy
mim	methylimidazolium
MWNT	Multi-walled carbon nanotube
NHC-Pd	N-heterocyclic carbenes
nm	Nanometer
NP	Nanoparticle
Pd	Palladium
Pd-$CuFe_2O_4$	Palladium copper iron oxide
PdNP	Palladium nanoparticle
PTFE	Polytetrafluoroethylene
PXRD	Powder X-Ray diffraction
SD	Standard Deviation
SWNT	Single-walled carbon nanotube
TGA	Thermogravimetric analysis
TOF	Turnover frequency
TON	Turnover number
wt	Weight
γ-Fe_2O_3	Iron oxide

Abstract

This report investigates the design of a recyclable palladium nanocatalyst to be utilised in the Suzuki cross coupling reaction. Palladium nanoparticles (PdNPs) were combined with graphitised nanofibers (GNF) and then developed to improve its properties as a catalyst. Different methods of deposition were employed, including an innovative use of magnetron sputtering, to attempt to improve catalyst performance. Other approaches such as changing the structure of the carbon support were also used to test the capabilities of this promising material. Magnetic Iron NPs (FeNPs) were also employed as a method of improving the recyclability of the PdNPs, making the extraction process between cycles easier and quicker. Each catalyst was tested for its activity and recyclability using a simple Suzuki cross coupling reaction, and utilised in up to five cycles. Conversion of the product was determined by ^{1}H NMR. High resolution transmission electron microscopy (HRTEM) was used to determine particle size and distribution, both before and after reactions. This was essential for determining which methods could be used to improve the performance and recyclability of the catalyst. Thermal gravimetric analysis (TGA) was used to determine metal loadings which in turn could produce quantitative measurements of activity, turnover number (TON) and turnover frequency (TOF). In total, ten variants of a PdNPs@GNF catalyst were synthesised and tested to determine the most effective one for Suzuki cross couplings and obtained a wide variety of results. It became evident that adding a hydrogenation step to the procedure was essential, as all the catalysts which involved this step had dramatically advanced performances (yields as high as 97 %). This excellent result opens up an exciting opportunity for this catalyst to undergo further testing to extend its use to more challenging starting materials and reactions. These exciting results proved the potential of PdNPs@GNFs as catalysts and were used to determine the best way of synthesising this material. This investigation involved making structural changes to this material to design an active recyclable catalyst for Suzuki cross coupling reactions.

Table of Contents

1 Introduction

1.1 The Suzuki Miyaura Reaction

1.1.1 Background and Mechanism

A cross-coupling reaction in organic chemistry describes the process of two organic fragments being joined together with the aid of a metal catalyst. The Suzuki-Miyaura reaction is a cross-coupling reaction that creates an sp^2C- sp^2C bond between organic boron compounds and organic halides and is typically catalysed by transition metals, allowing an efficient, viable reaction.[1] The Suzuki reaction is a powerful and efficient method of forming C-C bonds and strategically effective in drug synthesis and design due to its robustness and tolerance of heterocycles.[2] Due to its ability to construct C-C bonds, this reaction is among the most widely used protocols for biaryl synthesis; a prominent structural component of many essential compounds used in a variety of chemical sectors. There are numerous synthetic methods that are capable of producing biaryls, but it is desirable to obtain a selective, direct and versatile method of forming these compounds that minimises the waste of precious metal catalysts. The use of green solvents and mild reaction conditions are also preferred, ensuring minimal environmental impact. The popularity of the use of the Suzuki cross-coupling mechanism compared to other methods is a consequence of the mild reaction conditions, high tolerance toward functional groups, and the ease of handling and separating by-products from its reaction mixtures.[3] The reaction also allows the use of a wide range of catalysts with various selectivities and utitlises a diverse range of boronic acid derivatives which have high commercial availability, stability and are environmentally safer than the other organometallic reagents.[4]

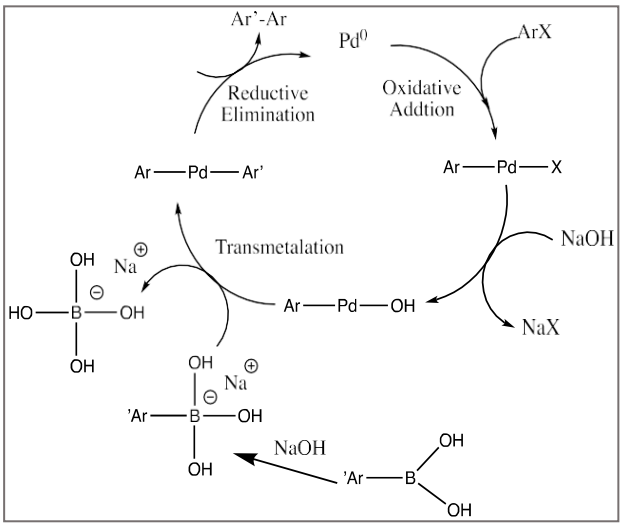

The Suzuki reaction has 3 main steps in the catalytic cycle: oxidative addition, transmetalation and reductive elimination (Figure 1.1).[5] In most cases, the oxidative addition step is the rate determining step, as this step involves the oxidation of the metal catalyst, this can be an important factor in determining reaction rate.

Figure 1.1.[5] Suzuki mechanism demonstrating the catalytic role of palladium which is first oxidised from Pd(0) to Pd(II) when it couples with aryl halide. The Pd then facilitates ligand transfer and elimination to afford the biaryl product. Made in ChemDraw and adapted from C.Len *et al.*[5]

1.1.2. Expanding the Scope

Expanding the scope of the Suzuki reaction by improving catalyst activity is a promising approach to overcoming the challenges caused by more complex and difficult coupling partners such as aryl chlorides and alkyl boranes. The capability of the borane reagent to conduct transmetallation increases with its Lewis acidity.[6] Therefore, alkyl substituents decrease the reactivity of the borane due to their electron donating properties. In order to successfully utilise these reactants, often the use of high temperatures, pressures and extended reaction times are required. Reducing the need for harsher reaction conditions whilst maintaining high yields, can be achieved by selecting an appropriate catalyst. Aryl chlorides and bromides are generally less expensive and more readily available than iodides, but the activation of aryl chlorides and bromides is considerably more challenging, as a result there is considerably less studies reporting on the use of these reagents in cross coupling reactions.[8] The high bond dissociation of C-Cl bonds makes aryl chlorides the most challenging of the three and requires higher quantities of catalysts and harsh reaction conditions, including the use environmentally undesirable solvents.[7] 1,4-Dioxane, THF, NMP, and DMF are all commonly used solvents in palladium-catalysed cross-coupling reactions however these dipolar aprotic and ethereal solvents pose significant concerns from an environmental, health, and safety perspective.[9] If aryl-chlorides could be successfully coupled by using a more effective catalyst to improve activity instead of these harsh solvents then this would be a 'greener' reaction.

When expanding the scope of the Suzuki reaction, the halide is not the only potential limiting factor. Steric interactions can have an impact on the progress of the reaction and the electronic or physical properties of functional groups can cause the reaction to slow or not proceed at all.[10] The discovery of a catalyst that can overcome these limitations would make cross coupling reactions considerably more applicable, easier and greener.

Jin *et al.* [11] reported the use of a magnetic Pd nanocatalyst for coupling reactions of aryl chlorides. They used silica coated Fe_3O_4 to support the PdNPs and aryl chlorides were successfully used as starting materials in the Suzuki reaction and satisfactory yields were obtained in neat water. This presents a promising prospect for green catalysis of the Suzuki reaction by removing the use of organic solvents that are normally required to couple challenging aryl chlorides. Outstanding catalytic activity was observed for some of the aryl chlorides and excellent recyclability of the catalyst due to its magnetic nature. Another example of successful aryl chloride coupling was achieved by Zhang *et al.* [12] who used microwave assisted organic synthesis in order to accelerate the formation of C- C bonds. However, microwave irradiation does have some limitations when used in industry, including needing to install new equipment, some solvents being unsuitable and uneven heating of the reaction leading to inconsistent yields.[13]

1.2. Catalyst Selection

1.2.1. Palladium

Transition metals are often used as catalysts because of their ability to manage different oxidations states and their ability to form complexes as a result of possessing partially filled d-orbitals. In Suzuki coupling, palladium and nickel are the most commonly used due to their ability to easily change redox state between Ni(II)/Ni(0) and Pd(II)/Pd(0). Their d^8 electronic configuration preferentially adopts square planar geometries, leaving two empty coordination sites which is key for the rate determining step.[14] In the earliest Suzuki reactions, only palladium was reported to be used as a catalyst but some recent investigations have utilised nickel instead. Both metals demonstrate great potential as catalysts, however palladium has thus far been shown to have overall better functional group tolerance and has been utilised for this reaction for a longer time. Therefore, palladium is generally a better understood and more established catalyst. However, palladium is a costly and rare metal and in 2020 took top spot as the most expensive of the four major precious metals - gold, silver, platinum, and palladium.[15] The chemical catalysis industry uses 21.63% of the world's palladium production, [16] therefore, improving the recyclability of palladium when used as a catalyst in a widely and frequently used reactions such as cross couplings is a pivotal issue.

1.2.2. Homogeneous *vs.* Heterogeneous

Homogeneous catalysts are advantageous for organic synthesis, they not only encourage high yields but also efficient selectivity and overall catalytic activity is superior. [17] This activity is often quantitatively represented by turnover number (TON) and turnover frequency (TOF), where TON is the molecules reacted per active site of catalyst and TOF is the TON per time. Nevertheless, various problems arise in the time-consuming separation process when using homogeneous catalyst, due to the materials all being in the same phase, often leaving impurities, which is particularly prevalent in the pharmaceutical, food and cosmetic industries.[18] Homogeneous catalysts can also have a straining effect on the catalyst, where compression and tension can change the way they perform, caused by processes such as distillation or extraction and sensitivity to temperature, A resultant in lack of reusability when using a precious metal like palladium also holds many sustainability issues.

Heterogeneous catalysts are generally easier to separate, aided by the different phases present, and have much improved reusability supported by reduced leaching. However, activity and selectivity are compromised. Heterogeneous catalysts are more applicable to industry, as a result, and so combining these catalysts with nanotechnology can maintain or even improve recyclability whilst overcoming their deficiencies (i.e., activity) in other areas.[19] For palladium catalysts, as a costly metal this is of both economic and sustainable importance. The benefits of using the palladium in nanoparticle form are extensive, including a much larger surface area to volume ratio than the bulk

metal which is significant in increasing the activity of the catalyst.[20]

Nanoparticles are a bridge between heterogeneous and homogeneous catalysts and their activity is increased by their low coordination number of the surface metallic atoms.[21] However, the stability can be impacted by this high activity and aggregation is common which may need to be considered and overcome.[22] A catalyst that can include the advantages of heterogenous and homogeneous properties whilst supporting mild reaction conditions, and with limited usage of harmful organic solvents is very desirable, ensuring "greenness" of the reaction.

1.2.3. Catalyst Supports

Palladium can be immobilised on a range on nanosupports, allowing easier separation and reducing agglomeration. The ideal support should have a high surface area and specific properties that allow optimum interaction with the catalytic NPs.[23] It is important that these interactions do not cause catalyst deactivation by leaching to the support or unwanted oxidations. Supports that are commonly selected for metallic nanoparticles include carbon, polymer or silica-based nanostructures and zeolites.[24] Carbon supported nanoparticles generally improves activity, can allow more control over porosity, easy catalyst recovery and resistant to acid/base media.[25]

Carbon nanotubes (CNTs) have been employed extensively in the field of catalysis as both an active catalyst itself and as a support for various catalytic species including inorganic metal catalysts.[26] The benefits of using these cylindrical sp^2 hybridised carbon structures in this include high surface area, thermal stability, mechanical strength as well as having high chemical stability.[27] This property allows nanoparticles to physically adsorb onto the nanotube, whilst avoiding reacting with it. The configuration of the carbon atoms in nanotubes can significantly impact the properties of the material, generally carbon nanotubes are formed from a hexagonal carbon lattice which are aligned into hollow cylindrical tubes. CNTs are generally divided into two categories, single-walled (SWNTs) – internal diameter 0.4 to 2 nm and multi-walled nanotubes (MWNTs) – external diameter 2-100 nm. The categorisation is dependent on the number of concentric nested nanotubes (Figure 1.2).

Additionally, the SWNTs can be constructed in different ways depending on how the graphene sheet is rolled up, armchair, zigzag and chiral.[28] (Figure 1.2). Both have shown to be effective catalyst supports in various settings but SWNTs, although possessing greater potential in the field, normally require a more complex synthesis process, demanding higher quality control and a catalyst.[29] Both electrical and structural characteristics of SWNTs can vary greatly depending on the chirality and diameter making it difficult to selectively grow SWNT with single or few chiralities.[30] Another point to note for some applications is that the inter-tube interactions in MWNTs encourage natural metallic properties. A study by Siamaki[31] demonstrated the use of PdNPs supported on MWNT *vs.* SWNT which demonstrated MWNT to have the better activity and recyclability which they deduce is due to the larger diameter of the MWNT. This provides stronger surface

interactions and more effective anchor for the PdNPs resulting in a greater number of particles on the surface.

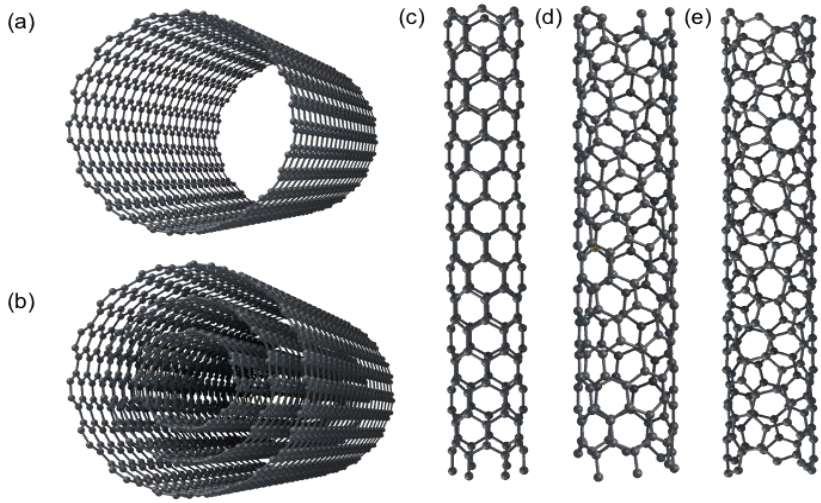

Figure 1.2. Structures of a) SWNTs, b) MWNTs, c) Zigzag, d) Armchair, and e) chiral nanotubes. Figures made in Samson Connect Nanotube Creator.

Carbon nanofibers possessing many appealing qualities as a catalyst support including electrical conductivity, chemical and thermal stability, high surface area and mechanical strength whilst maintaining low density.[32] Hollow graphitised nanofibers (GNFs) are grouped with multiwalled nanotubes and consist of an outer layer of concentric carbon cylinders and an inner layer of stacked cones forming a cavity (Figure 1.3). There is a distinct contrast between the smooth outer walls and uneven inner walls, which has the potential to affect its capability as a catalyst support.

These nanoreactors possess defined step-edges on the inside of the nanotube, made from rolled up graphene layers and so particles size and distribution are more controlled. They also possess a larger internal cavity diameter of normally over 50 nm, allowing GNFs to be applicable to a wider spectrum of reactions that may be inhibited in narrower tubes due to transport resistance.[33] However, thus far there is limited data regarding palladium nanoparticles adsorbed on the outside of the nanofiber structure as the step-edges are clear anchoring points.

Agasti *et al.* [34] used GNF to support cerium oxide nanoparticles and investigated the significance of the confinement of the nanoparticles inside the GNF and on the step edges. They also distributed CeO_2 nanoparticles onto activated carbon and graphite for comparison, which hold similar anchoring abilities as GNF, without the special confinement aspect. TGA results demonstrated a significant lack of stability of the nanoparticles on graphite compared to the activated carbon and a drop in conversion of product for both supports compared to GNF, demonstrating the advantageous effect of nanoconfinement. There are additionally forms of GNF which possess step edges on the outside as well as the inside which has the potential to support more nanoparticles. This can be used in conjunction with methods of

deposition that encourage the nanoparticles to favour the outside of the nanotubes. The properties of carbon nanotubes can be altered by creating physical changes to the structure or functionalisation. The functionalisation of carbon nanotubes has been widely discussed in the literature as this can have a significant impact on the applications for these structures. It has been shown that depositing chromium oxide onto the surface of GNFs and then heating can etch the sidewalls and create defects which can be used as anchoring points for metallic nanoparticles for applications such as catalysis.[35] Anchoring these particles can reduce agglomeration and improve the stability of the catalyst. Creating defects on the carbon support can also hold many other advantages including the control of the properties. M. Astle *et al*. [32] investigated this etching process to find optimum conditions for controlling the size of the defects and consequently successfully deposited RuNPs onto this support. They demonstrated that this is an effective way to secure metallic nanoparticles by successfully using this material for gas-phase sorption of CO_2 and liquid phase alkyne hydrosilylation.

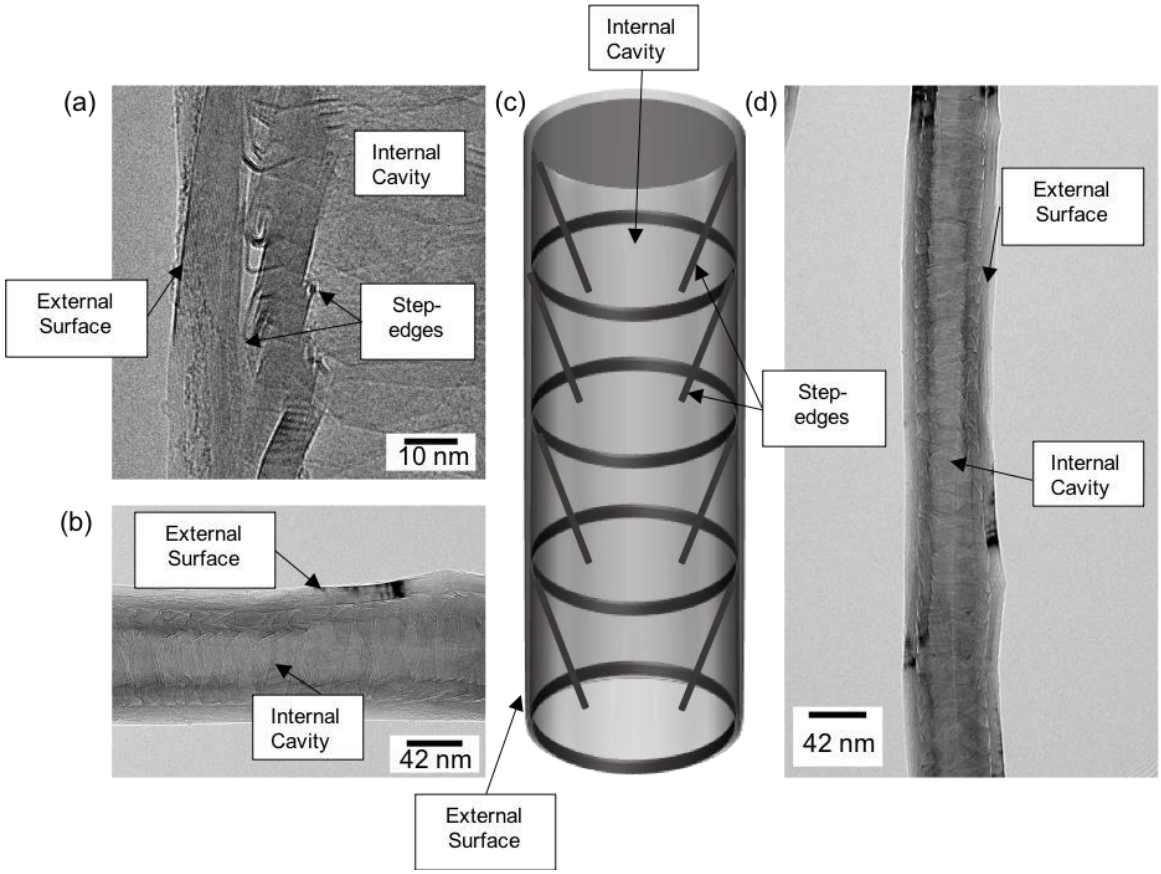

Figure 1.3. (a) TEM image highlighting step edges in GNF, (c) Schematic of GNF structure produced in Microsoft Powerpoint and (b, d) TEM images of GNF.

It has also been shown that step edges of the GNF that undergo transformation by opening up under hydrogenation conditions. Aygün[36] reported that the graphitic step edges on GNFs open up during continuous electrocatalysis which is caused by the hydrogen atoms forming covalent bonds with the carbon atoms at this point. The curvature of the GNF step edge weakens the

C=C bonds and results in the formation of sp^3 carbon centres in a chain of C-H bonds when exposed to hydrogen radicals in the electrocatalytic hydrogen evolution reaction (HER). The strain of these bonds causes a defect in the GNF step edge when the weakened bonds are broken forming flat graphene layers. The Pd NPs can embed themselves in this defect, securing the bonds between the carbon and palladium, thus reducing the migration of the particles. In theory this would aim to reduce leaching and aggregation of the nanoparticles. The original π bonds occurring at the step edge are thought to be converted into stronger σ covalent interactions between Pd-C. Overall, carbon nanoreactors have proven to be effective catalytic supports for metallic nanoparticles and have the potential to be utilised in a variety of reactions due to their unique properties and durability.

1.2.4. Nanoparticle Synthesis

In catalysis, performance of PdNPs depends strongly on size, shape and surface modification which can be controlled by the ligands on the metal precursor.[37] PdNP synthesis from palladium salts such as alkali tetrachloropalladates or palladium nitrates are popular options.[38] Many PdNPs synthesis methods also require stabilising agents that achieve this stability through electrostatic or steric forces or have to be carried out in unfavourable organic solvents.[39] Using a method that reduces the need for these solvents or the removal and disposal of hazardous ligands is desired. Choice of ligand on palladium complexes as precursors for naked PdNPs is very important to consider as this can significantly impact catalytic activity.

Tris(dibenzylideneacetone)dipalladium ($Pd_2(dba)_3$) is widely used as a precursor for PdNPs and has been applied as a catalyst to cross coupling reactions previously.[40] The weak coordination of Pd to the dba ligand allows for a thermodynamically favourable process for PdNPs to attach to the chemically reactive sites on carbon under mild conditions.[41] The stirring of $Pd_2(dba)_3$ in an organic solvent with gentle heating causes the ligands to dissociate, decomposing the precursor and leaving the Pd atoms to bond favourably with a support.[42] Then the dba can be easily washed away. Additionally, the solution chemistry of $Pd_2(dba)_3$ is complex due to ligand exchange reactions which cause Pd to change its redox state. This results in the formation of colloidal palladium as a by product.[43]

Dibenzylideneactone (dba) has many benefits as a ligand for the palladium nanoparticle precursor because it has relative stability in air and is phosphine free.[44] In some reports the dba has even been shown to actually participate towards the catalysis, but others report the dba ligands can impede the catalytic cycles.[45] At this stage it is not yet clear whether dba impedes or assists the reaction progression, and this requires further investigation.

When using palladium NPs as a heterogeneous catalyst it has been stated that nanoparticle size and shape is an influential factor, so the control of these properties is very important for catalysis. In a study conducted by El-Sayed,[46] it was shown that TOF generally increased with the decrease of particle size.

However, the smallest nanoparticle (3 nm diameter) had a lower TOF than expected due to having the strongest adsorption of reaction intermediates, resulting in poisoning of the active sites of the Pd nanoparticles. Zhang *et al.*[47] conducted in-depth investigation into the influence of size of PdNPs in catalytic denitrification of nitrite to nitrogen gas. They demonstrated clearly the detrimental effect that size of nanoparticle can have on catalytic activity. They used PdNPs with particle sizes between 2.7 and 22.1 nm. The results presented a large spread TOFs ranging from 462.9 to 1122.3 h^{-1}. The smallest particles with diameter of 2.7 nm had the highest mass catalytic activity of 602.6 mg g_{Pd}^{-1} min^{-1}, whereas TOF generally increased with size up to 1122.3h^{-1}. The PdNP with diameter of 5 nm displayed the best overall performance.

The use of ligands is a popular approach to stabilise PdNPs for the Suzuki reaction and phosphine ligands are commonly selected for this. However, these have significant limitations as they are sensitive to air, expensive, unrecoverable and toxic. Using phosphine ligands often demands the use of organic solvents which also results in considerable environmental pollution.[48] Therefore a ligand free system is desirable.

1.3. Deposition Methods

1.3.1. Comparison of Deposition Methods

When selecting an appropriate deposition method for the formation of Pd NPs onto a support many aspects need to be taken into consideration including, the greenness of the method, how well the Pd is distributed, the selectivity of the position of the particles, control of particle size. Nanoparticles can be synthesised by top-down or bottom-up approaches.[49] Top-down approaches tend to involve breaking down larger particles into smaller nanoparticles, examples include lithographic technique, etching, grinding and ball milling technique.[50] This method tends to be cheaper and greener. Contrastingly, bottom-up approaches involve the assembly of larger particles from molecules or atoms, although more costly, is less likely to produce defects in the nanostructure and offer a better size and shape control.[51] There are many ways to deposit NPs onto a support and some of the more frequently used methods include chemical reduction or thermal decomposition of a metallic precursor, vapour deposition and magnetron sputtering. Each of these methods have been reported to successfully deposit well-distributed Pd NPs onto a support for heterogeneous catalysis. The advantages and disadvantages of each method have been identified and presented by Manikam (Table 1). [52]

Method	Description	Advantages	Disadvantages
Molecular Beams	Beams are directed towards specific metal targets using a variety of methods; laser vaporisation, pulsed arc, ion and magnetron sputtering. This creates clusters of metallic nanoparticles including nanoalloys.	(1) Any type of nanoparticle or nanoalloy can be created from metallic/alloy targets. (2) Nanoparticle synthesis is quick and not lengthy.	(1) Process is expensive, and requires equipment setup in most cases.
Chemical Reduction	Use of precursor salts, reducing agents and stabiliser to synthesise nanoparticles. In most cases a catalyst and some heating are used.	(1) Can readily produce bulk quantities of nanoparticles and nanoalloys so process can be easily scaled up. (2) Process enables synthesis of particles close to 1 nm and this can easily be controlled. (4) Process is relatively cheaper compared to other synthesis methods since the technology is quite standard.	(1) Mass use of chemicals and some may be harmful to the environment. (2) Processing is time consuming and depends on many parameters.

Thermal Decomposition	Thermal decomposition of metal complexes (for nanoalloys) is produced using high temperatures or solvents.	(1) Nanoparticles can be created at relatively low temperatures. (2) Process can create nanoparticles in a wide range of sizes.	(1) Requires use of chemicals and solvents which may be harmful to the environment.

Table 1 [44] – Comparison of common bottom-up and top-down deposition methods of nanoparticles, outlining advantages and disadvantages.

1.3.2 Magnetron Sputtering

Magnetron sputtering (MS) is used to prepare thin films *via* physical vapour deposition under high vacuum.[53] (Figure 1.4.). The preparation of heterogeneous catalysts *via* this method of deposition of nanoparticles on a support holds many benefits. Control of size, composition and morphology in addition to the absence of solvent and ligand requirements. [54] This results in higher purity of the catalyst and highly active clean surfaces. [55] MS is a scalable top-down method for the synthesis of metal nanoparticles on surfaces that avoids the use of wet-chemistry which is more challenging to scale up. [56] Kohlrausch *et al.* [57] showed for the first time the deposition of atomically-dispersed metal catalysts (ADMC) into bulk powder using magnetron sputtering. They used Pt atoms onto graphitic carbon nitride and reported the highest rate of ADMC production out of all available methods.

Cano *et al.* [58] sputtered Pd nanoclusters into ionic liquids to produce a Pd@[NTf_2] system of which the catalytic performance was investigated in a cyclopropanation of alkenes. Good conversions and selectivity suggested an active catalyst as mercury poisoning and dibenzo[a,e]cyclooctatetraene (DCT) tests confirmed the heterogeneous nature of the catalyst and that Pd nanoclusters were the active sites. This catalyst was also shown to be recyclable for this reaction.

Magnetron sputtering has been used as a method for thin film deposition quite widely and extensively but the deposition of Pd nanoparticles on carbon supports is not as prevalent. As this is a fairly recent advancement, for this specific application of magnetron sputtering there is plenty of potential for further investigation. [60]

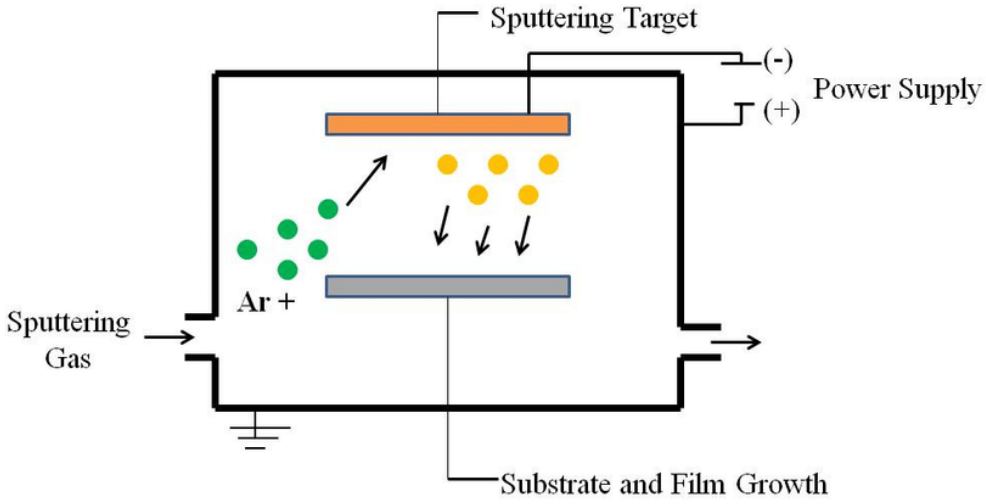

Figure 1.4. A schematic for magnetron sputtering set-up.[59] The sputtering chamber is evacuated to a high vacuum and filled with argon. The equipment creates a magnetic field combined with a negatively charged cathode to trap electrons near the target materials.

1.3.3. Chemical vapour deposition

Chemical vapour deposition (CVD) is a reaction in the vapour phase capabale of depositing metal nanoparticles onto supports. This method has previously been used extensively in the preparation of thin films.[61] More recently it has been investigated as a method used for catalyst preparation as it allows for direct deposition of the active material onto the support.[62] The encapsulation of Pd nanoparticles inside GNF is very advantageous as the encouragement of the Pd NPs to sit in a step-edge reduces migration of the particles. This can be achieved by the vapour deposition of the Pd NPs through sublimation of a Pd precursor which is then reacted with a support in the vapour phase.[35] The precursors previously reported in the literature include $Pd(acac)_2$ and Pd(allyl)Cp for the deposition of well- distributed Pd NPs on carbon supports. Liang *et al.* [63] reported the deposition of Pd NPs on carbon nanofibers using a Pd(allyl)Cp precursor via a two step chemical vapour deposition. First, the Pd(allyl)Cp was adsorbed dissociatively on the surface of the nanofibers. This resulted in evenly distributed PdNPs and the Cp ligand was dissociated off during the this step. Then a reduction step which reduced the allyl ligand to propane and was still bound to adsorbed Pd species. This was used in the hydrogenation of cycloocatene, producing excellent stability and activity allowing the potential for an excellent catalyst for other reactions. Cominos *et al.*[64] investigated the sublimation and deposition behaviour of $Pd(acac)_2$ when deposited on catalytic monoliths. After thermogravimetric analysis to determine the behaviour of the precursor a low temperature was used for the sublimation (100-120 ^oC) and deposition (130- 150 ^oC), lowering the risk of carbon contamination.

1.4. Recyclability Studies

1.4.1. Improving the recyclability of PdNPs

Recyclability studies have been conducted with palladium nanoparticles when used as a catalyst in Suzuki couplings using various approaches to improve the reusability of the catalyst. These include, investigating the effect of supports, reaction conditions, and methods of deposition onto the supports and extraction from reaction mixtures.

Veisi *et al.* [65] used PdNPs on functionalised multi walled carbon nanotubes (MWNTs) as an efficient and recyclable catalyst for the Suzuki reaction. The MWNT were functionalised with mercapto-melamine groups. This catalyst was used for the Suzuki coupling of iodobenzene and bromobenzene with phenylboronic acid. The performance of the catalyst was compared with seven other palladium catalysts reported in the literature. This catalyst achieved the highest yields and very good TOFs of 480 h^{-1} and 240 h^{-1} respectively. This catalyst even obtained good yields of 65-70% for three aryl chlorides - chlorobenzene, 4-chlorotoluene and 1-chloro-4-methoxybenzene in relatively mild reaction conditions. The recyclability of the catalyst was investigated with just 4-bromotoluene as a reactant and the catalyst was separated successfully using centrifugation and found that over three cycles of Suzuki reaction the yield decreased from 96 % to just 90%. The high stability of this catalyst was also confirmed by ICP-OES (inductively coupled plasma optical emission spectroscopy) that showed only a 1.58% leaching of Pd after three runs. This demonstrates that the catalyst is recyclable however further cycles would need to be conducted to conclude that the catalyst would be reusable enough times for it to be an alternative to other current methods.

The use of magnetic nanoparticles can make catalysis less time consuming, greener and more effective and has been extensively researched in the literature. Despite these advantages, when using magnetic NPs it is important to consider ferromagnetism, as their magnetic dipole-dipole interactions can encourage aggregation of the nanoparticles, hence a decrease in catalyst efficiency.[66] There are both *in situ* and *ex situ* ways to deposit magnetic nanoparticles onto supports, each holding their benefits and drawbacks.[67] *In situ* methods prevent particle agglomeration and maintain good spatial distribution whereas *ex situ* methods tend to be more suitable for large scale industrial applications.[68] CVD is a popular *in situ* method of magnetic nanoparticle development.

An alternative use of magnetic nanoparticles was presented by Pineux *et al.*, [69] who applied successful chemical vapour deposition of ferrocene (based on their previous work [70]) to synthesise conjugated FeNPs@CNT for cancer treatment, impressively, these hybrids can categorise cancer cells from healthy cell lines. Using this method, they can achieve 36 wt% loading of Fe on CNT. The authors took this knowledge forward to utilise Fe@CNTs conjugates that are antagonists of a A_3AR (an adenosine receptor that has been shown to have some role in tumour development) and managed to achieve successful binding to said receptor. They used a pyrazolo[4,3-e]-1,2,4-triazolo[1,5-c]-pyrimidine

core with tri- or hexa(ethyleneglycol) chains to study steric impact. This demonstrated the effectiveness of *in situ* methods for magnetic nanoparticles synthesis and opened a really exciting and novel use of magnetic nanoparticles on CNTs supports.

Cano *et al*.[71] synthesised and utilised Fe_3O_4@SiO_2@(mim)[$FeCl_4$] nanoparticles (mim = methylimidazolium) to catalyse the glycolysis of Poly(ethylene terephthalate). This novel nanomaterial appears to be the first example of the surface modification of nano-magnetite materials with paramagnetic ionic liquids. These ionic liquid coated nanoparticles demonstrated excellent recyclability, being used up to 12 times whilst maintaining an impressive almost 100 % yield throughout, highlighting the exciting potential of the magnetic recovery of catalysts.

Melchionna *et al.* [72] developed Fe-filled CNTs also using CVD, and employed this material as palladium nanocatalyst supports, for photocatalytic H_2 evolution. The authors used two variants of a Fe@CNTs/Pd@TiO_2 hybrid system and utilised magnetic sieving as an alternative method of separation that appeared to be extremely effective and over 3 cycles showed very little decrease in activity. One of the catalysts demonstrated particular excellent activity, with stable H_2 productivity amounting to 1092 mmol per gram of catalyst after 20 hours of irradiation. Comparing that with CNT-free Pd@TiO_2 which produced approximately 150 $mmolg_{Pd@TiO2}^{-1}$ in the same time, demonstrates clearly the catalytic benefits of CNTs. With the combination of the low cost and versatility of the procedure, this has demonstrated a successfully designed novel, magnetic catalyst with plenty of useful potential in industry.

In an investigation by Aygün,[73] magnetic carbon coated Fe or Co nanoparticles were deposited onto GNF alongside palladium and used in the reduction of nitrobenzene. The PdNPs@(($Fe@C_n$)/GNF) and PdNPs@(($Co@C_n$)/GNF) from both $Pd_2(dba)_2$ and $Pd(acac)_2$ and found that $Pd(acac)_2$ produced larger NPs resulting in decreased activities. Both catalysts synthesised from $Pd_2(dba)_3$ achieved good yields of 72 and 74 % respectively for this reaction. When using these catalysts over 5 cycles, the nitrobenzene conversion did decrease (72 to 47 % and 74 to 46 %) but less significantly than for just PdNPs@GNF (77 % to 37 %) demonstrating that magnetic separation helps to maintain catalyst activity. Studies were also conducted into the cause of these decreases in activity, but no evidence of Ostwald ripening or coalescence was found. Inductively coupled plasma optical emission spectroscopy (ICP-OES) demonstrated a small (3.76 %) leaching of Pd, leaving a space for further investigation into the source of this decrease in activity.

These examples demonstrate the powerful potential of using magnetically recoverable nanocatalyst for a variety of applications, making it more recyclable and in some cases more active, and there have also been reports of the successful use of these catalysts for cross coupling.

1.4.2. Using magnetic nanocatalysts for Suzuki reactions

Magnetic nanocatalysts supporting palladium have proven to be effective catalysts for Suzuki reactions. Many different types of magnetic catalyst have been deployed and achieved excellent results. Stevens *et al.*[74] synthesised iron oxide-Pd using Pd complexes and N-heterocyclic carbenes (NHCs) coated magnetic maghemite (γ-Fe_2O_3). After five consecutive cycles of Suzuki the yield only very marginally decreased suggesting that no significant loss of catalytic activity was observed. This catalyst was able to obtain high pre-isolated yields of 93-99% across a variety of functional group including iodide and bromide functionalised aryl halides under fairly mild reaction conditions. A comparison study between iron oxide NHC-Pd and polystyrene resin supported NHC-Pd was also conducted that determined via GC that showed that when using the iron-oxide-Pd reactions proceeded faster. The catalyst was able to be retrieved each time simply by using an external magnetic field, removing the need for another solvent. The authors conclude that this superparamagnetic nanoparticle is a promising catalyst support for industrial use.

Similarly, Ye *et al.*[75] synthesised a very effective recyclable palladium catalyst using magnetic nanoparticles and applied this to Suzuki coupling. In this study, the support used was N-heterocyclic carbene which presents many advantages including low toxicity, environmental stability and excellent bonding with Pd. They obtained excellent activity and recyclability for the coupling of bromobenzene with phenylboronic acid. The yield after 5 cycles was maintained at 92 % within 10 min under 70 °C. However, significant decrease in reaction rate was observed with each cycle, with the first cycle at approximately $8x10^{-3}$ and the 5^{th} at $1x10^{-3}$ $kmol/m^3 \cdot min$. Their research highlights the importance of insuring strong bonds between the support and NPs which could prevent the deactivation of the catalyst when being recycled as there is less likely to be agglomeration of the NPs or leaching into the reaction solution. Although green from a recyclability point of view, this method reports use of mixture of DMF and water as the most effective solvent. DMF is an undesirable solvent, and so if this activity could be maintained with more desirable solvents, such as neat water, the significance of this work would improve.

In 2021, there have been many reports on the use of magnetic nanoparticles in conjunction with Pd on different supports being used for cross coupling reactions. One significant example being a study conducted by Chutia *et al.* [76] who reported the very effective use of a Pd-$CuFe_2O_4$ magnetic nanocatalyst to be used in Suzuki Miyaura reaction and was successful even in the coupling of challenging chlorobenzene with a variety of arylboronic acids and managed to obtain yields between 72-95 %. The reactions were also performed in mild conditions and the Pd was ligand-free. Normally ligands are required to stabilise the active Pd but they can be toxic and hold many environmental and synthetic issues. The reaction also utilised readily available starting materials, solvents and bases, all without any loss of catalytic activity.

This is very promising progress towards affording a catalyst that can perform well in green conditions to Suzuki couple more challenging reagents and is very recyclable. The catalyst was easily removed with an external magnet and a recyclability test revealed only a 5 % decrease in yield (95-90%) over 5 cycles. All of these examples demonstrate the exciting potential that magnetic nanoparticles can have on creating active, recyclable catalysts for a variety of reactions, including cross couplings.

1.5. Summary

This chapter reviews some current insight on catalytic nanostructures, palladium nanoparticles and the Suzuki coupling reaction. Since the first paper published on the Suzuki Miyaura reaction in 1981, its use across many chemical industries has significantly increased, revealing that it was the second most used rection after amide bond formation in drug discovery in 2014. [77] As a powerful tool in organic synthesis, this reaction is widely used and significant to the chemical industry. Palladium has proven to be a very effective catalyst for this C-C bond formation, but it is an expensive and finite resource. So far nanoparticles have proven to have high activity due to their high surface area. However, their recovery can be challenging in the homogeneous system. Therefore, designing a heterogeneous nanocatalyst which can possess equivalent or better activity as homogeneous systems with low palladium loading, whilst also making it recyclable to reduce waste may

be a solution to the current issues surrounding the sustainability of cross coupling reactions. Therefore, it is important to investigate the most suitable support for the nanocatalyst, efficient method to fabricate the nanoparticles and deposit them onto the support and effective approach to ensure ease of separation for recyclability. My research will combine all of these aspects to report a design for an active, recyclable palladium nanocatalyst for the Suzuki reaction.

2. Aims and Objectives

This report will focus on the use of PdNPs on GNFs as a catalyst the Suzuki-Miyaura cross coupling reaction. The main aim is to improve the recyclability of this catalyst whilst maintaining or improving other important properties including activity. The approaches selected are: the use of magnetic nanoparticles to improve catalyst recyclability, altering the structure of the carbon support and investigating alternative Pd deposition methods.

2.1. Using magnetic nanoparticles to improve recyclability

The use of magnetic NPs has been reported as an effective method of improving recyclability of catalysts in the literature. An Fe@C_n/PdNPs@GNF catalyst is utilised which has been previously used as an active, recyclable catalyst for the reduction of nitrobenzene.[33] The main objective in this part of the project is to further develop this catalyst and evaluate its utility in the Suzuki coupling reaction.

2.2. Improve stability by altering the structure of the carbon nanosupport

GNFs are effective supports for metallic nanoparticles and create particularly stable anchoring points at their step edges. However, this could be further developed to create more sites for the palladium to bond to for stability. The approaches undertaken are to create defects in the GNF by etching holes for the nanoparticles to sit in and using GNFs with step-edges on the outside of the tube as well as inside, possessing more stable points for the palladium to attach to. The focus of this section is to improve the stability of the catalyst by mitigating factors, such as leaching and coarsening, by reducing the migration of the NPs.

2.3. Investigation into deposition methods

There are many ways to deposit nanoparticles onto supports, each holding pros and cons. Magnetron sputtering is a more recent approach to synthesising catalyst and has previously produced very active catalysts.[57] It is considered a greener method than using wet chemistry as it does not require solvent use. Properties of the NPs are also able to be easily controlled, including size and spatial distribution, making this is an exciting advancement in catalysis. There is no record of Pd fabricated by sputtering methods on GNF and used as a catalyst in published scientific literature, so this is a very novel and exciting method to be explored. Other methods of deposition of metal nanoparticles onto GNF have been reported, including encapsulation *via* vapour deposition, which encourages the NPs to settle inside the GNF in stable positions at the step- edges which has been adapted and utilised in this work.[32] The objective of this section of my project is to uncover the most desirable method to deposit PdNPs onto GNF to produce the most recyclable, efficient and active catalyst.

3. Results and discussion

Metal nanoparticles supported on carbon nanoreactors can be active, recyclable catalysts and are of great interest for use in coupling reactions. Palladium on graphitised carbon nanofibers has the potential to possess these properties for Suzuki cross coupling reactions, hence this material has been investigated and further developed in this project.

3.1 Synthesis and use of PdNPs@GNF from $Pd_2(dba)_3$

This section outlines the formation of PdNPs onto GNF from $Pd_2(dba)_3$ to be used as a catalyst in a Suzuki cross coupling. Two methodologies were utilised, one using $Pd_2(dba)_3$ dissolved in chloroform and the other using the commercially available solvate form, revealing some interesting results.

3.1.1. Synthesis of PdNPs@GNF-1 from Pd_2@$(dba)_3$

Using a simple stirring procedure adapted from work reported by Aygün,[33] PdNPs@GNF-1 was synthesised (Scheme 3.1.) and then used for up to five cycles of the Suzuki cross coupling reaction. The precursor used was $Pd_2(dba)_3$, which Aygün observed triggered a spontaneous growth of PdNP mainly at the graphitic step-edges, inside the GNF. Due to the fluxional nature of dba, the ligand then easily detaches itself and can be washed away.

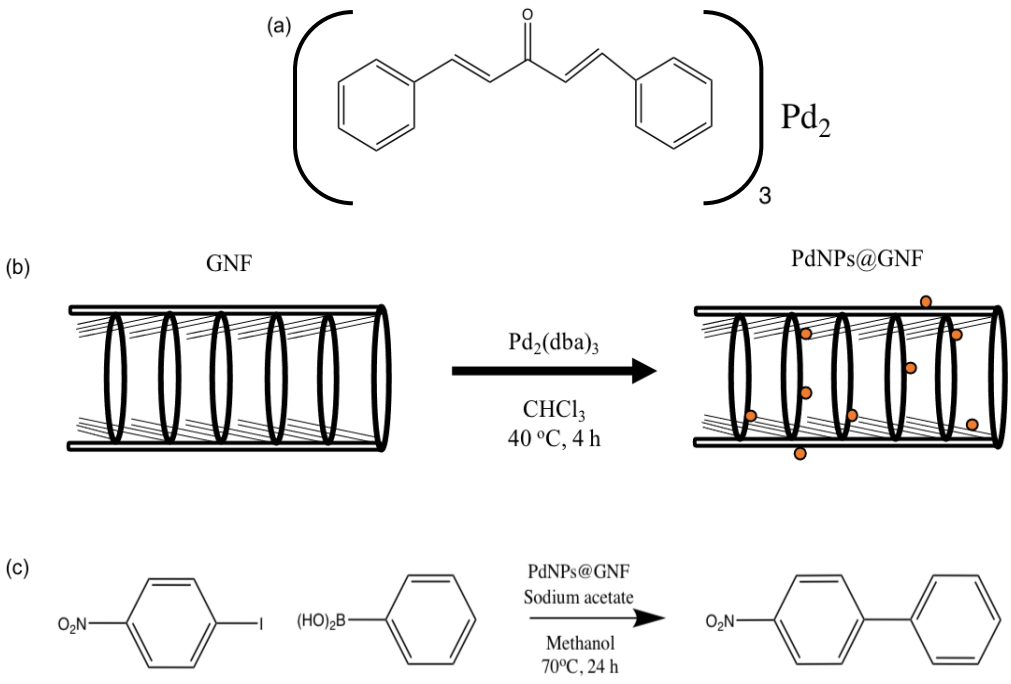

Scheme 3.1. (a) Structural diagram of Pd2(dba)3, (b) reaction scheme of synthesis of PdNPs@GNF from Pd2(dba)3, (c) Suzuki reaction between 1- iodo-4-nitrobenzene and phenylboronic acid.

TEM images were taken of the PdNPs@GNF-1 (Figure 3.1. (a-d)) which demonstrated a good distribution of nanoparticles, with many of the particles encapsulated on the inside of the GNF, where the step edges are. The images also showed many of the particles to be sitting on the anchoring points and have a generally consistent size. The diameter distribution was measured, which provided a 3.4 nm mean particle size with standard deviation (SD) of 2.06 nm prior to the Suzuki reaction cycles (Figure 3.1. (e)). From these images, it would be expected that this catalyst should perform well in a catalytic reaction and this was tested in a Suzuki coupling.

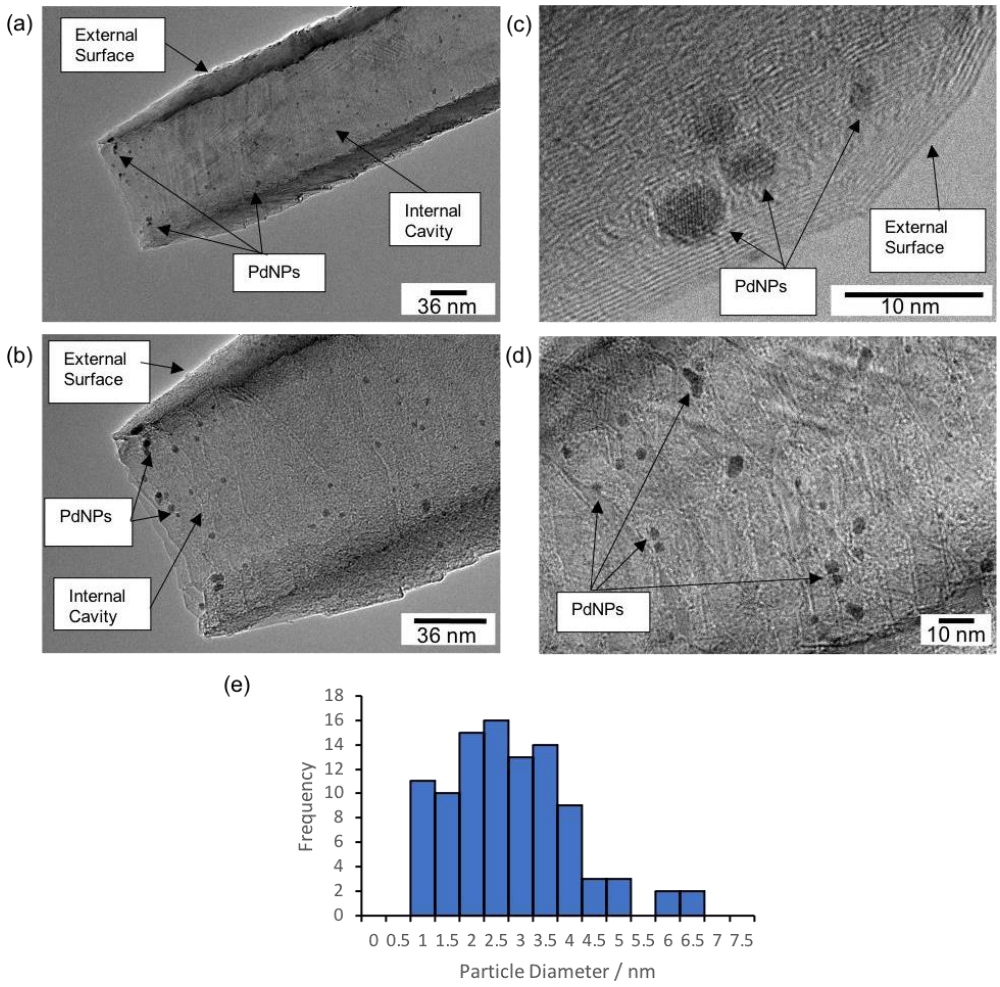

Figure 3.1. TEM images and particle diameter distribution histogram of PdNP@GNF-1 before Suzuki reaction with (a, b) NPs at end of GNF, (c) magnified image of Pd particles, (d) NPs encapsulated inside of GNF and on step-edges, (e) particle diameter distribution histogram showing a uniform size of 3.4 nm.

3.1.2. Suzuki cross coupling using PdNPs@GNF-1

The synthesised PdNPs@GNF-1 catalyst was used for the Suzuki cross coupling of 1-iodo-4 -nitrobenzene and phenylboronic acid (Scheme 3.2.). The temperature used was 70°C and the reaction was performed in methanol, a relatively green solvent. The first reaction cycle achieved a very poor conversion (6.7%) of 4-nitro-1,1'-biphenyl, determined by ^{1}H NMR (See Appendix A). A further two cycles of the reaction were then attempted (Table 3.1.) with the same catalyst. After each cycle, the reaction mixture was separated from the catalyst by centrifugation. The catalyst was washed, centrifuged again and dried, ready for the next cycle. After each reaction the conversion results continued to exponentially decrease until the 3rd cycle, where there was no product at all. Thermo-gravimetric analysis (TGA) was used to determine the Pd metal loading of the catalyst as a weight percentage before the reaction, which indicated a 1% loading of Pd for this material. Using this value, TON was calculated to be 99.7 and TOF of 4.1 h^{-1}. Comparing this to a TOF of 4.2 x 10^{4} h^{-1} which was achieved by Lodge *et al.*[70] (for the same reaction using a different catalyst) these values are very low.

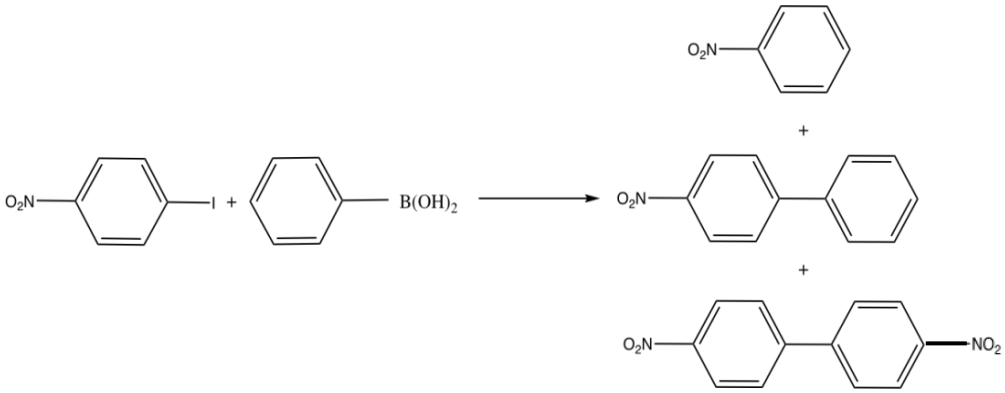

Scheme 3.2. Suzuki cross coupling reaction scheme of 1-iodo-4-nitrobenzene and phenylboronic acid producing the desired product 4-nitro-1,1'-biphenyl and two by-products nitrobenzene and 4,4'-Dinitro-1,1'-biphenyl.

Cycle Number	Conversion / %	Mass of Catalyst / mg
1	6.68	5.00
2	0.33	4.65
3	0.00	4.21

Table 3.1. Percentage conversion of product for three Suzuki cycles and the mass of catalyst PdNPs@GNF-1 used at the start of the reaction.

After three cycles, TEM images of the catalyst were taken again and showed a significant reduction of PdNPs present (Figure 3.2), in addition to some much larger aggregates of particles, presenting evidence of agglomeration, explaining this significant decrease in activity, a 4.9 nm average diameter of the NPs post reaction with SD of 4.12 nm, showing that the particles sizes were more varied post reaction.

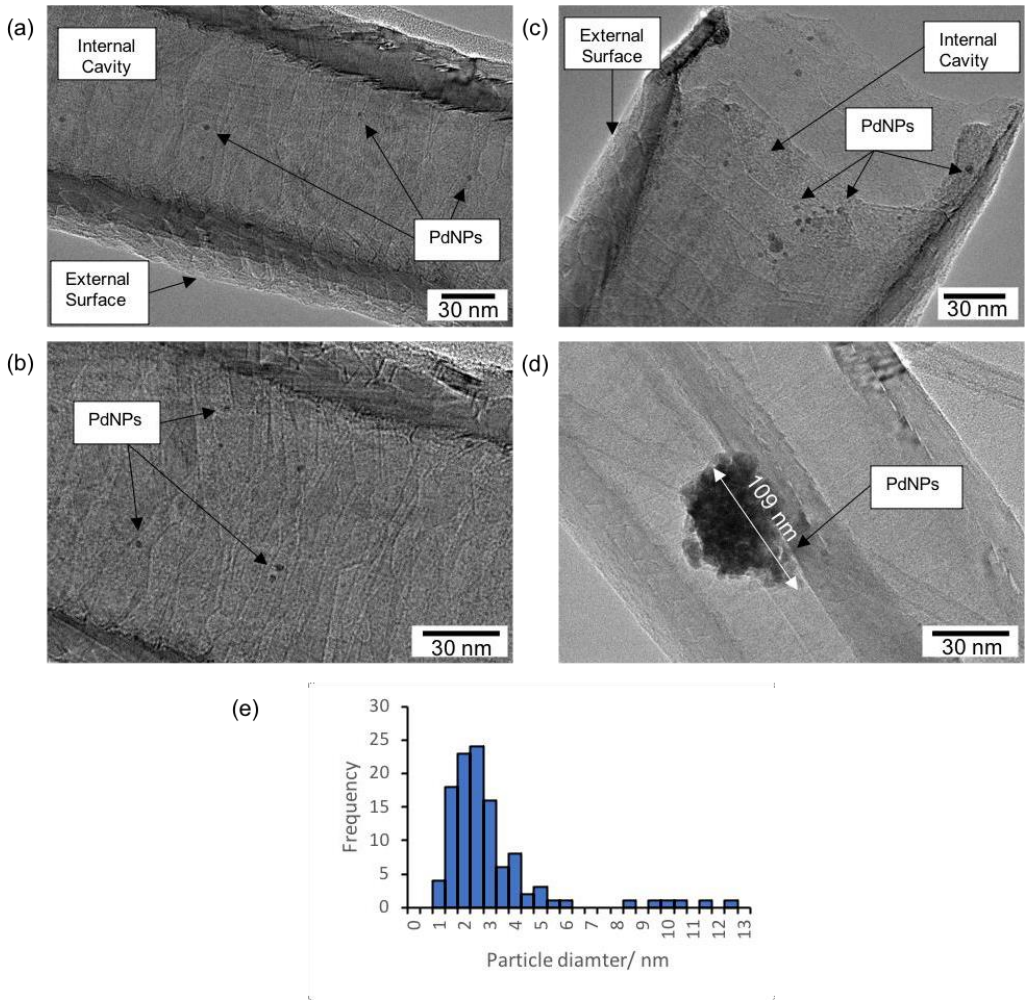

Figure 3.2. TEM images of PdNPs@GNF post three cycles of Suzuki where (a and b) show the inside of the GNF with a small number of PdNPs, (c) shows the end of the GNF, (d) showing a large agglomeration of NPs with diameter 109 nm, (e) particle diameter distribution histogram showing a uniform size of 3.4 nm.

In the literature, $Pd_2(dba)_3$ has been utilised successfully as a precursor for PdNP synthesis.[42] However, many opt to use this material in its solvate form, crystallised with chloroform.[36] [41] [43] The reason for this is that commercially available $Pd_2(dba)_3$ is often not a pure compound. It may contain elemental Pd and free dba ligands as impurities which can affect formation of NPs and quality of catalyst. This was investigated by A.J. Reay[78] who conducted analysis of this compound and demonstrated how the quality of catalyst is compromised as dba plays a non-innocent role in the catalytic activity of $L_nPd(0)$ complexes. By crystallising the $Pd_2(dba)_3$ into a chloroform solvate, they removed any free ligand and any elemental Pd, preventing negative effects on the catalytic system caused by poor characterisation of the compound. This is consistent with my results which demonstrate that catalytic activity is low when NPs are synthesised from this compound. Following this discovery, synthesising PdNPs@GNF from a $Pd_2(dba)_3$-$CHCl_3$ complex was then conducted.

3.1.3. Synthesis of PdNPs@GNF-2 from $Pd_2(dba)_3$ chloroform solvate

The same method to produce PdNPs@GNF-1 was then used but synthesised from $Pd_2(dba)_3$-$CHCl_3$. TEM images of PdNPs@GNF-2 were taken before the reaction (Figure 3.3) and revealed a good distribution of many PdNPs with relatively uniform size. A mean diameter of 2.5 nm and SD 1.15 nm (Figure 3.3. (f)) was also measured. This average size is ca. 1 nm smaller than the PdNPs@GNF-1 which suggests a larger surface area to volume ratio, potentially increasing activity. The size distribution was also smaller, showing that the nanoparticles were more uniform in size. The majority of these particles were encapsulated on the inside of the GNF. There were also more particles present on step-edges compared to the previous catalyst, suggesting that they would be less likely to migrate. From the images, this catalyst was expected to perform well so it was utilised in the Suzuki reaction. However, a large agglomerate of NPs (diameter 61 nm) was also identified, suggesting there could be some decrease in activity due to reduction in active catalytic surface area. The presence of an agglomerate at the NP synthesis stage is very undesirable and further synthetic methods will try to reduce this affect. Several reports state that smaller NPs are more likely to agglomerate so a method that involves the better control of NP size may reduce this effect.[79], [80] Although smaller NPs in theory should have better activity due to their larger surface area to volume ratio, if they are more likely to form large agglomerates this counteracts this effect.

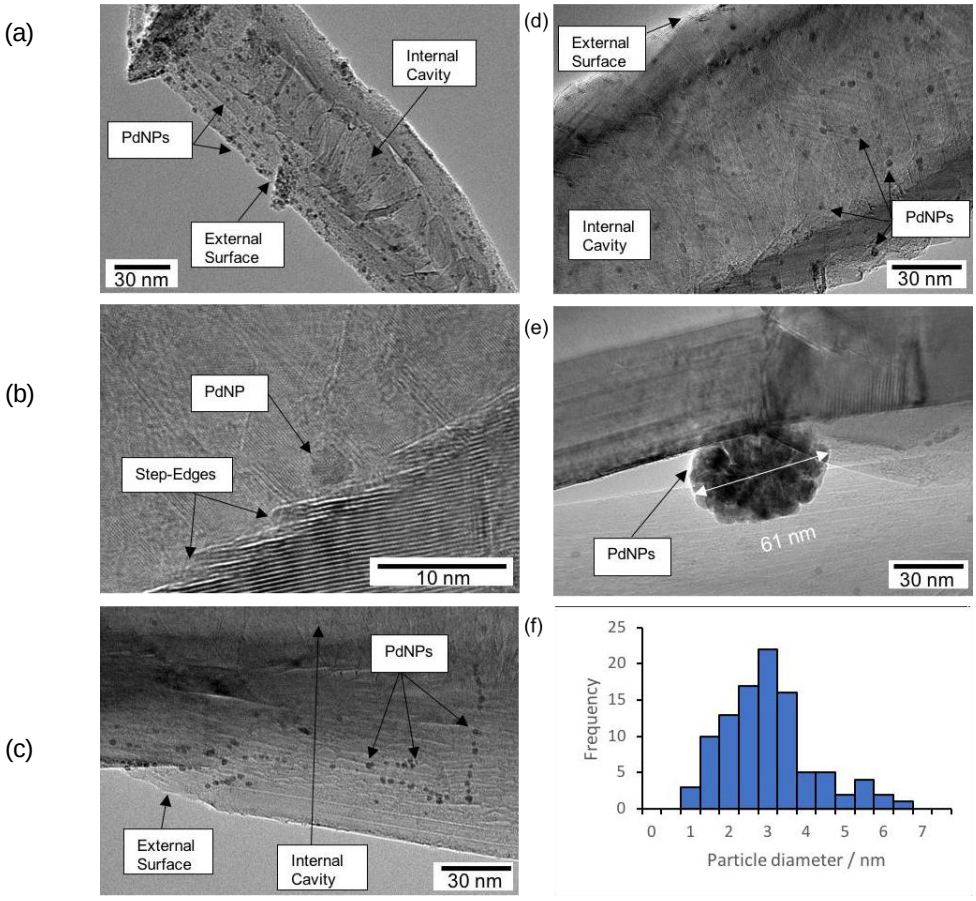

Figure 3.3. TEM images of PdNPs@GNF-2 from $Pd_2(dba)_3$-$CHCl_3$ where (a) large field of view showing distribution of NPs, (b) higher magnification showing on PdNP secured in a step-edge, (c) NPs on outer surface of GNF, (d) NPs encapsulated inside GNF, (e) an agglomerate of nanoparticles with diameter 61 nm, (f) particle diameter distribution histogram showing a uniform size of particle with average diameter of 2.5 nm.

3.1.4. Suzuki cross coupling using PdNPs@GNF-2

The catalyst was used in four cycles of Suzuki reaction. This catalyst was a lot more active than PdNPs@GNF-1, with a first cycle conversion of 33.01% (See Appendix B). This confirms the theory that when $Pd_2(dba)_3$ is confined into the $CHCl_3$ lattice in adduct form, better NPs are formed due to an improvement in purity of the precursor complex. The conversion still was low, however, and after the first cycle, the same precipitous decrease in conversion was observed. (Table 3.2) until a 0% yield was obtained at the end of cycle 4.

Cycle Number	Conversion / %	Mass of Catalyst / mg
1	33.08	5.00
2	1.85	4.22
3	1.01	3.18
4	0.00	1.22

Table 3.2. Percentage conversion of product for four Suzuki cycles and the PdNPs@GNF-2 mass of catalyst used at the start of the reaction.

Prior to the reaction a TGA was performed (See Appendix M-1) to determine an approximate 1% metal loading of Pd in order to calculate activity of catalyst. Using this value, TON of 364.7 and TOF of 15.2 h^{-1} was calculated, these values show that the activity of this catalyst was higher for the first cycle than PdNPs@GNF-1 catalyst but still much lower than desirable. Across the literature, TOF and TON values are very varied however it appears that TON values that are greater than 10^{-4} and TOF values greater than 10^{-3} tend to be considered as "good", dependent on the reaction time and catalyst used.[47], [65]

TEM images (Figure 3.4) determined an average nanoparticle diameter of 5.4 nm post reaction, showing a significant increase which may explain the observed deactivation of the catalyst. The SD of 4.96 nm also demonstrates how the particles are more varied in size post reaction. The image analysis showed a significant reduction of number of NPs present on the GNF and the presence of more large agglomerates. One of the agglomerates was measured to be 42 nm. Although this was not as large as the pre-reaction agglomerate (61 nm), there may have been larger ones in the sample that was not identified by TEM. Additionally, there appeared to be more agglomerates that had formed post reaction. Reduction of number of NPs could also be due to leaching of the particles into the reaction mixture and therefore having fewer active particles

on the GNF. However, this could not be determined by ICP-OES due to the small scale of the reaction. $Pd_2(dba)_3$ also produces fairly amorphous PdNPs therefore may lack defined catalytic sites. Any residual dba ligand from the precursor may also still be present and blocking some sites. It was thought that further development of this catalyst would reveal the cause of this poor performance.

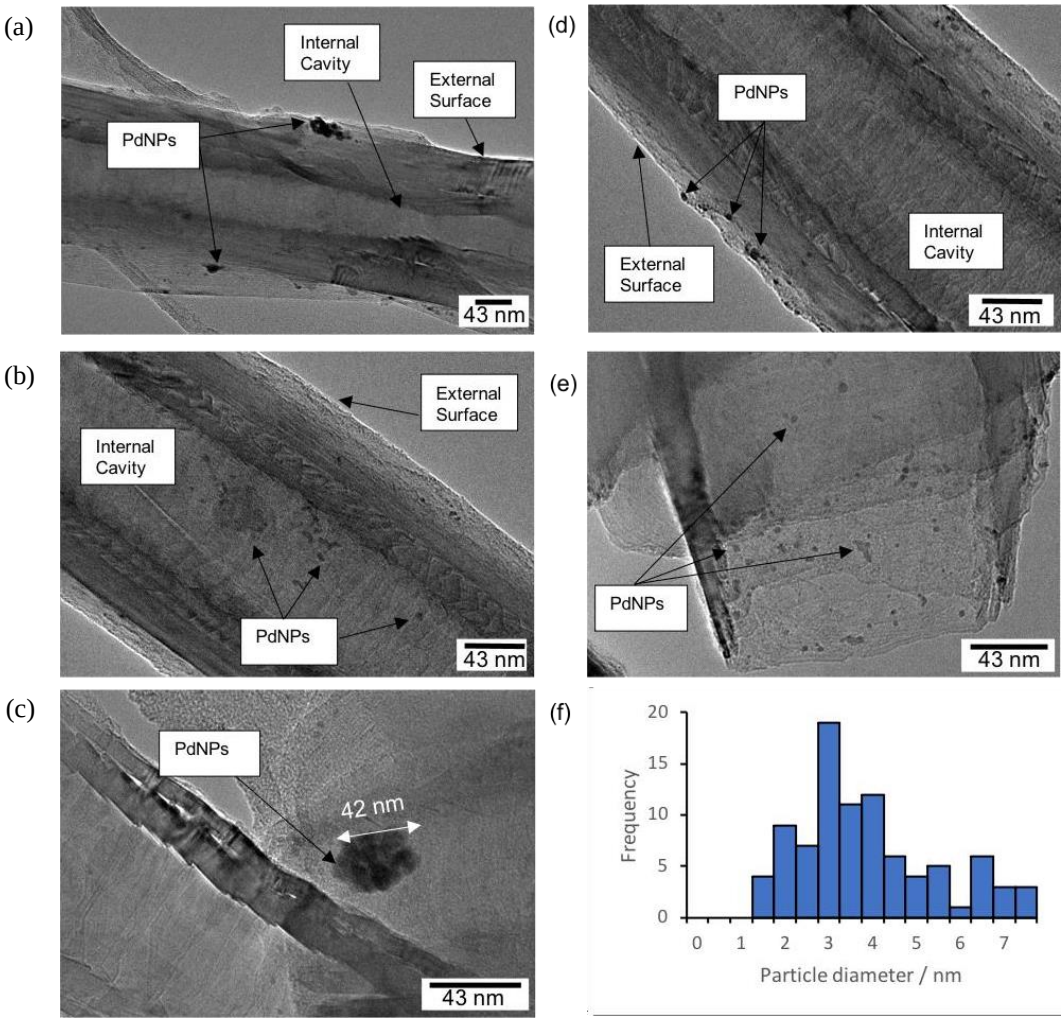

Figure 3.4. TEM images of PdNPs@GNF-2 post reaction (a) large agglomerates of NPs on outside wall of GNF with no Pd encapsulated, (d) distribution of nanoparticles mostly on outer surface of GNF, (b) small number of NPs encapsulated, (e) end of GNF with some NPs and (c) a large agglomerate of nanoparticles with diameter 42 nm, (f) particle diameter distribution histogram showing a uniform size of particle with average diameter of 5.4 nm.

3.1.5. Conclusion

$Pd_2(dba)_3$ can be a precursor to distribute PdNPs onto GNF but has not proven to produce an effective catalyst for the Suzuki cross coupling reaction. The catalyst performs better when produced from $Pd_2(dba)_3$ in a chloroform solvate complex and not just dissolved into the solution. However, the conversion of product and recyclability was very low for both catalysts. The TEM images showed large clusters of particles forming where the Pd had migrated and aggregated due to the Pd not being secured in the stable GNF step-edges.

Therefore, an approach to prevent migration of NPs by securing it onto the support and to develop a more effective approach to recovering the catalyst after each reaction cycle could be solutions to significantly increasing catalyst activity and recyclability. The next section will focus on the improving these factors of this PdNPs@GNF catalyst by utilising magnetic NPs.

3.2. Use of magnetic NPs to improve recyclability

Magnetic NPs have been used on catalyst supports as an easier, cheaper and more effective way of extracting a catalyst in order to improve recyclability, as well as being used as catalysts themselves. Therefore, combining a PdNPs@GNF with magnetic NPs has the potential to significantly improve the performance of this catalyst.

3.2.1. Synthesis of Iron (Fe) functionalised PdNP@GNF

By thermally decomposing ferrocene, a carbon coated Iron (Fe@C_n) functionalised GNF was synthesized. $Pd_2(dba)_3$-$CHCl_3$ was then introduced to the system and PdNPs encouraged to attach to the Fe@Cn/GNF via the same solution stirring method used in the previous section (Scheme 3.3.) to produce Fe@C_n/PdNPs@GNF-1.

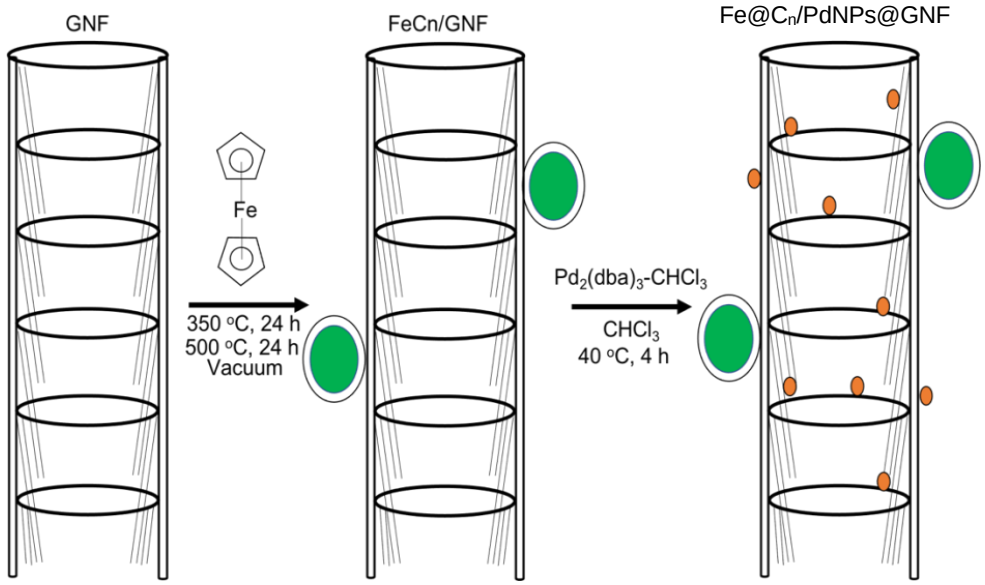

Scheme 3.3. Two-step synthesis of Fe@C_n/PdNPs@GNF. Produced in Microsoft Powerpoint.

The TEM images of the catalyst (Figure 3.5. (a, c, d)) showed the clear presence of Fe@C_n both attached to the outer surface as well as encapsulated in the internal cavity. The images also revealed the presence of PdNPs (Figure 3.5. (b, e)) with an average diameter of 2.3 nm prior to reactions, similar to PdNPs@GNF-2, and a relatively uniform size shown by a SD of 1.25 nm (Figure 3.5. (f)). However, a smaller fraction of the particles appeared to be encapsulated in the GNF than in the previous catalysts, therefore suggesting that more of the particles would be likely to migrate and coalesce. As the PdNPs particles mostly appeared to be settled on the outside of the GNF instead of in the more secure step edges they would also be more likely to leach into the reaction solution, leaving less Pd available for the next reaction cycle. A large agglomerate of PdNPs with diameter 57.1 nm was also present on this catalyst. Once again, this may be due to the small NP size but requires further investigation.

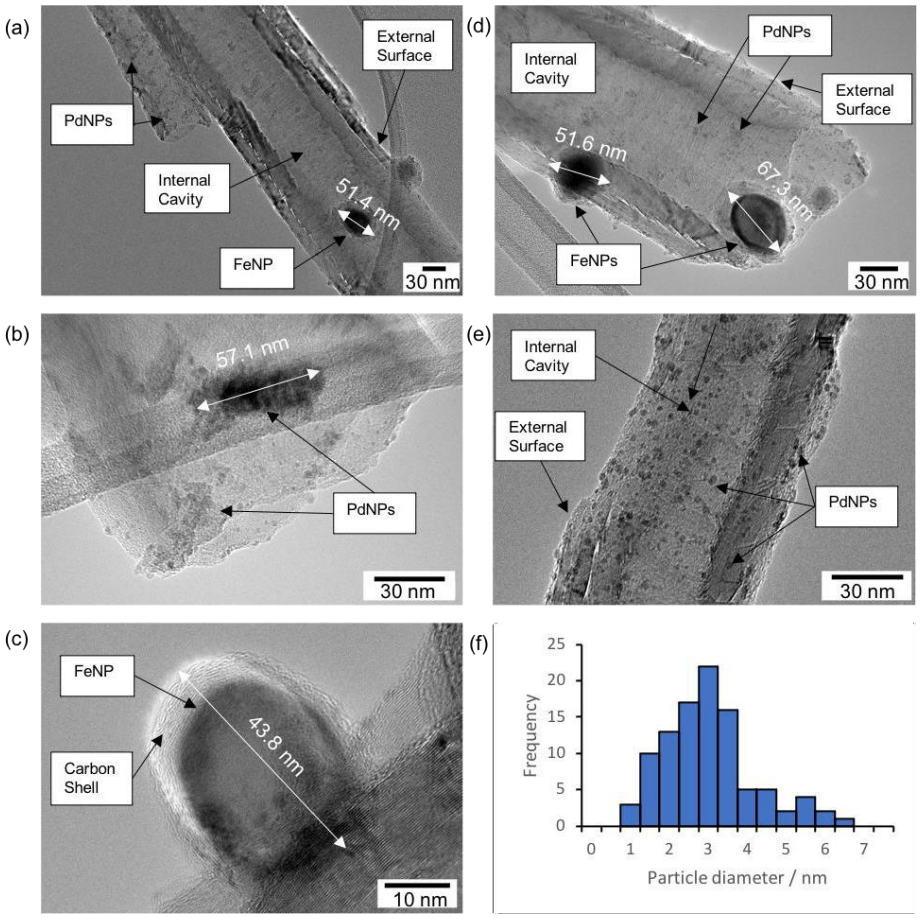

Figure 3.5. TEM images and particle diameter distribution histogram of Fe@C_n/PdNPs@GNF before Suzuki reactions with (a) a Fe@C_n encapsulated inside GNF with diameter 51.4 nm, (b) a large agglomerate of PdNPs with diameter 57.1 nm, (c) higher magnification images of Fe@C_n NP displaying the carbon shell structure consisting of c.a. 10 layers of graphitic carbon with diameter 43.8 nm, (d) two Fe@C_n NPs, one encapsulated inside GNF and the other settled on the external surface with diameters 67.3 and 51.6 nm respectively, (e) large field of view showing distribution of PdNPs, (f) particle diameter distribution histogram showing a uniform size of particle with average diameter of 2.3 nm.

3.2.2. Suzuki cross coupling using Fe@C_n/PdNPs@GNF-1

This catalyst was used for four consecutive Suzuki reactions and each time the catalyst was extracted from the system using an external magnet. The reaction mixture was extracted and the catalyst washed with methanol, extracted again with a magnet and then left to dry in air. This proved to be much quicker and easier and less catalyst mass was lost compared to the non-magnetic catalysts in the extraction process, displaying some of the benefits of using a magnetic catalyst. The conversion obtained on the first cycle was 60.7 % (See Appendix C), which was almost double the result obtained by PdNP@GNF-2, demonstrating that not only can magnetic nanoparticles maintain better recyclability but can also improve the activity of catalysts. One possible explanation for this could be the increase in surface area to support the catalyst due to the presence of Fe@C_n. However, once again a critical loss of catalytic activity was observed from cycle to cycle shown by the conversion. As a result, after four cycles the reactions were stopped after <1% conversion was observed.

Cycle Number	Conversion / %	Mass of Catalyst / mg
1	60.72	5.00
2	9.80	4.62
3	1.19	4.03
4	0.60	3.59

Table 3.3. Percentage conversion of product for four Suzuki cycles and the mass of catalyst used at the start of the reaction.

Due to the presence of Fe, TGA was not able to be used to calculate Pd metal loading (See Appendix M-2). However, as the PdNPs were synthesised in exactly the same way as PdNPs@GNF-2 from $Pd_2(dba)_3$ and all of the Pd will become PdNPs using this method, an assumption that the catalyst contained 0.92% loading of Pd on was made in order to calculate activity of catalyst. The weight loading obtained for the Fe and Pd combined was 9.7% which was used to calculate and Pd loading of 0.92% of the whole system. Using this value, TON of 1087 and TOF of 45.3 h^{-1} were calculated, these values show that the activity of this catalyst was higher for the first cycle than both the previous catalysts but still could be improved.

The TEM images post four reactions (Figure 3.6. (a-e)) revealed clear agglomeration of particles as the average particle size increased to 5.8 nm, a similar to that of the PdNPs@GNF-2 catalyst. The variation in sizes in the particles had additionally increased demonstrated by the large spread in the size distribution histogram (Figure 3.6. (f)) and a SD of 5.35. Large agglomerates of particles and considerably fewer individual particles appeared to be present in the post cycles images, particularly encapsulated inside the GNF, all of which can explain the large decreases in activity observed.

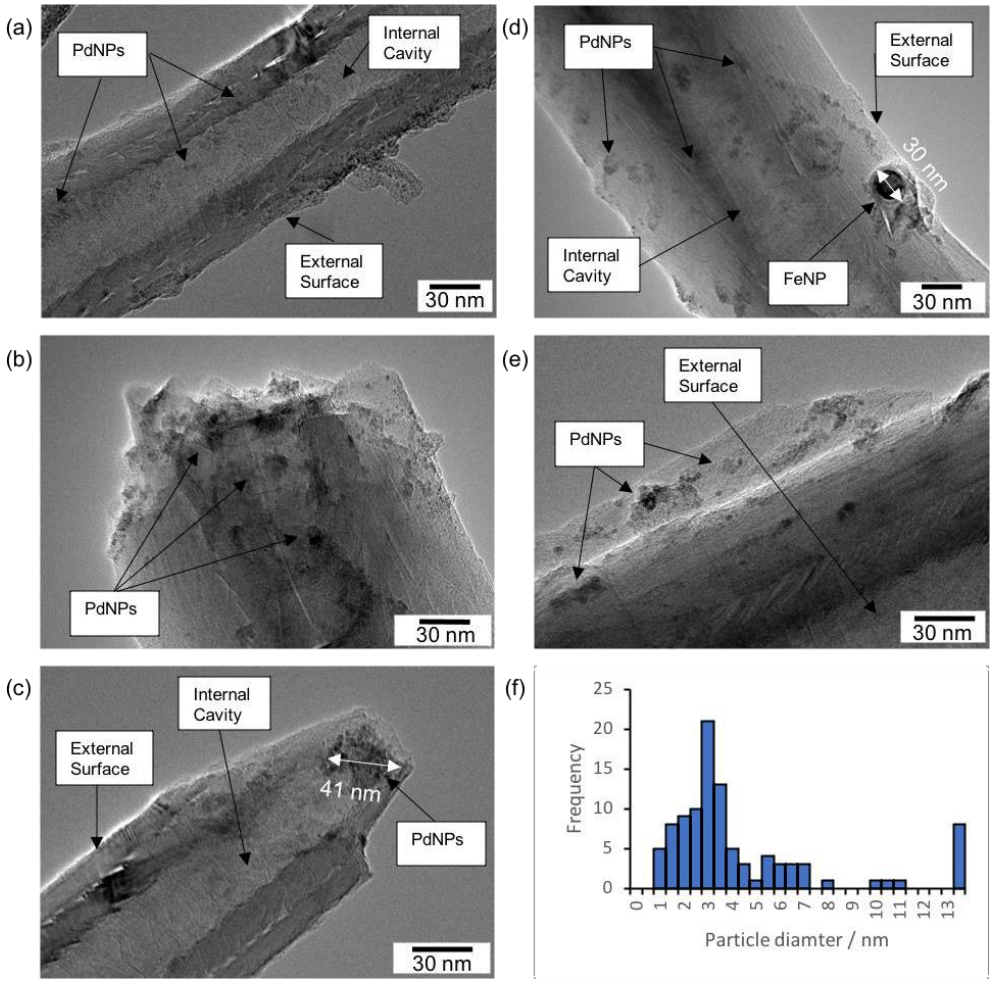

Figure 3.6. TEM images of Fe@C_n/PdNPs@GNF post four reactions (a) small number of PdNPs encapsulated in GNF with large number of particles located on external surface, (b) end of the GNF with larger particles present, (c) end of GNF with large agglomerate of PdNPs with diameter 41 nm, (d) larger PdNPs on GNF with an Fe@C_n NPs with diameter 30 nm embedded on external surface, (f) particle diameter distribution histogram showing a large spread of particle sizes with average diameter of 5.8 nm.

3.2.3. Conclusion

The magnetic NPs on GNF provided a much quicker and easier separation process and retained more mass of catalyst between cycles overall compared to PdNPs@GNF without the magnetic NPs. However, this catalyst did not show evidence of being recyclable. Although good activity for the first reaction cycle was observed compared to the previous catalysts, this was followed by a significant decrease after the 2nd cycle. TEM analysis after all reactions

revealed significant agglomeration and lack of individual PdNPs, explaining this reduction in activity. Therefore, in the next section an approach was taken to try and improve the activity and stability of the catalyst by investigating an alternative deposition method.

3.3. Magnetron Sputtering

Magnetron sputtering is a technique that has been employed as a method of NPs deposition on supports and is capable of producing very active catalysts. [56] As a result of its past successes that have been reported in scientific literature and many advantages including control of properties and environmental benefits, this method was utilised to try and improve the PdNPs@GNF catalyst.

3.3.1. Synthesis of PdNPs/GNF-3 via magnetron sputtering

Another PdNPs combined with GNF catalyst was synthesised using this novel, solventless method to attempt to improve activity. Sputtering allows control over particle size and metal loading, and so an optimum particle size of 3 nm was selected and a loading of 1 wt % of palladium.

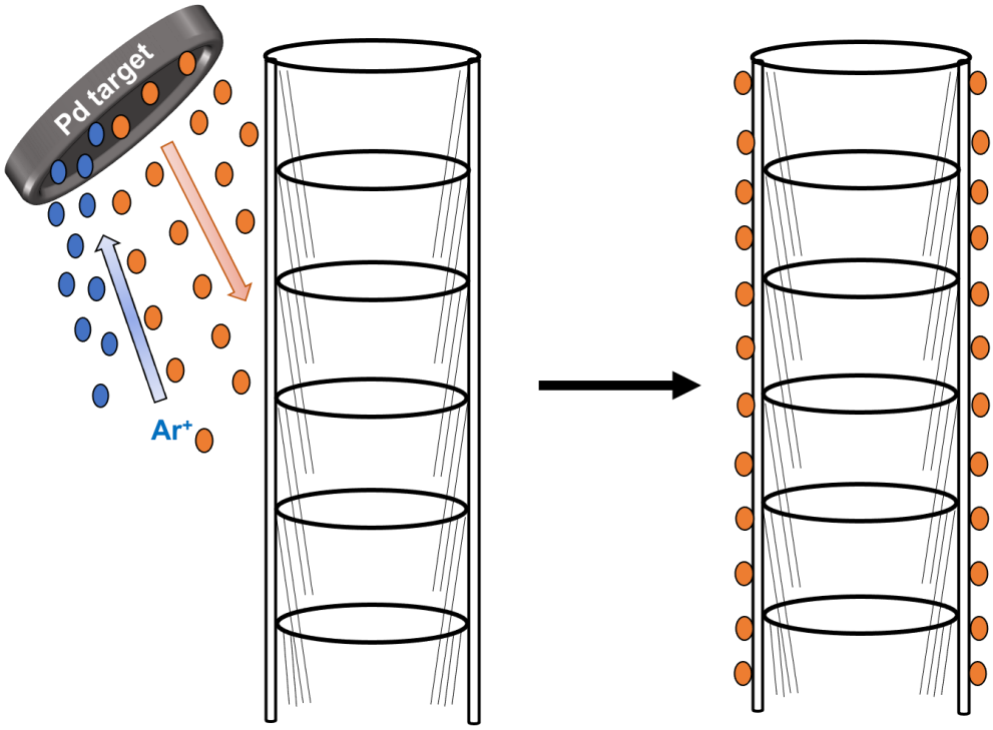

Scheme 3.4. Scheme of magnetron sputtering deposition of PdNPs onto GNF.

TEM analysis of the catalyst prior to the reaction (Figure 3.7. (a-e)) showed an excellent, equal size and even distribution of PdNPs on the GNF external surface and a very uniform particle size averaging at 3.4 nm with SD 1.02 nm (Figure 3.7. (f)), a very close value to the diameter that was expected. No agglomerates were present in this material, and the singular particles were larger than that of the previous catalyst. This may be the effect of the small particle size on amount of agglomeration.

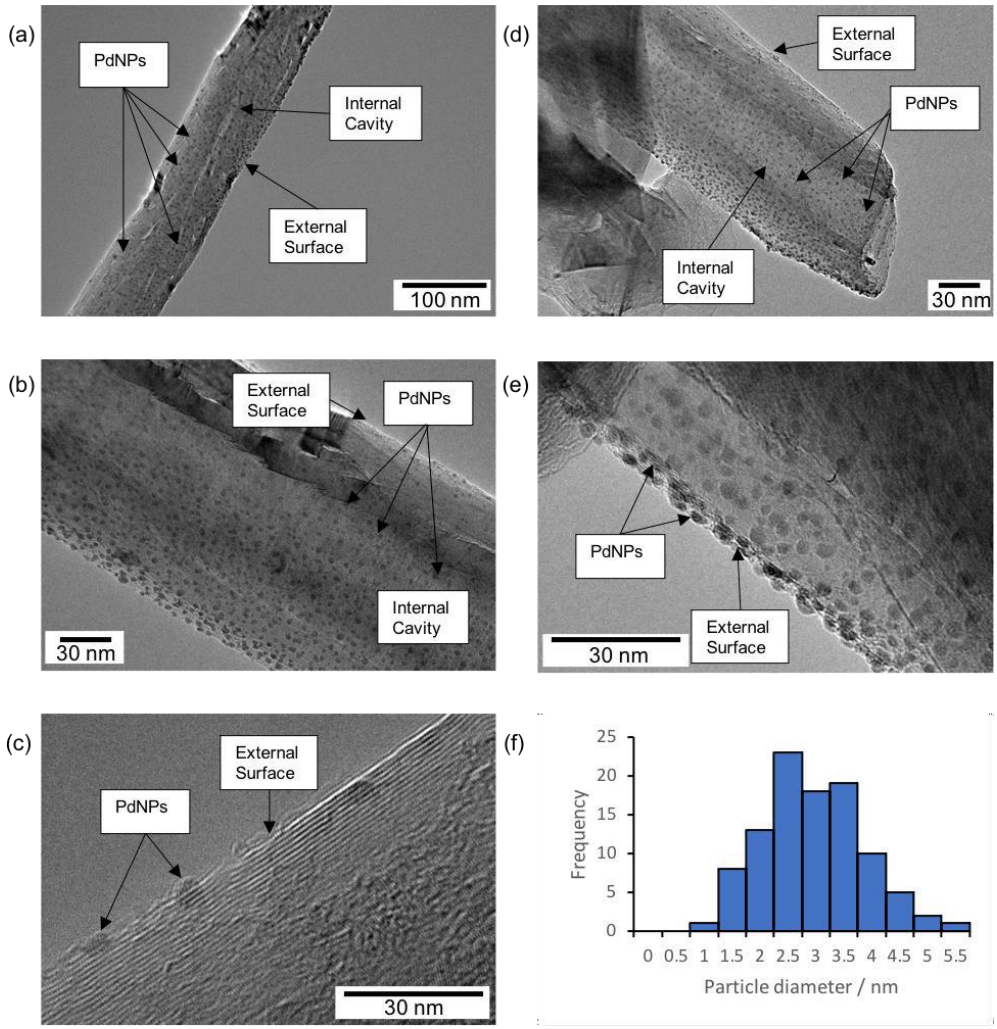

Figure 3.7. TEM images of PdNPs/GNF-3 and particle diameter distribution of NPs where (a, b) large field of view showing distribution of NPs, (c, e) NPs deposited on external surface, (d) distribution of NPs at end of GNF, (f) particle diameter distribution histogram showing very uniform size of particle with average diameter of 3.4 nm.

3.3.2. Suzuki cross coupling with PdNPs/GNF-3 using magnetron sputtering

This catalyst was used for four cycles of Suzuki reaction and displayed very similar conversion results as the Fe@C_n/PdNPs@GNF catalyst. Initially this catalyst produced a good conversion of 60% (See Appendix D), double that

of PdNPs@GNF-2, but unfortunately then displayed a large decrease between the first and second cycle to 6%. The results displayed a considerable decrease after the first cycle, rendering this neither an active nor recyclable material. TGA provided a Pd metal loading of 1% and from this value a TON of 872 and a TOF of 36.3 h^{-1} was calculated, both values higher than the other PdNPs@GNF catalysts but not quite as high as FeC_n/PdNPs@GNF.

Cycle Number	Conversion / %	Mass of Catalyst / mg
1	59.97	5.00
2	5.68	4.25
3	1.53	3.73
4	0.00	2.86

Table 3.4. Percentage conversion of product for four Suzuki cycles and the PdNP/GNF-3 mass of catalyst used at the start of the reaction.

This significant reduction in conversion could be explained by the TEM images conducted after the reactions (Figure 3.8. (a-e)) which showed that after three cycles of the reaction displayed similar behaviour to the other catalysts with considerably fewer PdNPs present, and some larger clusters of particles, demonstrating evidence of agglomeration and an increase in NP mean diameter 5.5 nm (Figure 3.8. (f)). The SD increased to 3.87 nm, the smallest increase so far post reaction, demonstrating a more uniform particle size.

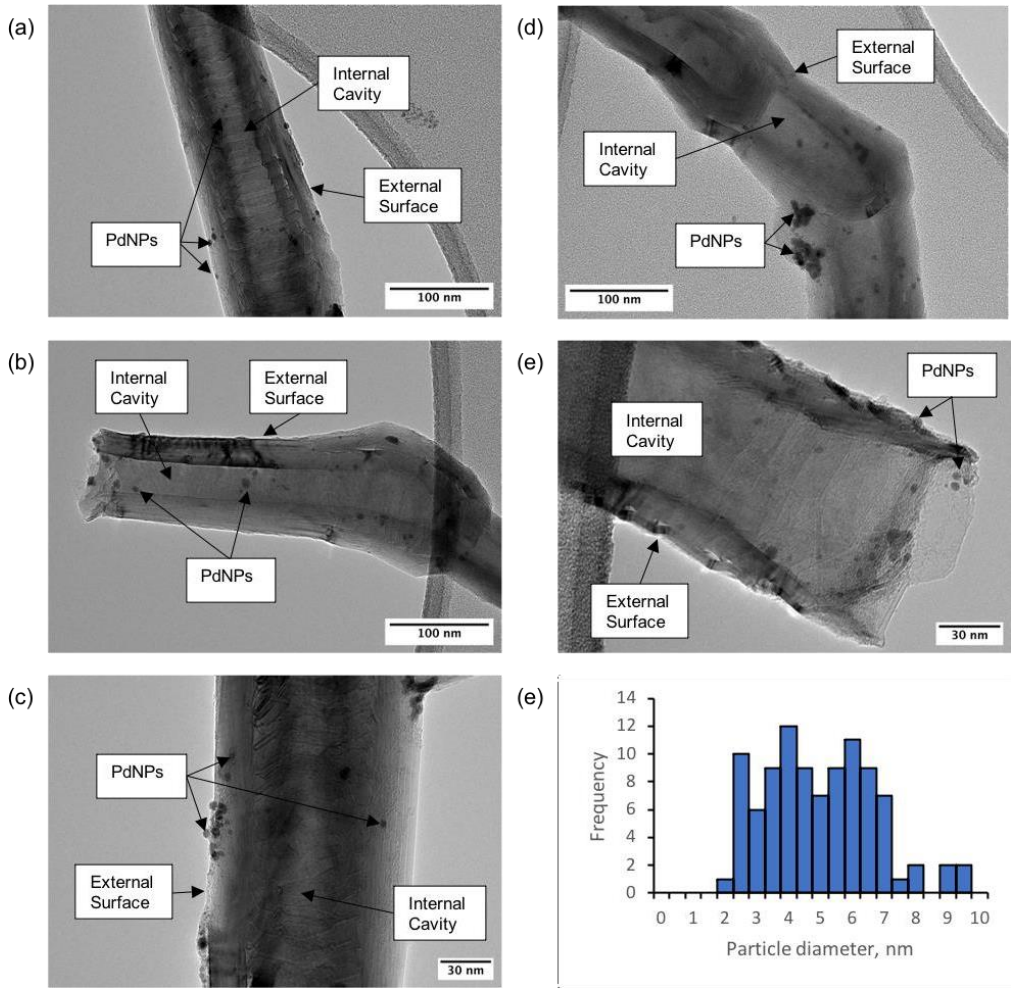

Figure 3.8. TEM images of PdNPs/GNF-3 after four Suzuki reactions and particle diameter distribution of NPs where (a, b) large field of view showing distribution of NPs, (c, d) larger clusters of NPs deposited on external surface, (e) distribution of NPs at end of GNF, (f) particle diameter distribution histogram showing a larger distribution of particle size with average diameter of 5.5 nm.

3.3.3. Conclusion

Magnetron sputtering is a novel way of depositing metal NPs onto supports and has been utilised to synthesise catalysts. It has previously been used to produce very active, successful catalysts and so this was an alternative method used to try to improve the activity of the catalyst. Both the activity and recyclability were improved in comparison to the previous PdNPs@GNF catalysts but still only achieved 60 % conversion on the first cycle with limited recyclability, and in terms of activity had very similar results to Fe@C_n/PdNPs@GNF. All the catalysts tested so far have followed the same pattern of activity decrease between cycles (Graph 3.1.) and are therefore not recyclable. All catalysts have shown evidence of agglomeration which may be the cause of this pattern.

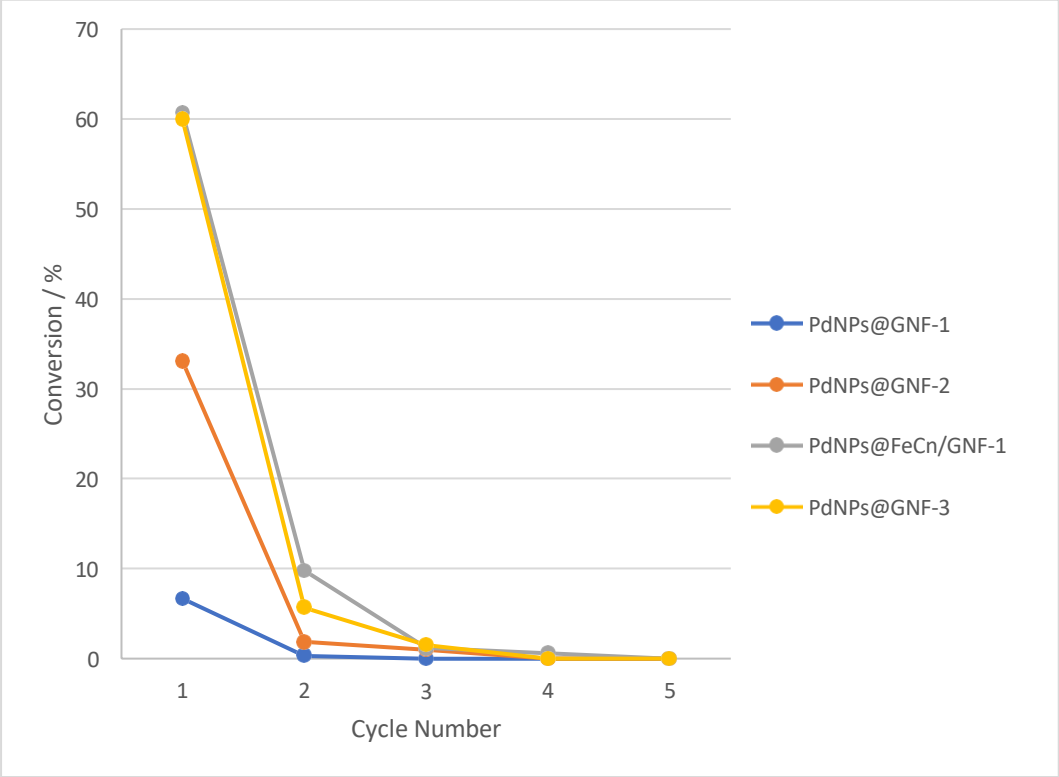

Graph 3.1. Comparison of the conversions achieved by the four PdNPs@GNF catalysts used so far up to five cycles of Suzuki cross coupling, demonstrating the significant decrease between cycles and overall Fe@C_n/PdNPs@GNF was the best performing catalyst.

3.4. DCT Test using Crabtree's catalyst

Due to the poor results demonstrated by the catalyst, the catalyst was tested to check if the reaction was being catalysed by the heterogeneous nanoparticles on the support or by NPs that have leached in the solution. Dibenzo[a,e]cyclooctatetraene (DCT) (Figure 3.9.) is a potent selective poison for homogeneous catalysts was first reported by Anton and Crabtree as a way to determine the homogeneous nature of a catalyst.[81] When a catalyst is mixed with DCT before a reaction the DCT will block the active sites of any homogeneous catalysts (Scheme 3.5.). If the reaction still proceeds with the same conversion this suggested that the non-homogeneous supported NPs are the active sites. This test was used to confirm that the heterogeneous NPs were the active sites for the reaction and was performed using PdNPs@GNF-2. ^{1}H NMR confirmed a 33 % conversion (See Appendix E), which shows no loss of activity suggesting that the NPs on the GNF were responsible for catalysing the reaction.

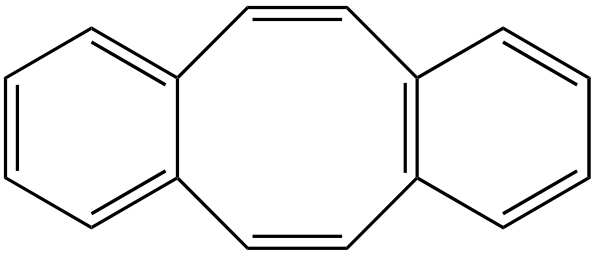

Figure 3.9. Schematic diagram of DCT. Produced in ChemDraw.

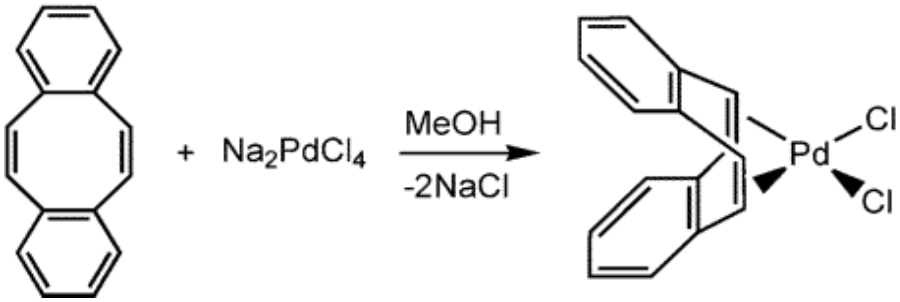

Scheme 3.5. Example reaction scheme of DCT reacting with Pd complex, demonstrating the bonding formation.[82]

3.5. Hydrogenation

It has been highlighted in the literature that hydrogenation is a method capable of changing the structure of GNF step edges by breaking the C=C bonds resulting in the formation of stronger covalent bonds between C and Pd.[33] These defects in the GNF step-edge, allow a structure that is more stable for the PdNPs to bind stronger to carbon support. The step edges play a large role in the effectiveness of GNF as a catalyst support as they secure the Pd to prevent its migration and subsequent deactivation. It was theorised that a hydrogenation step could also remove excess dba ligands that may be blocking potential interaction between Pd and the GNF. Thus, after synthesising PdNPs@GNF-2 a hydrogenation step was added to determine if this could improve the recyclability of the catalyst.

3.5.1. Hydrogenation of PdNPs@GNF-4

PdNPs@GNF-4 was synthesised by solution stirring with $Pd_2(dba)_3$-$CHCl_3$ as a precursor for the NPs, using the same methodology that was used to produce PdNPs@GNF-2. Following this, the catalyst was then stirred in a hydrogenation reactor in THF for 18 hrs under 10 bar of H_2 at 40 ˚C to achieve the desired effects.

TEM images (Figure 3.10. (a-e)) after synthesis demonstrated a smaller number of particles compared to the previous catalysts prior to Suzuki

reactions. Although an even distribution NPs was not present, the NPs were very uniform in size with a mean diameter of 5.7 nm (Figure 3.10. (f)) and SD of 2.21, which were both larger than PdNPs@GNF-2 catalysts. However, the majority of these particles appeared to be encapsulated inside the GNF, settled on the desirable step-edges. There is a large agglomerate of NPs with diameter 66.6 nm present which is likely to deactivate some of the catalyst.

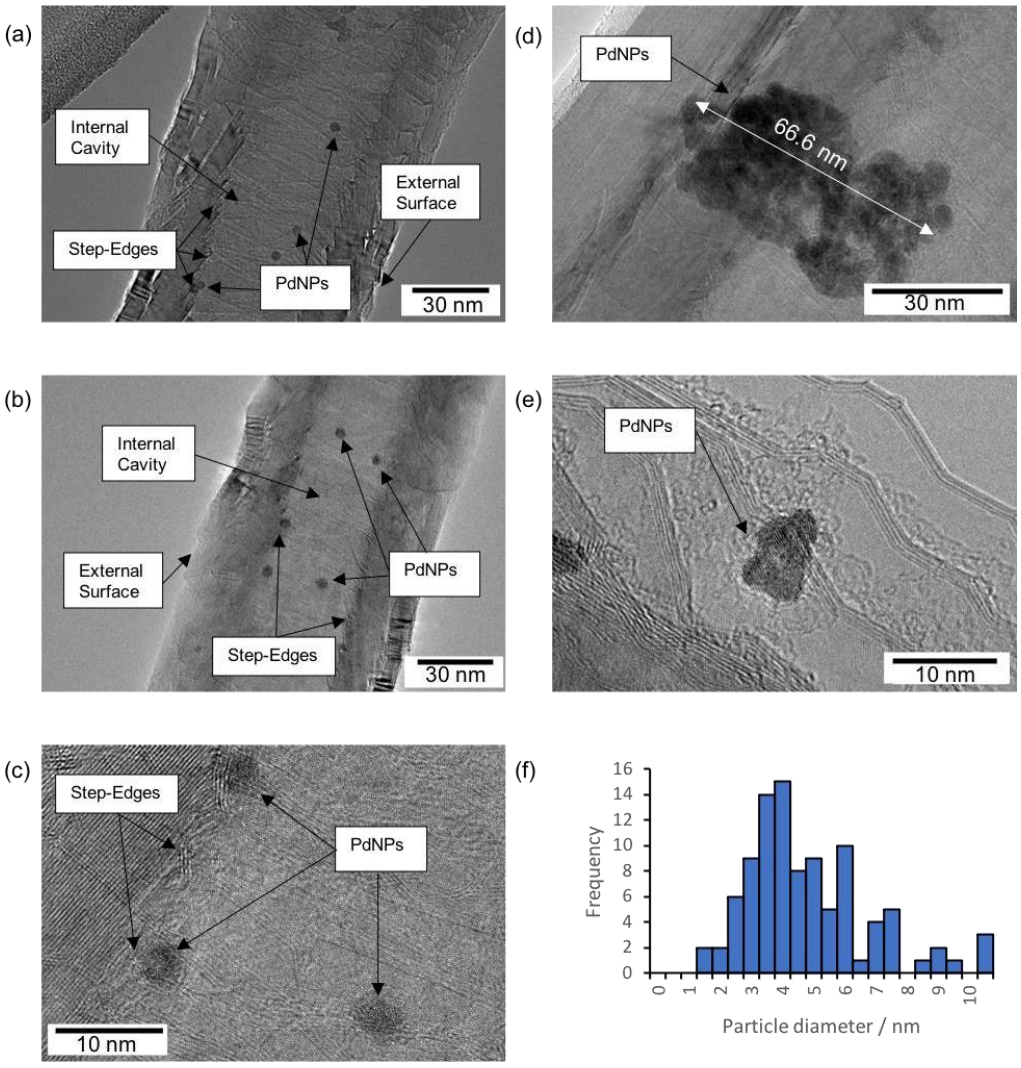

Figure 3.10. TEM images and particle diameter distribution histogram of PdNPs@GNF-4 before Suzuki reaction with (a, b) PdNPs encapsulated inside GNF, (c) magnified image of PdNPs settled onto step-edges, (d) large agglomerate of NPs with diameter 66.6 nm, (e) PdNP secured inside GNF, (f) particle diameter distribution histogram showing a generally uniform size of particle with average diameter of 5.7 nm.

3.5.2. Suzuki cross coupling using PdNPs@GNF-4

The hydrogenated catalyst was then used for five cycles of Suzuki coupling and the results were outstanding. The conversion for the first cycle was a remarkable 98% (See Appendix F) and did not display the same exponential decrease in activity as the previous catalysts had. On the 5th cycle the catalyst was still achieving a very good 81% conversion and was dropping at a steady rate of approximately 5% per cycle (Table 3.5.). TGA determined a 2.4% metal loading which was a higher percentage than the other catalysts suggesting that this catalyst was capable of supporting more Pd (See Appendix M-3). Using this value, a good TON of 1001.3 and a satisfactory TOF of 41.7 h^{-1} of was calculated, both much higher than any previous catalyst.

Cycle Number	Conversion / %	Mass of Catalyst / mg
1	97.89	4.72
2	90.59	3.53
3	86.27	2.59
4	89.18	1.91
5	80.93	1.55

Table 3.5. Percentage conversion of product for five Suzuki cycles and the mass of catalyst used at the start of the reaction.

The TEM images post reaction (Figure 3.11. (a-e)) showed some large agglomerates of Pd on the outside of the GNF and some singular particles still supported by the step edges. A mean NP diameter of 6.5 nm was determined and maintained a relatively uniform size (Figure 3.11. (f)), showing minimal increase in size, compared to previous catalysts. The SD was 3.17 nm, showing minimal difference in particle size variation between pre- and post-reaction.

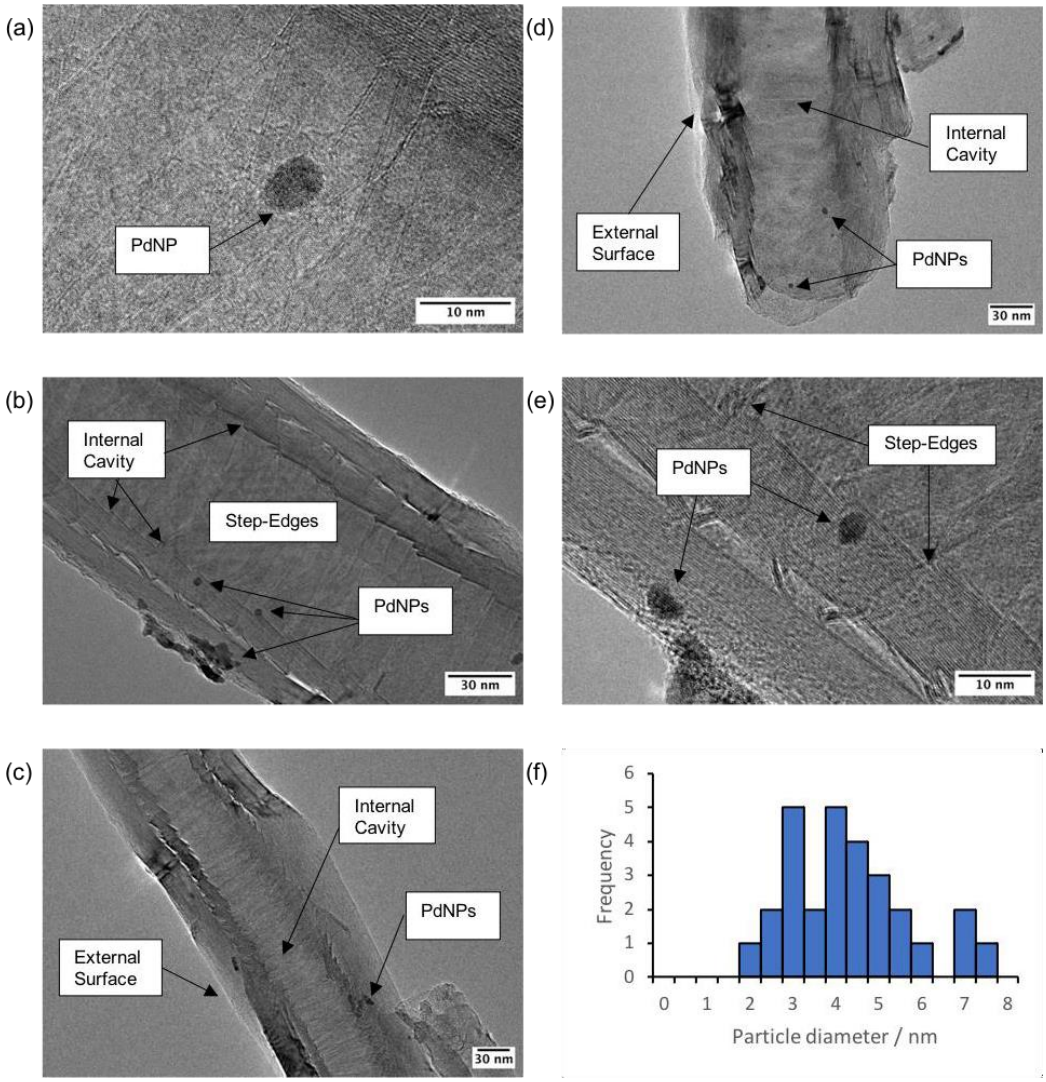

Figure 3.11. TEM images and particle diameter distribution histogram of PdNPs@GNF-4 after Suzuki reactions with (a) a NP encapsulated inside the GNF, (b) NPs settled on step-edges with a larger agglomerate on external surface, (c) large field of view of GNF, (d) end of GNF with some particles encapsulated, (e) NP on step-edge, (f) particle diameter distribution histogram showing the formation of some larger particles and a mean diameter of 6.5 nm.

To ensure the repeatability of these results, a repeat of the synthesis of the catalyst and five cycles of Suzuki were conducted, which presented very similar results, producing a conversion of 95% on the first cycle and 87% on the 5th cycle (Table 3.6.) (See Appendix G).

Cycle Number	Conversion / %	Mass of Catalyst / mg
1	95.34	5.00
2	85.48	4.36
3	88.24	3.89
4	90.51	3.15
5	87.31	2.58

Table 3.6. Percentage conversion of product for five Suzuki cycles and the mass of catalyst used at the start of the reaction.

Although the catalyst was very active, presumably due to the very active Pd NPs on the step edges, agglomeration still appeared to be a prominent issue, so the next steps were to try and reduce this effect in order to reduce the Pd that was being wasted and improve recyclability. These results demonstrate that a hydrogenation step is vital in ensuring that PdNPs@GNF is an active catalyst for Suzuki couplings.

3.5.3. Magnetron Sputtering with hydrogenation to make PdNPs/GNF-5

Using magnetron sputtering for the synthesis of heterogeneous catalysts has the potential to be a very successful methodology, with its ability to provide an even distribution and particle size control of metallic NPs and greener methodology. However, thus far the results in this report for PdNPs sputtered on GNF and then used as a catalyst for the Suzuki cross coupling reaction has not yet shown this to be very active or recyclable. The approach was then combined the newly implemented hydrogenation step to uncover whether it could achieve the same or even better activity and recyclability whilst simultaneously presenting less evidence of agglomeration than PdNPs@GNF-4. Once synthesised, TEM images of the catalyst (Figure 3.12. (a-e)) were taken. The images revealed a small number of NPs but most of these were sitting in step-edges. This confirms that hydrogenation encourages the PdNPs to attach to step edges as NPs were only present on the outside surface before hydrogenation. Some small clusters of NPs had formed in the internal cavity of the GNF but this appeared to be minimal. The particle distribution histogram demonstrated a little variation in size but with most particles smaller than 6 nm with a mean size of 3.6 nm (Figure 3.12. (f)) and SD of 1.4 nm, very similar to PdNPs/GNF-3 which was also sputtered but not hydrogenated.

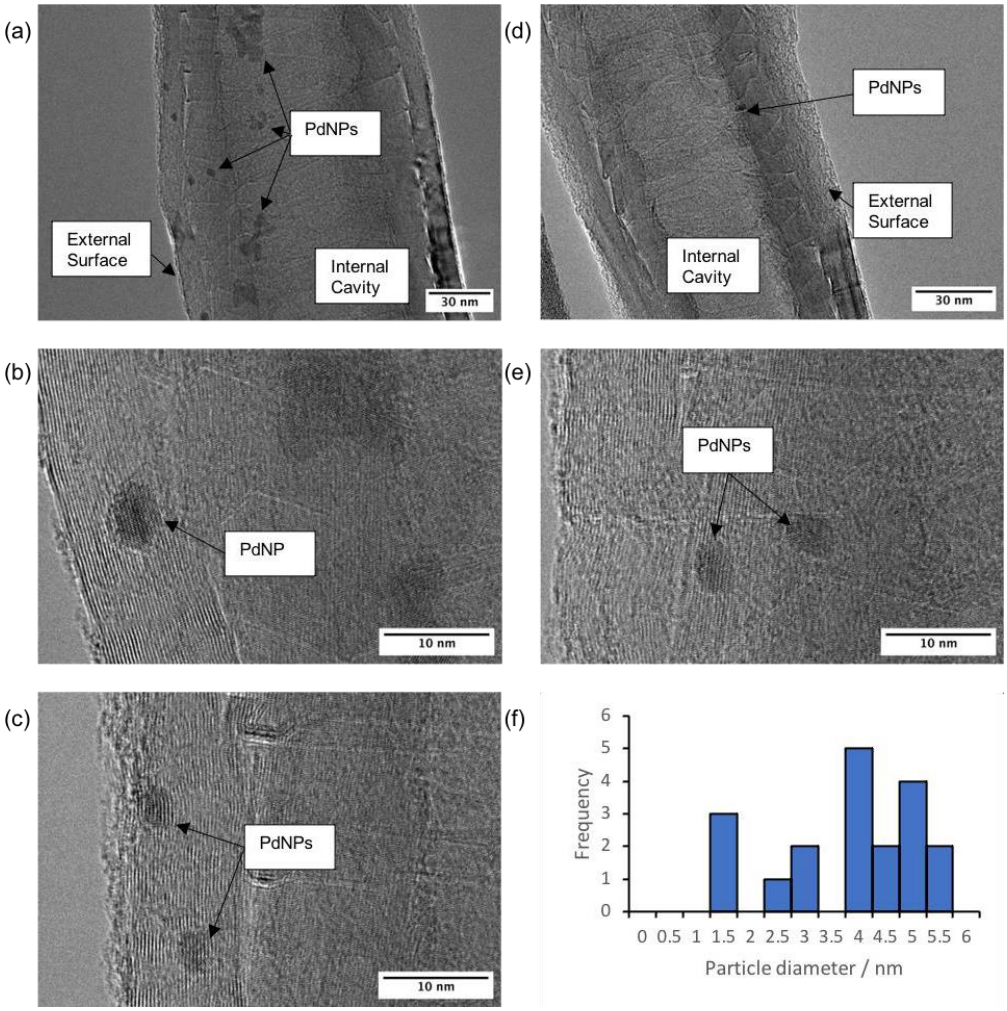

Figure 3.12. TEM images and particle diameter distribution histogram of PdNPs/GNF-5 before Suzuki reactions with (a) PdNPs on step-edges and some larger clusters of particles present, (b, c, e) magnified image of individual particles, (d) GNF with only one particle shown on step-edge, (f) particle diameter distribution histogram showing the formation of some larger particles and a mean diameter of 3.6 nm.

3.5.3. Suzuki cross coupling using PdNPs/GNF-5

The PdNPs/GNF-5 catalyst was used in five cycles of the Suzuki reaction. On the first cycle an excellent conversion of 97%, the same as PdNPs@GNF-4, was obtained and the activity was maintained until the 5th cycle which had a conversion of 95% (Table 3.7.) (See Appendix H). This exceeded the recyclability of all other catalysts used so far, showing how this combination of techniques produces a very active recyclable catalyst. The decrease in conversion between cycle 1 and cycle 5 was a very small 2%, suggesting that when extrapolating the data, this has the potential to hold up approximately 92.5 % conversion at 10 cycles.

These incredibly exciting results really display the advantageous effect of both magnetron sputtering and hydrogenation techniques in this kind of catalysis. TGA gave a weight loading of 14.2% which was significantly higher than the other results so far, as this appeared to be too high compared to the other results suggesting the presence of other metals (See Appendix M-4). Energy dispersive analysis (EDX) was used to determine elemental composition metal loading and showed the presence of some silicon, copper and titanium dioxide which could be responsible for some of the excess weight. It is assumed these have come from some cross contamination in the hydrogenation step as these impurities only appeared in the hydrogenated samples. ICP-OES was not able to be conducted to give a more precise value due to lack of material so the only way to obtain a metal loading was to use EDX (Appendix N-1, N-2 and N-3). Although this is not considered the most accurate way to determine metal loading this was used to gain an approximation. Using this technique, a *ca.* 0.74 % loading was measured which better aligned with the results obtained by the previous catalysts and the TEM images which showed very few particles. From this value a TON of 2025.7and TOF of 84.4 h^{-1} were calculated, the highest values calculated so far.

Cycle Number	Conversion / %	Mass of Catalyst / mg
1	96.59	5.00
2	97.29	3.35
3	94.16	2.96
4	95.49	2.50
5	94.57	2.04

Table 3.7. Percentage conversion of product for five Suzuki cycles using PdNPs/GNF-5 and the mass of catalyst used at the start of the reaction.

TEM images post reactions (Figure 3.13. (a-d)) showed similar results to the pre reaction images, suggesting that the catalyst structure had not changed significantly after the Suzuki reactions, this is very promising for recyclability purposes. No large clusters of NPs appeared to be present, showing fewer signs of agglomeration, an improvement on previous catalysts. However, a mean particle diameter of 7.4 nm was obtained, which is a significant increase on the pre reaction diameter, and the last post reaction particle size obtained by any catalyst thus far which could have an impact on activity with further cycles. Unfortunately, not enough particles were present in the images to obtain a particle distribution histogram.

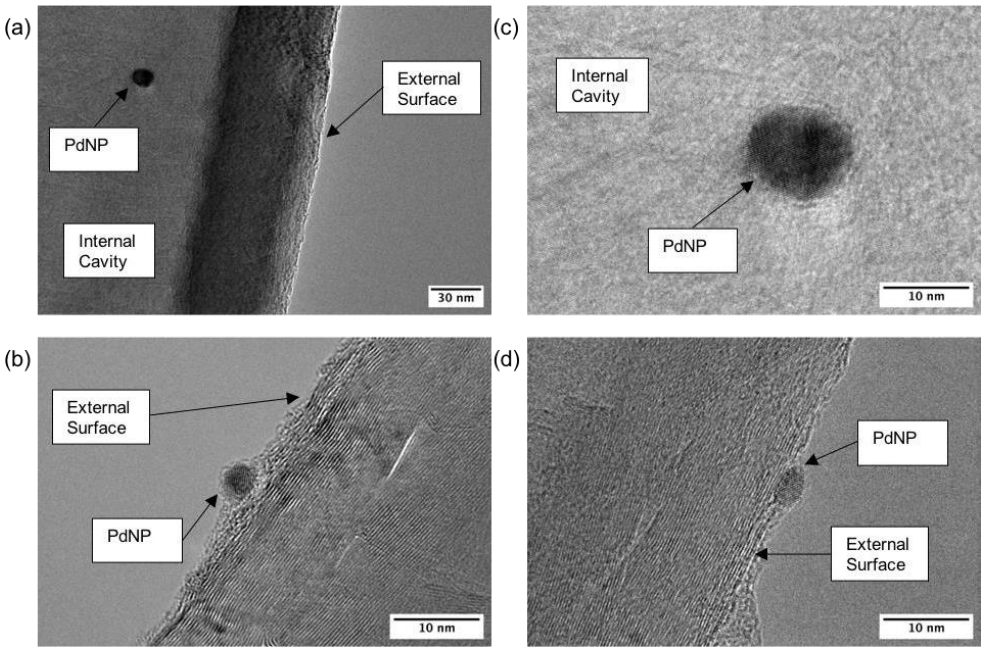

Figure 3.13. TEM images singular PdNPs on PdNPs/GNF-5 after five Suzuki reactions with (a, c) a NP encapsulated inside GNF, (b, d) NP on external surface of GNF.

Although this catalyst showed a lot of promise, a repeat of this experiment in another environment would need to be applied to either identify the source of the contaminant metals and to confirm whether these are effecting the result. However, there is no reports in the literature of a titanium oxide catalyst having an effect on the Suzuki reaction and it is described as inert and non-toxic.[82] It has only been used previously as a support for PdNPs or as a photocatalyst, requiring very specific conditions, in order to improve catalytic activity.[83],[84] Additionally, it is unlikely that the presence of the copper on the GNF had any effect on catalytic activity, as copper based catalysts are rarely known to perform aryl–heteroaryl and heteroaryl–heteroaryl couplings.[85] In addition, Cu-catalysed aryl–aryl couplings generally have low catalytic turnovers, requiring high loadings of catalysts and ligands.[86] An investigation was conducted into the source of these materials, but it was confirmed that these were not present in the sputtering chamber, therefore it was most properly a lab error causing contamination. The first hydrogenated catalyst tested (PdNPs@GNF- 4) did not show any signs of unwanted materials and still obtained excellent conversion suggesting that the results for this catalyst were not affected by the containments. A repeat of this experiment in future work may confirm these theories and if these metals are still present, determine the source of this excess metal, so this is something to consider.

3.5.4. Synthesis of Fe@C_n/PdNPs@GNF-2 with hydrogenation step

After discovering the effectiveness of the hydrogenation step in stabilising the catalyst, the next approach was to combine this step to the magnetic catalyst. First Fe@C_n/PdNPs@GNF-2 was synthesised using the same method used to synthesise Fe@C_n/PdNPs@GNF-1 and then hydrogenated before being run

through five cycles of the Suzuki cross coupling reaction. This was predicted to combine the stabilising effects of the hydrogenation with the simplicity and efficiency of physical recovery of the catalyst by removing the need for centrifugation and recovering a greater amount catalyst for the next cycle.

The TEM images before the reaction (Figure 3.14. (a-e)) showed clearly the presence of Fe@C_n NPs both on the external surface and internal cavity of GNF. The PdNPs appeared to vary in size considerably (Figure 3.14. (f)) with a SD of 2.14 nm. The distribution of the particles was very uneven but most of the particles were encapsulated. The measurements of particle diameter provided an average of 4.2 nm, which was higher than all catalysts so far except for PdNPs@GNF-4.

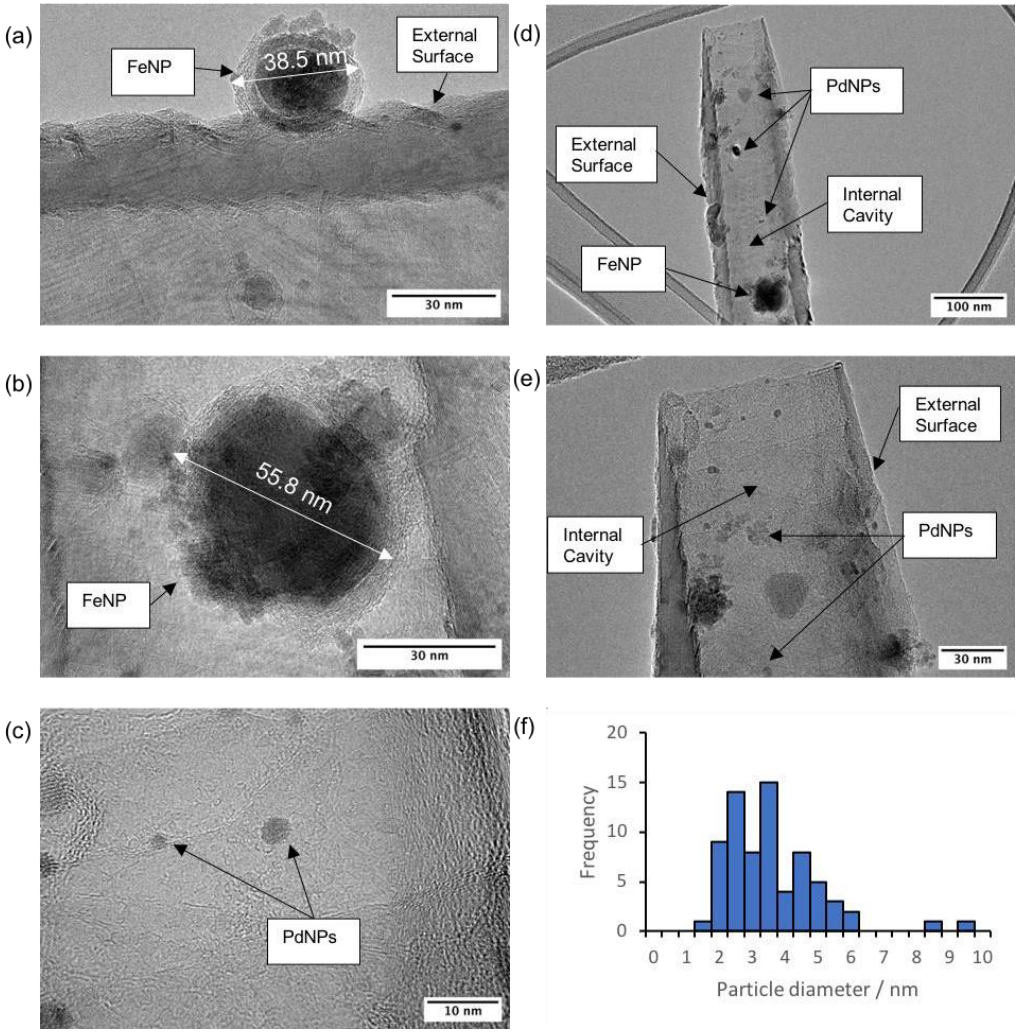

Figure 3.14. TEM images of singular PdNPs on Fe@C_n/PdNPs@GNF-2 before Suzuki reactions with (a) an FeNP on external surface of GNF with diameter 38.5 nm, (b) FeNP encapsulated in internal cavity of GNF with diameter 55.8 nm, (c) PdNPs encapsulated inside GNF, (d) larger field of view showing distribution of PdNPs and an encapsulated FeNPs, (e) PdNPs at end of GNF, (f) particle diameter distribution histogram showing the formation of some larger particles, a not very uniform size of particle and a mean diameter of 4.2 nm.

3.5.5. Suzuki cross coupling using Fe@C_n/PdNPs@GNF-2

Five consecutive Suzuki reactions were performed using Fe@C_n/PdNPs@GNF-2 obtained very good conversion results. The first cycle obtained a 90% conversion which stayed almost constant as the last cycle obtained a 91% conversion, showing this catalyst to be very recyclable (Table 3.8.) (See Appendix J). Despite this, the conversion results are overall lower than the other hydrogenated catalysts thus far. As TGA and ICP-OES were not able to be used for metal loading an approximation was obtained by EDX (See Appendix N-4) which revealed a metal loading of 0.41 %, providing a very good TON of 3992 and a TOF of 166 h^{-1}. Both values the highest observed so far.

Cycle Number	Conversion / %	Mass of Catalyst / mg
1	90.44	5.00
2	92.82	3.67
3	89.59	3.10
4	86.37	2.69
5	91.13	2.10

Table 3.8. Percentage conversion of product for five Suzuki cycles using Fe@C_n/PdNPs@GNF-2 and the mass of catalyst used at the start of the reaction.

TEM images taken after the reactions (Figure 3.15.) revealed the presence of FeNPs both encapsulated inside the GNF and on the external surface. There were not many individual PdNPs present in the images, but some larger clusters of particles were common, this made it very challenging accurate identify Pd particles to gauge a mean particle diameter or distribution, so this data was not collected.

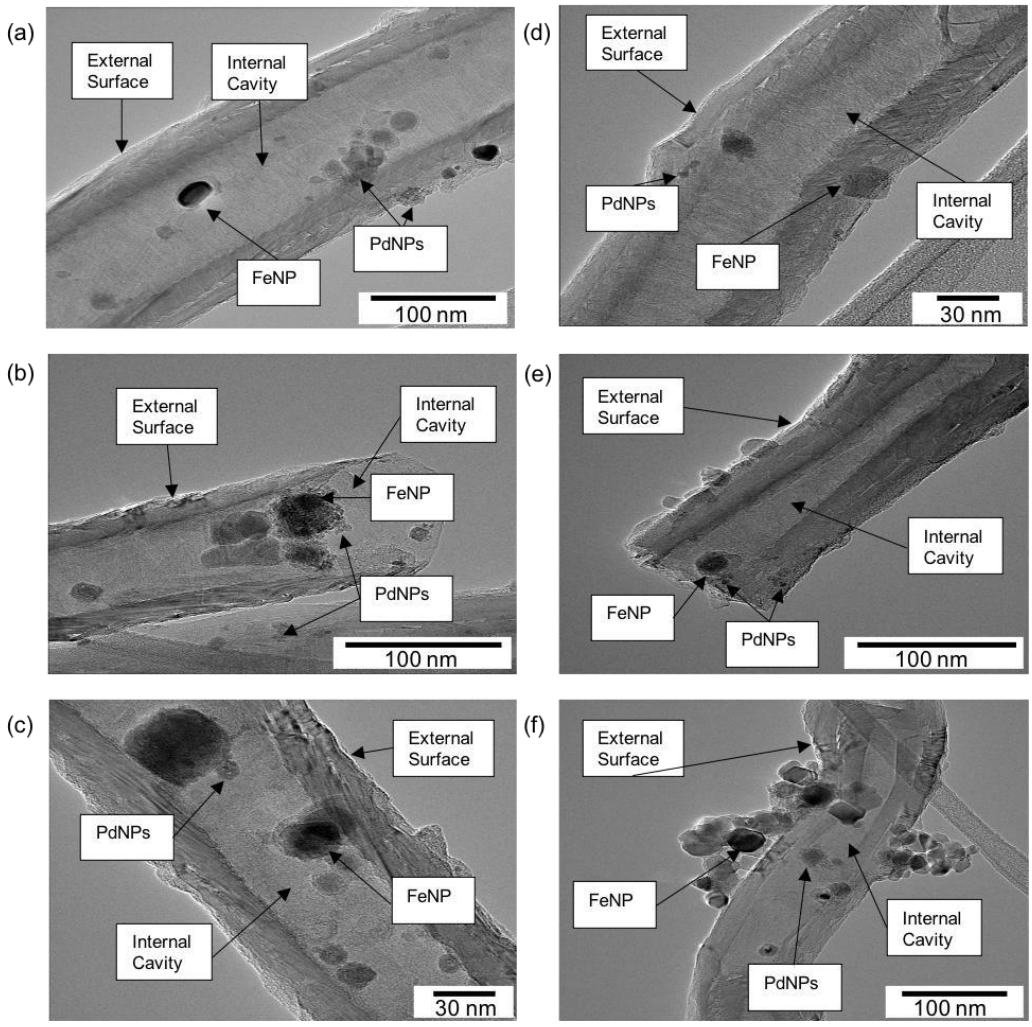

Figure 3.15. TEM images and particle diameter distribution histogram of Fe@C_n/PdNPs@GNF-2 after five Suzuki reactions with (a, b, c) showing large Pd and Fe NPs and clusters encapsulated inside the GNF, (d, e) NPs settled on both internal and external surfaces, (f) large clusters of Fe and Pd NPs mostly on external surface of GNF.

3.6. Vapour deposition of PdNPs onto GNF via $Pd(acac)_2$ precursor

The vapour deposition Pd(II)bis(acetylacetonate) ($Pd(acac)_2$) to form PdNPs onto supports has previously been investigated[53] and so this technique was use to try and encourage the PdNPs to encapsulate inside the GNF. As the step edges are thought to have a positive effect on the stability of the NPs, it was theorised that encouraging the NPs to encapsulate inside the GNF, where the step edges are located, may increase the stability of the catalyst and decrease migration. Once synthesised, this catalyst was treated under the same hydrogenation conditions as before.

The TEM images taken prior to the Suzuki reactions (Figure 3.16. (a-e)) revealed that the encapsulation on the inside of the GNF had worked very well

and there was a large proportion of PdNPs present inside the internal cavity on the step edges of the GNF. It appeared to be the highest fraction of encapsulated particles and the largest mean diameter and SD of NP size (7.59 nm and 4.12 nm respectively, Figure (3.16.(f))) compared to every other catalyst.

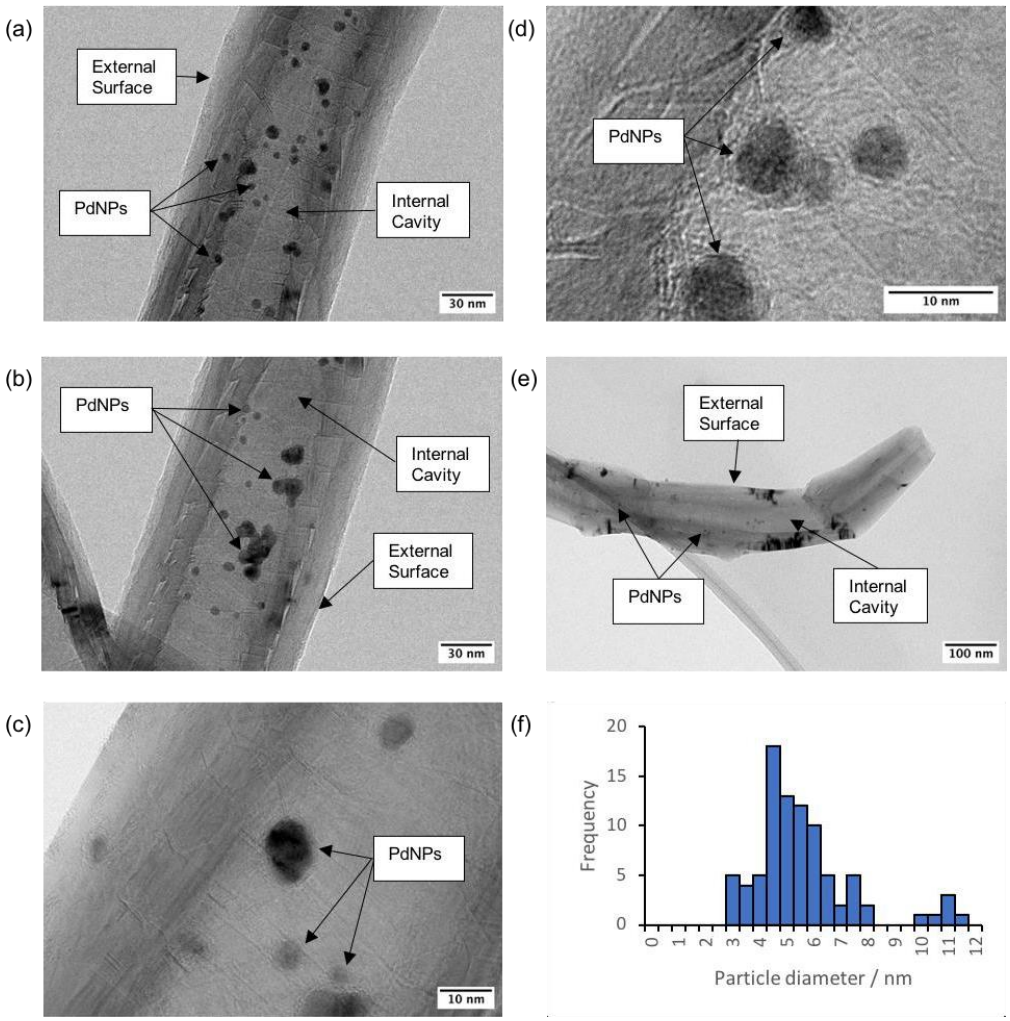

Figure 3.16. TEM images and particle distribution histogram of PdNPs@GNF-6 showing (a, b) Many PdNPs encapsulated inside GNF, (c, d) magnified images of PdNPs supported on step-edgs in the internal cavity, (e) a large field of view displaying a larger proportion of PdNPs on the external surface of GNF, (f) particle diameter distribution of PdNPs showing a wide spread of size and a mean particle diameter of 7.59 nm.

3.6.1. Suzuki cross coupling using PdNPs@GNF-6

Five Suzuki reactions were performed which revealed some very interesting results (Table 3.9.). The conversions obtained for this catalyst were generally the lowest of all the hydrogenated catalysts, particularly for the first cycle which only achieved a conversion of 54% (See Appendix I). Interestingly, the conversion showed an increasing trend with a large difference (~28%) between the results of the 2nd and 3rd cycle. TGA gave an overall 21% loading

(See Appendix M-5) which once again was a lot higher than the previous results and EDX provided a 1% loading of PdNPs (See Appendix N-7)
Pd which was used to calculate a TON of 1813.4 and TOF of 75.6 for the first cycle. These values are quite high compared to other catalysts but not as high as PdNPs@GNF-5.

Cycle Number	Conversion / %	Mass of Catalyst / mg
1	54.31	5.00
2	62.43	4.59
3	89.89	3.85
4	86.65	3.36
5	84.27	2.90

Table 3.9. Percentage conversion of product for five Suzuki cycles using PdNPs@GNF-6 and the mass of catalyst used at the start of the reaction.

The good distribution of PdNPs present in the TEM images contradict the poor conversion result for the first and second cycle. Initially it was hypothesised that the decomposition of the acac ligand had produced groups that were interfering with the catalytic activity. TGA was performed to on $Pd(acac)_2$ which showed many by products so this could be a factor in explaining this result. Additionally, the TEM images revealed that carbon shells had formed around the palladium, reducing the surface area of the active sites, which would most likely the main cause of this significant reduction in activity.

TEM images taken after the reaction (Figure 3.17. (a-e)) visually showed little change to the catalyst from before the cycles and this was further supported by the mean particle diameter of 6.7 nm and SD of 4.38 nm (Figure 3.17. (f)) which was very close to the mean and distribution of particle size before the reactions. Some evidence of agglomeration was present as there were some larger clusters of particles however there were still many individual PdNPs encapsulated. The carbon shells can be seen clearly in the images which would probably be responsible for some loss in activity.
Therefore, it can be concluded that vapour deposition from $Pd(acac)_2$ is not the most effective deposition method for the synthesis of PdNPs@GNF.

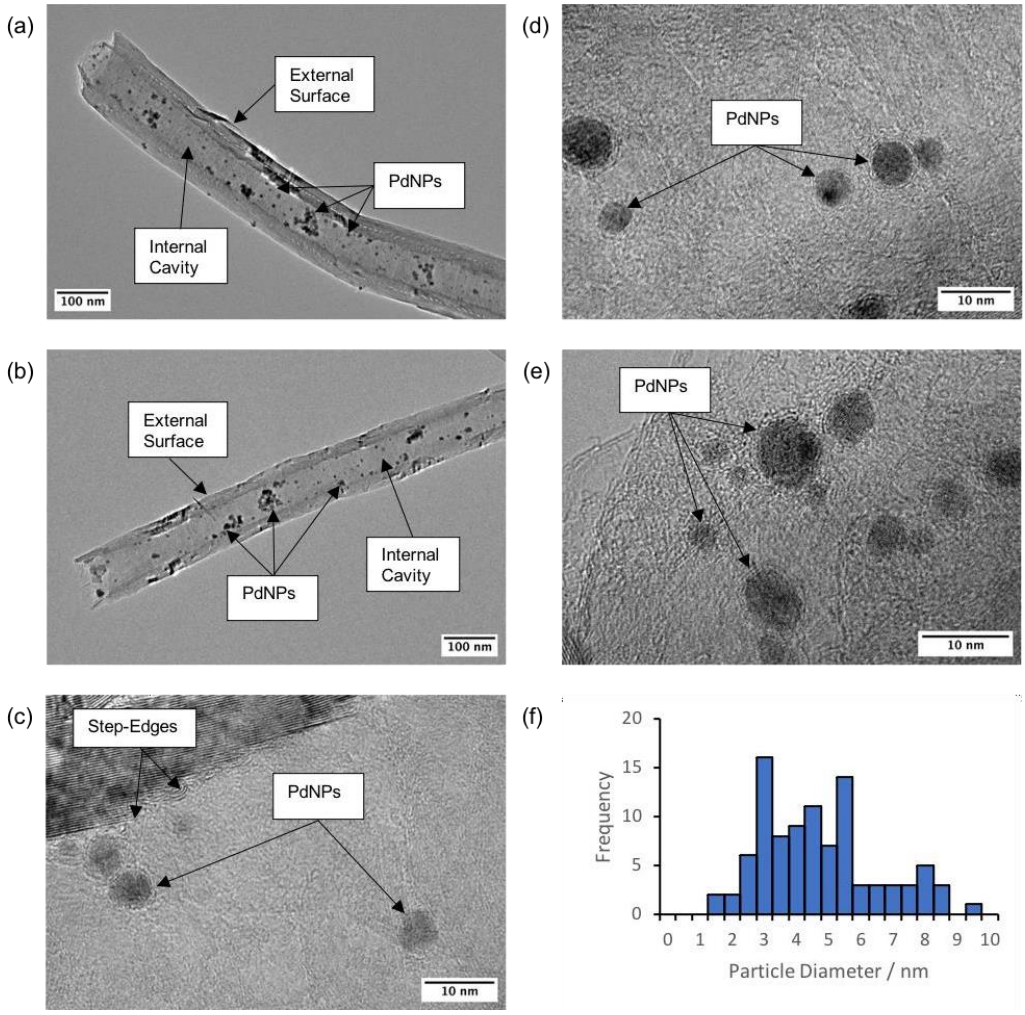

Figure 3.17. TEM images and particle diameter distribution histogram of PdNPs@GNF-6 after five Suzuki reactions showing (a, b) large field of view with most particle encapsulated inside GNF and some larger clusters of NPs, (c, d, e) NPs located inside internal cavity (f) NP diameter distribution histogram showing wide spread of particle size with average diameter 6.7 nm.

3.7. Development of hydrogenated magnetron sputtered PdNPs/GNF-5

3.7.1 Synthesis of PdNPs/GNF-7 from magnetron sputtering using PR24 GNF

The high activity of the magnetron sputtered PdNPs/GNF-5 after hydrogenation presented exciting opportunities for further development, as this process deposits the nanoparticles on the outside of the GNF and step edges are typically the anchoring sites, it was predicted that using PR24 GNF instead of PR19 would further improve the stability and activity of this catalyst. PR24 GNF possess step edges on both the external surface as well as inside the

internal cavity. Securing the NPs on the external surface more effectively could further reduce agglomeration of particles by being able to anchor more of them onto the support, thus improving recyclability between cycles.

TEM images taken after synthesis (Figure 3.18. (a-e)) show PdNPs successfully distributed onto GNF with a higher proportion on the external surface than shown by the other catalysts. The PdNPs are fairly evenly distributed and very uniform in size (Figure 3.18. (f)) and have a mean diameter size of 3.6 nm and SD of 1.26 nm.

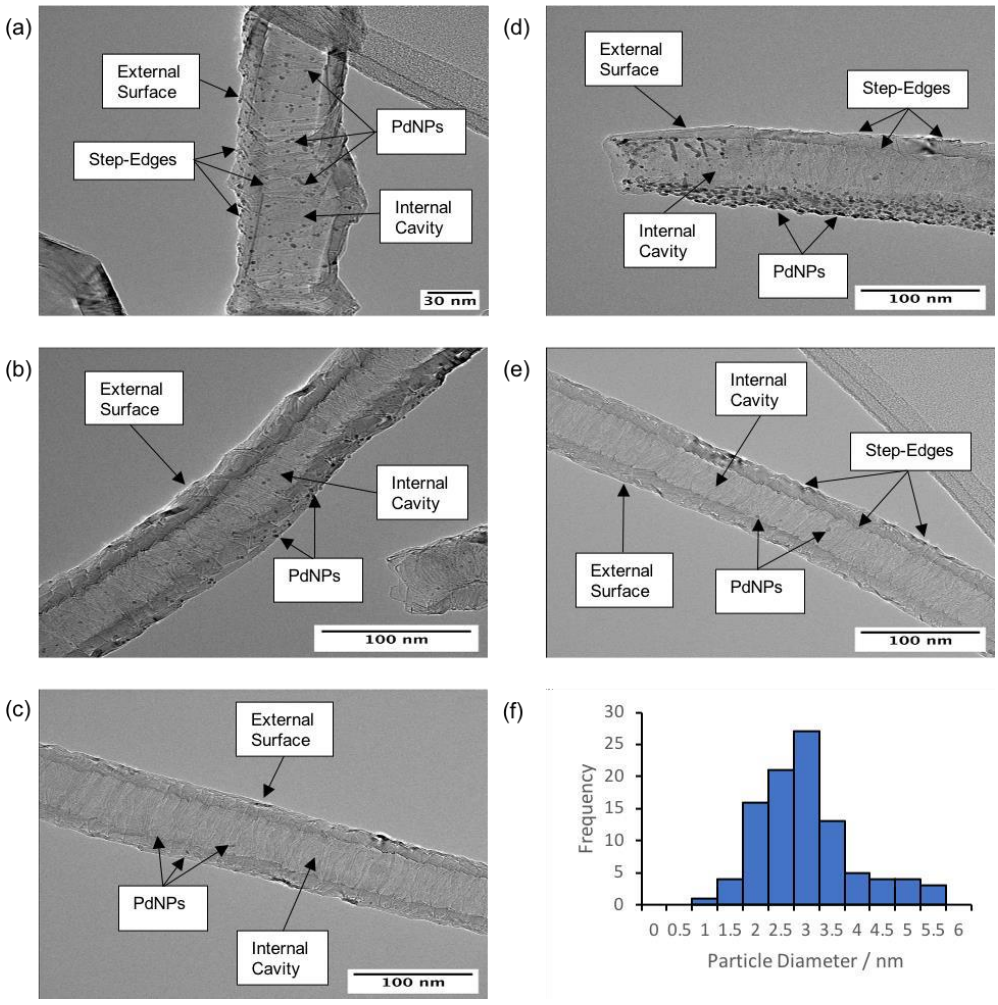

Figure 3.18. TEM images and particle diameter distribution histogram of PdNPs/GNF-7 before Suzuki reactions showing (a) large proportion of PdNPs encapsulated inside GNF, (b, c, e) large field of view with smaller number of NPs present and distributed both on the external surface and internal cavity, (d) large proportion of PdNPs on the external surface of GNF on step-edges, (f) NP diameter distribution histogram showing very consistent sizes with average diameter 3.6 nm.

3.7.2. Suzuki cross coupling using PdNPs/GNF-7

Five cycles of the Suzuki cross coupling were performed with PdNPs/GNF-7. The conversion results were outstanding again and achieved a 97% conversion on the first cycle which only dropped by ~5% by cycle five (Table 3.10.)(See Appendix K). Showing very similar results to the PdNPs/GNF-5 catalyst which was sputtered PR19 however this catalyst maintained higher conversions up to cycle 5 showing better potential for recyclability. TGA provided a 29% loading (See Appendix M-6) which was a lot higher than expected again so EDX was used to determine elemental composition which revealed the presence of some titanium dioxide contaminant. EDX was used to provide an estimation Pd loading of ~4.9% (See Appendix N-5 and N-6), In order to calculate approximate values of TON of 304.5 and TOF of 12.7, which were low compared to the other hydrogenated catalysts.

Cycle Number	Conversion (%)	Mass of catalyst used / mg
1	96.63	5.00
2	95.20	4.30
3	91.50	3.78
4	92.07	3.15
5	92.40	2.78

Table 3.10. Percentage conversion of product for five Suzuki cycles using PdNPs/GNF-7 and the mass of catalyst used at the start of the reaction.

TEM images (Figure 3.19. (a-e)) after the reaction presented very surprising results. The NPs present were considerably larger and differently shaped than any of the PdNPs shown so far. The d-spacing measurements of some particles were taken that gave a 0.35 nm spacing which is the same as the (101) plane of TiO_2 confirming its presence. The PdNPs that were present were also significantly larger, suggesting agglomeration and a mean particle diameter 27.3 nm was calculated (Figure 3.19. (f)) and a very large SD of 13.1 nm.

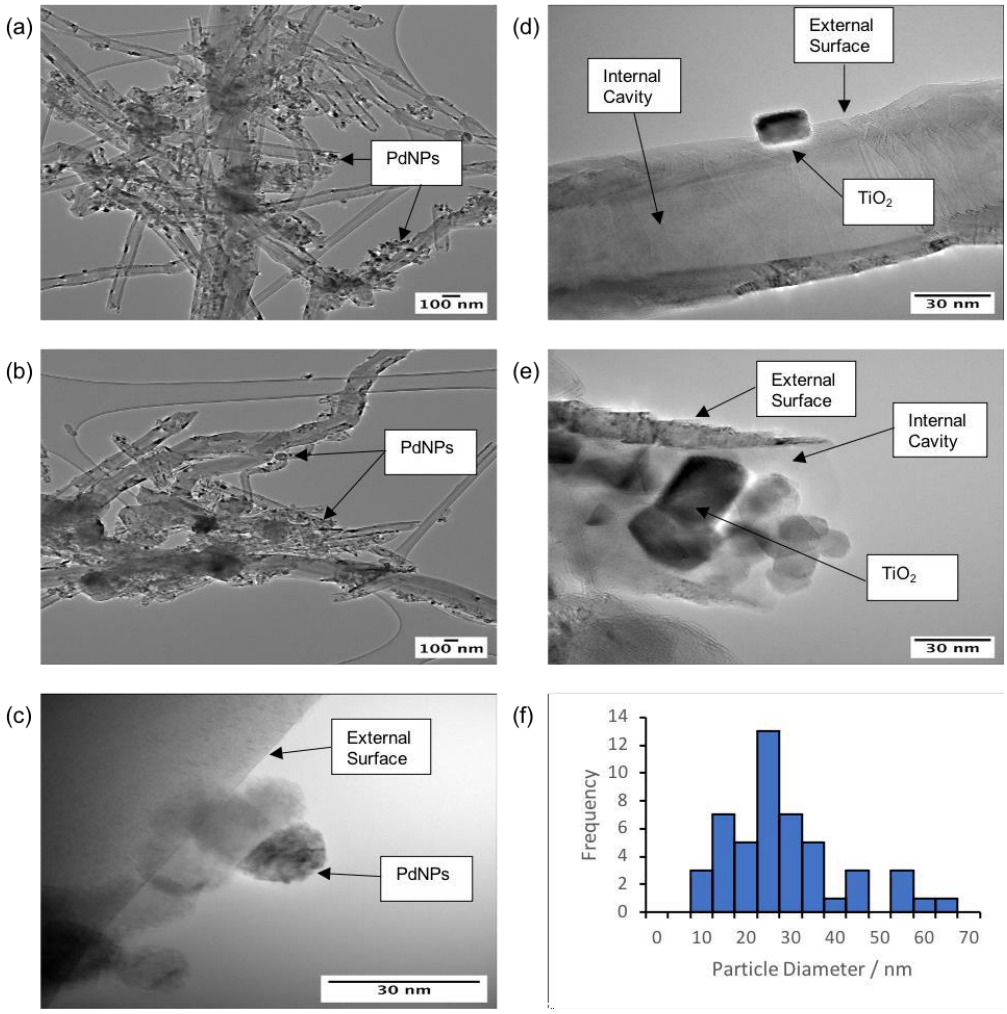

Figure 3.19. TEM images taken after five cycles of Suzuki cross coupling with (a, b) large field of view showing distribution of large PdNPs inside internal cavity and on external surface, (c) small cluster of PdNPs, (d) large oblong particle on external surface of GNF identified as Pd through d-spacing measurements, (e) large cluster of PdNPs at end of GNF inside internal cavity, (f) particle distribution histogram showing a wide variety of sizes and considerably larger particles with average diameter of 27.3 nm.

3.7.3. Synthesis of defected PdNPs/GNF-8 with hydrogenation step

Depositing PdNPs onto GNF has been shown to be most effective when performed using magnetron sputtering and then hydrogenating the product. It has been attempted to use PR24 to try to reduce agglomeration by allowing more anchoring points however larger PdNPs formed and its recyclability was not as good as the PR19. Therefore, a different approach was taken which was to use chromium acetylacetonate ($Cr(acac)_3$) to etch holes in the GNF were the

NPs could be supported on to reduce their migration. The resultant material was then washed with concentrated nitric acid to remove the chromium, sputtered with Pd and then hydrogenated as before. TGA and powder X-ray diffraction (PXRD) were both utilised to monitor the presence of chromium. Three washes were conducted until TGA indicated clean GNF (See Appendix M-7).

TEM images were taken after synthesis (Figure 3.20.) and unfortunately showed the presence of some chromium oxide still on the GNF. As three washes were attempted and did not work, this method will need some further development. A particle diameter measurement was not conducted due to the small number of PdNPs present in the image.

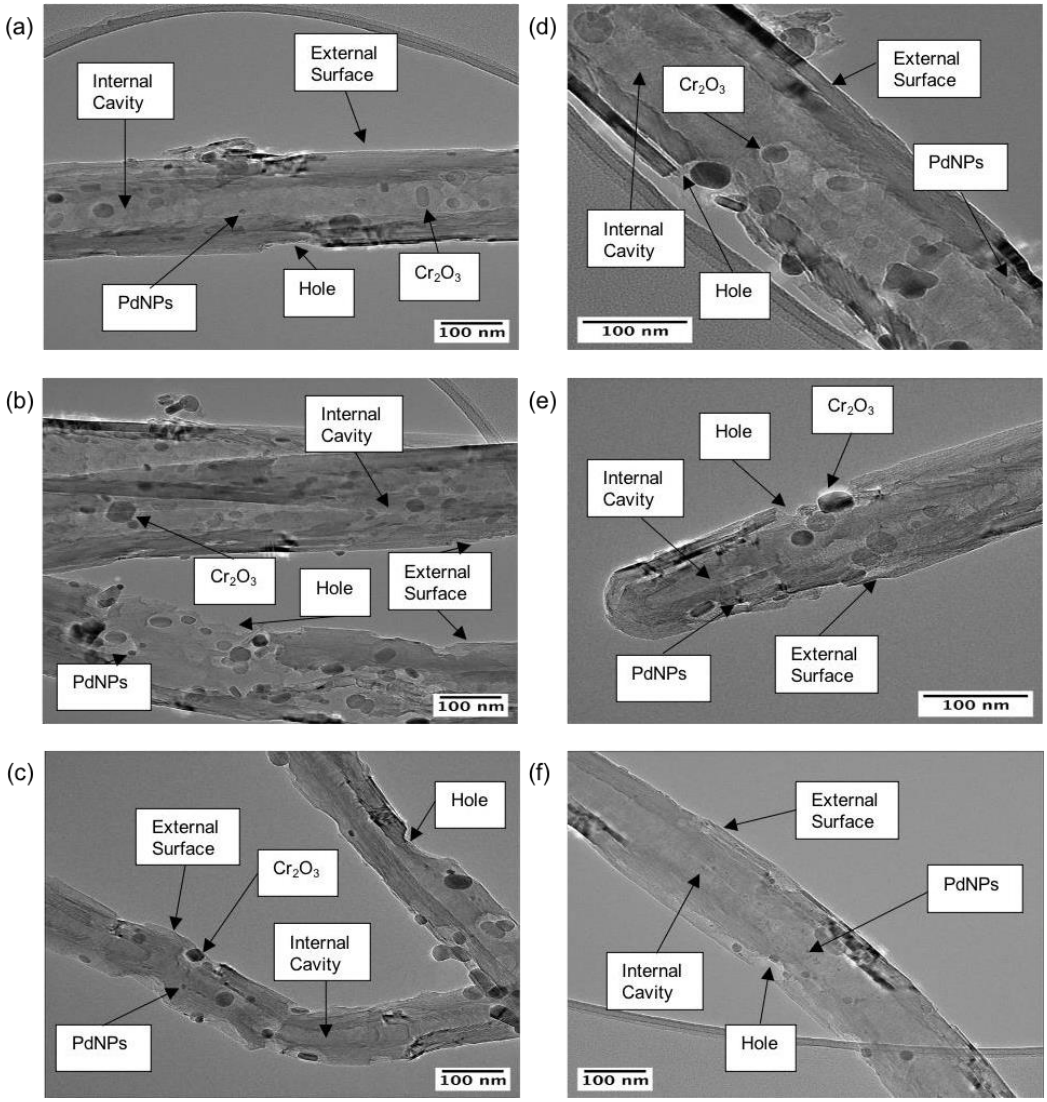

Figure 3.20. TEM images taken of PdNPs/GNF-8 prior to Suzuki reactions where all images show the distribution of both PdNPs and Cr_2O_3 in the internal cavity and on the external surfaces of the GNF in addition to the clear presence of defects on the external surface.

3.7.4. Suzuki cross coupling with PdNPs/GNF-8

Three Suzuki cycles were still attempted and achieved very good conversion results of 92 % on both the first and last cycle, displaying excellent recyclability (Table 3.11.) (See Appendix L). Showing very similar results to $Fe@C_n$/PdNPs@GNF-2. However due to the presence of unwanted chromium it cannot be definitively stated that this result was the Palladium acting alone as a catalyst. This catalyst also did not show any improvement on the conversion achieved by the original magnetron sputtered PdNPs/GNF-5 so further development would be required. TON and TOF could not be calculated as an accurate average particle size could not be determined or an accurate Pd loading.

Cycle Number	Conversion / %	Mass of Catalyst
1	91.47	5.00
2	86.76	4.65
3	91.52	4.30

Table 3.11. Percentage conversion of product for three Suzuki cycles using PdNPs/GNF-8 and the mass of catalyst used at the start of the reaction.

TEM images that were taken after the reaction (Figure 3.21.) show the presence of defects that were created in the GNF with PdNPs clearly positioned at these points. This demonstrates the potential this approach has to secure PdNPs onto GNF and with further development could create a very effective catalyst. The presence of chromium was also indicated by EDX (See Appendix N-8) and not enough particles were present to determine a particle distribution histogram.

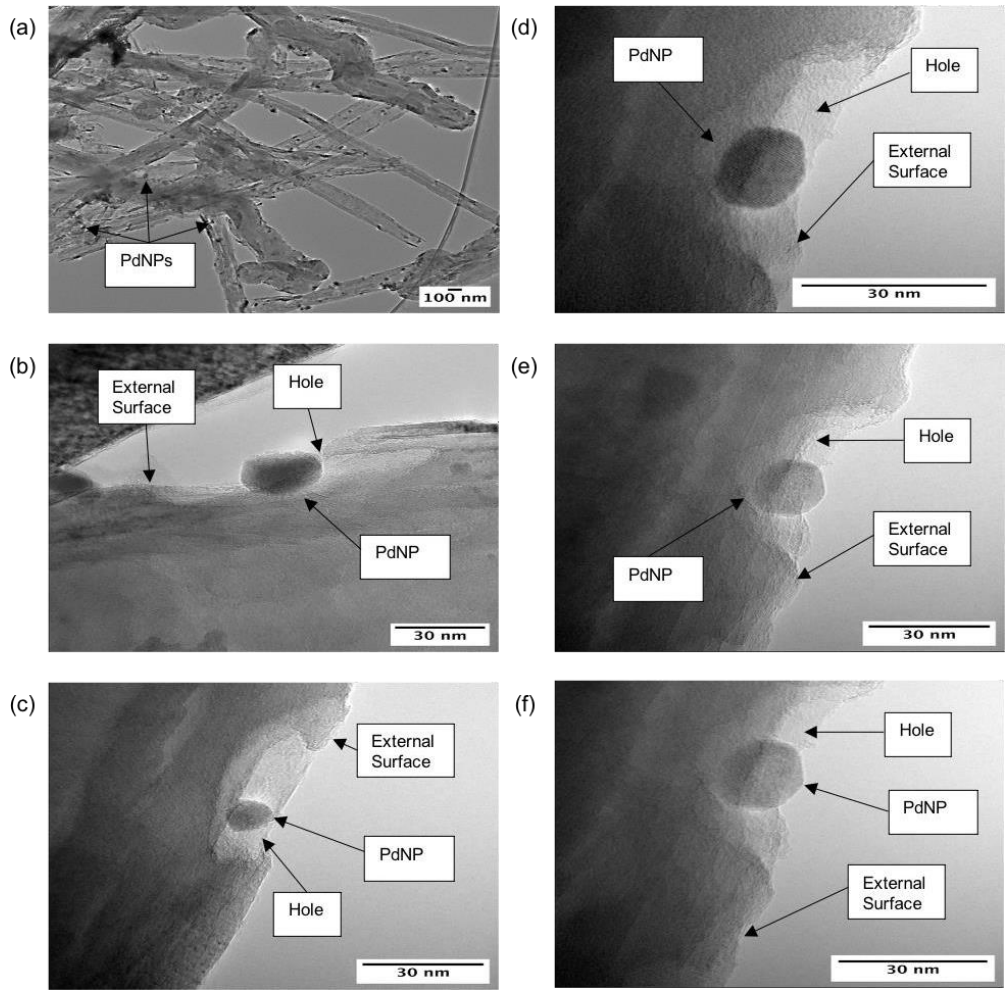

Figure 3.21. TEM images taken after three Suzuki cycles of PdNPs/GNF-8 with a) large field of view showing distribution of PdNPs and Cr_2O_3 on GNF, (b-f) individual PdNP supported in a hole on external surface of GNF.

3.8. Comparison of catalysts

Overall, ten different catalysts have been synthesised using five different methods of deposition (Figure 3.22.) and the use of magnetic nanoparticles has also been tested. When comparing the performance of all the catalysts presented in this work overall PdNPs/GNF-5 (magnetron sputtered, hydrogenated) and Fe@C_n/PdNPs@GNF-2 were the best catalysts and showed the most potential for further development. The product conversions recyclability for PdNPs@GNF-5 were the highest out of all catalysts shown (Table 3.12.) and the TON and TOF were the highest for Fe@C_n/PdNPs@GNF-2 whist also showing very high activity and excellent recyclability. This shows the exciting potential and abilities of both magnetron sputtering as a deposition method and the use of magnetic nanoparticles as an extraction method. It is also clear that the catalysts that have undergone hydrogenation as part of their synthesis generally performed a lot better than those that weren't, displaying the importance of adding this step. The changing in structure of the GNF step edges under these conditions (Figure 3.22) creates flat graphene layers where the PdNPs are able to form stronger bonds with the hydrogenated carbon and are therefore more secure in these positions. This

may reduce migration of the particles and in turn deactivation which explains why hydrogenation increases the recyclability of the catalysts. In addition, more active sites on the Pd are available in this structure, explaining the high activity. In both the hydrogenated and non-hydrogenated cases, the magnetron sputtered catalyst and magnetic catalysts displayed the best performance comparatively. However, three of the hydrogenated materials showed signs of contamination from other metals, although an investigation was conducted, the source of these metals is unknown, some more repeats of these experiments would potentially reveal this. It was assumed this was contamination as it did not appear in all of the hydrogenated catalysts. It was assumed that these contaminants were not the main reason for the fantastic catalyst performance as the catalysts that did not have these contaminants also performed very well. However, this would require further investigation in future work to confirm this.

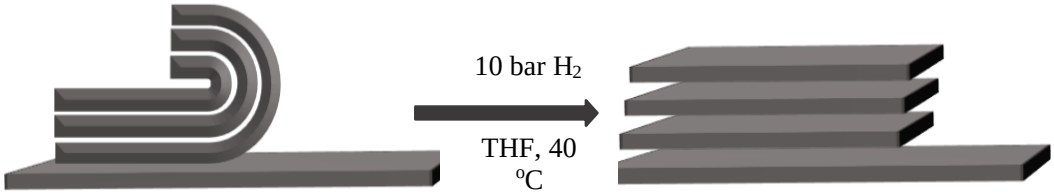

Figure 3.22. Schematic representation of the opening of the graphitic step edges a) shows the rolled step edge before hydrogenation, b) shows the opened step edge after reacting with hydrogen.

Catalyst	TON	TOF / h^{-1}	Conversion achieved 1st cycle / %	Conversion achieved final cycle / %
PdNPs@GNF- 1	99.7	4.1	6.68	0
PdNPs@GNF-2	364.7	15.2	33.08	0
Fe@C_n/PdNPs@GNF-1	991.2	41.3	60.72	0
PdNPs/GNF-3	872.4	36.3	59.97	0
PdNPs@GNF-4	1429.1	59.5	97.89	80.93
PdNPs/GNF-5	2025.7	84.4	96.59	94.57
Fe@C_n/PdNPs@GNF-2	3992.3	155.3	90.44	91.13
PdNPs@GNF-6	1813.4	75.6	54.31	84.27
PdNPs/GNF-7	304.5	12.7	96.63	92.40
PdNPs/GNF-8	-	-	92.40	91.52

Table 3.12. Comparison of all the PdNPs@GNF catalysts' performances measured where activated is determined by TON and TOF and recyclability shown by the different between the conversion of the first cycles and final cycle. The hydrogenated catalysts are shown in blue.

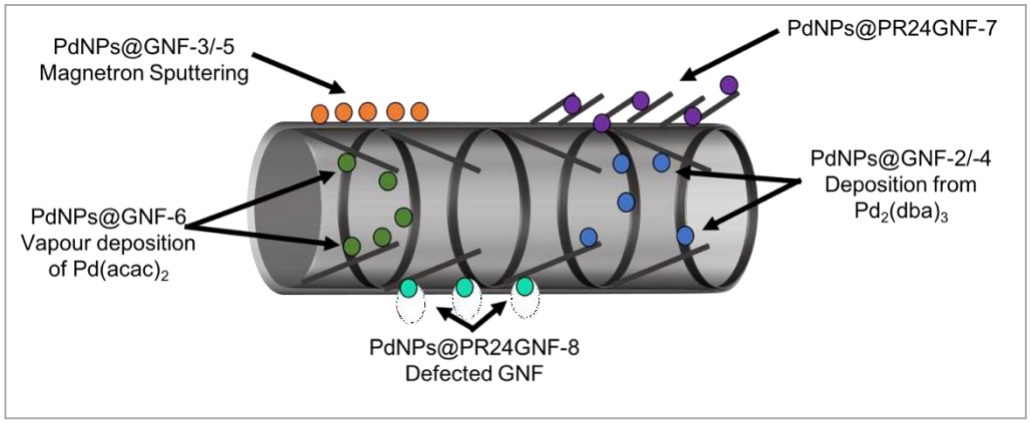

Figure 3.23. Shows the five main deposition methods utilised to synthesise PdNPs@GNF.

4. Conclusion

In conclusion, variations on PdNPs@GNFs have been designed and developed to be active and recyclable catalysts when used in Suzuki cross coupling reactions. Pd is a very expensive and finite resource, so the conservation and reusability of this material is incredibly important, hence this work was focussed on improving this. Out of the ten catalysts synthesised the most effective catalysts producing product conversion of up to 97 % were the ones that had been hydrogenated, proving that this was an essential step in the synthesis. Adding magnetic FeNPs showed some excellent potential in making the catalysts additionally easier to separate from the reaction mixture after each cycle. Additionally, the hydrogenated magnetic catalyst also presented the best quantitative activity and shown excellent recyclability. Most of the catalysts were synthesised using a $Pd_2(dba)_3$ precursor which did not initially prove effective but when a hydrogenation step was added a massive improvement was seen and this ended up being one the most active catalyst in the first cycle. The best performance overall was displayed by the hydrogenated catalyst synthesised via magnetron sputtering, an incredibly exciting result as this is a solventless method that holds many benefits. Not only did it achieve a 97 % conversion on the first cycle but almost completely maintained this to the five cycle. This was attempted to be further developed by using PR24GNF (with step edges on the outside) and creating defects on the GNF to further stabilise the NPs, however these methods were not as effective as theorised but have potential to be with further work. Overall, several very active, recyclable Pd nanocatalyst has been designed and successfully tested using a Suzuki cross coupling reaction.

5. Future work

The research presented in this project has many exciting development opportunities for future work. The most successful catalyst proved to be the hydrogenated magnetron sputtered PdNPs@GNF, which has a lot of potential to be used in future work, however still evidence of agglomeration was presented which could cause problems with recyclability if more cycles were attempted. There are many ways that this work can be further developed some of which are presented here:

1) Repeats of all catalysts that contained additional metals would need to be conducted in future work. Although very active and recyclable, some of the catalysts contained impurities so these methods would need to be repeated to create purer catalysts to determine if these metals are having any effect on the results. Additionally, creating defects on the GNF was attempted, however washing off Chromium oxide did not work so attempting this again with a better washing procedure in the future could be very effective.

2) Adding magnetic FeNPs showed a lot of potential in making the extraction process easier, quicker and more effective in addition to having the TON and TOF so combining the magnetron sputtered PdNPs@GNF-5 with FeNPs could further improve its activity and recyclability which is an area that could be explored.

3) The scope of this newly developed catalyst can be further tested by applying it to more challenging reagents and reactions. This has the potential to be active enough to couple sterically hindered coupling partners or even aryl chlorides and could allow reaction conditions to be a lot milder.

6. Experimental

GNF (PR19 and PR24) were purchased from Pyrograf Products. All other reagents and solvents were purchased from Sigma-Aldrich (UK) and used without further purification. All of the glassware required to perform the experiments was thoroughly cleaned with „aqua regia" (concentrated hydrochloric and nitric acids (3:1)) and rinsed with deionised water prior to use.

6.1. Characterisation Techniques

HRTEM analysis was performed on a JEOL 2100 Field emission gun with an information limit of 0.12 nm at 100 kV. Samples for HRTEM analysis were prepared by dispersing the materials in HPLC grade iso-propanol using ultra-sonication, then drop casting the resultant suspension onto a lacey carbon film coated copper grid.

TGA analysis was performed on a TA Instruments TGA-SDTQ600 analyser. Samples for TGA analyses were heated in air up to 1000°C with a heating rate of 10°C/min.

Pro diffractometer equipped with a Cu K(α) radiation Source (λ=1.5432, 40kV 40mA) in Bragg-Brentano geometry using a Si zero background holder. All samples were wetted with isopropyl alcohol to aid GNF adhesion. The parameters for a typical experiment were: Start angle: 5°, Stop angle: 80°, Step size: 0.0525°, Time/step: 6080s, Scan speed: 0.00220°/s.

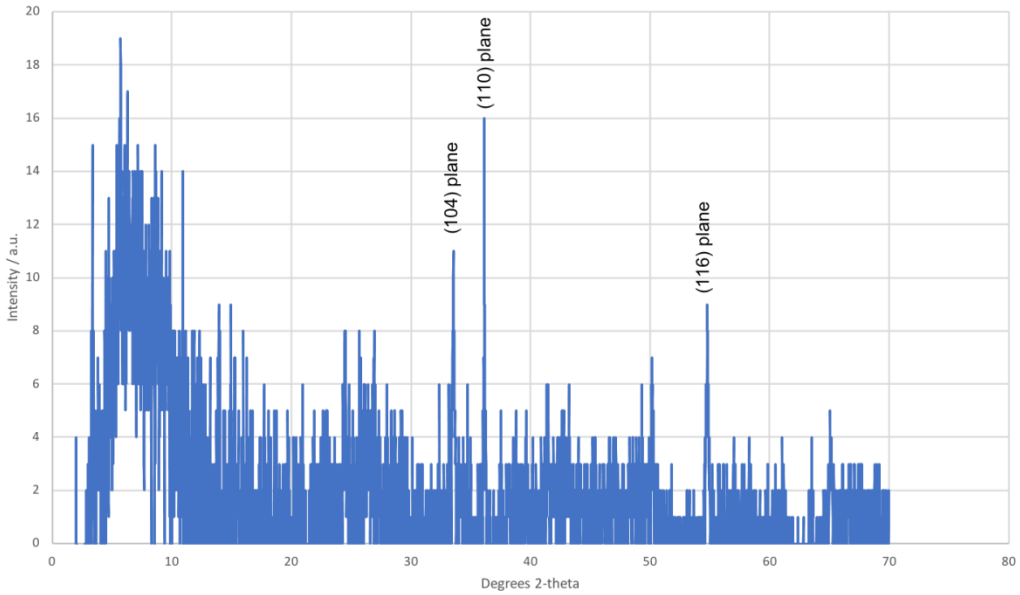

Figure 6.1. XRD pattern of PdNPs@GNF-8 showing presence of Cr_2O_3 from the 3 peaks labelled at ~33.6, ~36.2 and ~54.9 degrees respectively.[87] The spectrum is noisy due to the small amount of sample on the plate.

Figure 6.2. Photograph of PXRD plate.

1H NMR spectra were recorded using a Jeol EX270 NMR spectrometer. 1H NMR spectra were taken in $CDCl_3$ and were referenced to residual trimethysilane (TMS) (0 ppm) and reported as follows: chemical shift, multiplicity (s = singlet, d = doublet, t = triplet, dd= doublet of doublet, m = multiplet).

The calculation for the conversion of product from ^{1}HNMR was adapted from Lodge et al[88] 4-iodo-1-nitrobenzene to 4-nitro-1,1'-biphenyl was calculated by a comparison of the integrated peak areas (PA) from the four protons from 4-iodo-1-nitrobenzene at 7.96 ppm against the two protons of the product, 4-nitro-1,1'-biphenyl, at 8.31 ppm.

Phenylboronic acid (400 MHz, CDCl3) δH/ppm: 8.25 (m, 2H, 2 x Ar-H), 7.61 (tt, J 7.3, 1.4 = Hz, 1H, 1 xAr-H), 7.52 (m, 2H, 2 x Ar-H). The -B(OH)2 protons undergo deuterium exchange and were not evident in the spectrum.
4-iodonitrobenzene (400 MHz, CDCl3) δH/ppm: 7.96 (m, 4H, 4 x Ar-H)
4-nitrobiphenyl (400 MHz, CDCl3) δH/ppm: 8.31 (dt, J = 9.0, 2.1 Hz, 2H; 2 × Ar H), 7.75 (dt, J = 9.0, 2.1Hz, 2H; 2 × Ar-H), 7.64 (dt, J = 6.9, 1.8 Hz, 2H; 2 × Ar-H), 7.54-7.43 (m, 3H, 3 × Ar-H).

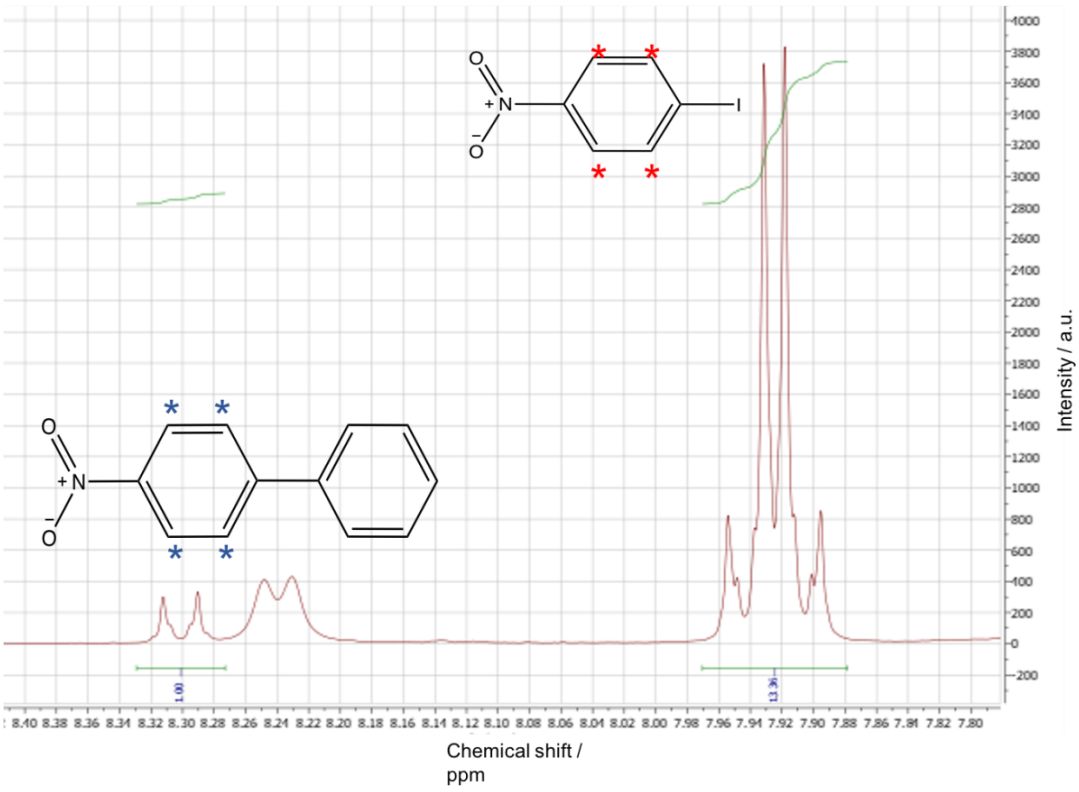

Figure 6.3. ^{1}H NMR spectroscopy of the reaction mixture showing the integral of the starting material, 1-iodo-4-nitrobenzene (protons responsible for peak denoted by *), and the product, 4-nitro-1,1'-biphenyl (protons responsible for peak denoted by *). The doublet peak at ~8.25 ppm is a signal from the remaining phenylboronic acid as this example did not reach reaction completion.

6.2. Synthesis of PdNPs@GNF from $Pd_2(dba)_3$

A solution of tris(dibenzylidenacetone)dipalladium(0) ($Pd_2(dba)_3$) (0.332 mg, 1 % loading) dissolved in $CHCl_3$ (2 mL) was added to GNF (annealed at 400 °C for 1 hr) in $CHCl_3$ (3 mL). The resultant mixture was stirred at 40 °C for 4 hrs

until the formation of a colourless solution. The black powder of PdNPs@GNF was obtained by filtration and washed with acetone.

6.3. Synthesis of PdNPs@GNF from $Pd_2(dba)_2$-$CHCl_3$

A solution of tris(dibenzylidenacetone)dipalladium(0)-chloroform adduct ($Pd_2(dba)_3.CHCl_3$) (0.375 mg, 1 % loading) dissolved in $CHCl_3$ (1 mL) was added to GNF (annealed at 400 ^oC for 1 hr) in $CHCl_3$ (2 mL). The resultant mixture was stirred at 40 ^oC for 4 hrs until the formation of a colourless solution. The black powder of PdNPs@GNF was obtained by filtration and washed with acetone.

6.4. Suzuki Cross Coupling Reaction

To a two necked round bottomed flask containing 4-iodionitrobenzene (14 mg, 0.056 mmol), phenylboronic acid (8.9 mg, 0.073 mmol), sodium acetate (10.6 mg, 0.13 mmol) and Pd@GNF catalyst (5 mg), was added methanol (degassed for 10 minutes). The resultant solution was ultrasonicated to disperse the catalyst and then heated at 70 ^oC for 24hrs. After which the reaction mixture was left to cool, centrifuged and the catalyst separated by pipetting off the solution. The catalysed was washed with methanol, centrifuged again and dried by pipetting of the methanol and leaving to dry overnight in air. The product was obtained by rotary evaporation and then HNMR performed to determine conversion. Once dried, the catalyst was weighed, and the process was repeated for 5 consecutive cycles.

6.5. Sublimation of Ferrocene

Impure Ferrocene (100 mg) was distributed onto a petri dish heated gently on a hot plate with another plate placed on top. The dish was heated until pure ferrocene crystals formed on the covering petri dish.

6.6. Synthesis of (FeCn)/GNF

GNF (15 mg, annealed at 400 ^oC for 1 hr) and ferrocene (5mg) were combined, sealed under vacuum in a pyrex tube using vacuum pump and heated for 350 ^oC for 24 h and then at 500 ^oC for a further 24 h. The resultant powder was cooled, and the tube opened to yield the black power (FeCn)/GNF.

6.7. Synthesis of PdNPs@(FeCn/GNF)

($Fe@C_n$)/GNF (15 mg) was dispersed in $CHCl_3$ (2 mL) using ultrasonication. $Pd_2(dba)_3$ CHCl (0.34 mg) dissolved in $CHCl_3$ (1 mL) was added to GNF dispersion and stirred at 40 ^oC for 4 hrs until colourless solution formed. The resultant mixture was separated using centrifugation and magnet and washed with acetone (20 mL).

6.8. Suzuki Cross Coupling Reaction Using Magnetic Catalyst

To a 25 mL two necked round bottomed flask containing iodionitrobenzene (14 mg), phenylboronic acid (10.6 mg), sodium acetate (8.9 mg) and catalyst (5 mg), methanol (5 mL, degassed for 10 minutes) was added. The resultant solution was ultrasonicated to disperse the catalyst and then heated at 70 ^{o}C for 24 hrs. After which the reaction mixture was left to cool, centrifuged and the catalyst separated by pipetting off the solution. The catalysed was washed with methanol, centrifuged again and dried by pipetting of the methanol and leaving to dry overnight in air. The product was obtained by rotary evaporation and then HNMR performed to determine conversion. Once dried, the catalyst was weighed, and the process was repeated for 5 consecutive cycles.

Figure 6.4. Photograph of magnetic catalyst being separated using a magnet.

6.9. Magnetron Sputtering

Pd metal was sputtered onto GNF (100 mg) as nanoparticles using a custom-built magnetron sputter chamber from AJA International. Work distance 90 mm target tilt 0.31, work pressure 3 mTorr at 80W for 15 minutes.

Figure 6.4. Photograph of sample in magnetron sputter chamber

6.10. Experimental for DCT test

DCT (1 mg, 0.5%) and PdNPs@GNF were mixed in methanol (5mL) and stirred for 2 hrs at 70 ^{o}C. Then phenylboronic acid (8.9 mg, 0.073 mmol), 4-iodionitrobenzene (14 mg, 0.056 mmol) and sodium acetate (10.6 mg, 0.13 mmol) was added, and the resultant solution was stirred at 70 ^{o}C for 24 h. The catalyst was separated by centrifugation and dried in air. ^{1}HNMR analysis was performed to determine conversion of product.

6.11. Hydrogenation procedure

Pd@GNF (10 mg) was stirred with THF (10mL) in a hydrogenation reactor at 40 ^{o}C and exposed to 10 bar H_2 for 18 hrs. Once complete, the mixture was filtered, washed with acetone (2x10 mL), and left to dry overnight.

6.12. Encapsulation of Pd NPs onto GNF via $Pd(acac)_2$ precursor

$Pd(acac)_2$ (1 mg) was inserted into an ampoule with GNF (15 mg, annealed at 450 ^{o}C for 1 h) and heated at 160 ^{o}C under vacuum for 72 h to sublime the $Pd(acac)_2$. The mixture was then cooled immediately in an ice bath and then heated under argon at 500 ^{o}C for 1 hr to decompose the ligand.

6.13. Synthesis of defected GNF

GNFs (150 mg, annealed at 500 ^{o}C for 30 minutes) was mixed with Chromium acetylacetonate (54 mg) and distributed evenly between four 18 cm long ampoules and then sealed under vacuum 1.5 x 10^{-4} mbar. The ampoules were heated to 160 ^{o}C for 2 days. Once sublimed, the ampoule, still closed, was cooled rapidly for 5 min. The resultant solid was transferred to four new ampoules, which were then evacuated and then any oxygen and moisture was eliminated by backfilling with argon three times. The ampoules were then filled with argon (0.5 bar) and then heated to 500 ^{o}C for 1 hr. The ampoules

where then left to cool for 4 days. The resultant material was heated in air at 10^{o}C/min to 495^{o}C, isotherm 8 min, and then the etching process was halted by cooling under Ar. The composite was then heated in concentrated nitric acid (15.8 M 60 mL) for 1 h at reflux to remove the Cr_2O_3. The sample was then diluted and filtered using PTFE membrane. This washing step was repeated 3 times but did not remove all the Cr_2O_3. The remaining solid was heated to 1000 ^{o}C for 2 h and cooled slowly under Ar atmosphere to remove any oxygen containing groups left from the acid treatment, yielding the defected GNF product.

6.14. Working out TON and TOF

Atomic radius of Pd atom = 0.137 nm

Surface area of atom = $4 * (22/7) * (0.137)^2 = 0.236\ nm^2 = 2.36*10^{-19}\ m^2$

Average diameter of PdNP in GNF = 2.32 nm (measured from HRTEM)

Volume of PdNP = $4/3*(22/7)*(2.32/2)^3 = 6.54\ nm^3 = 6.54*10^{-21}\ cm^3$

Density of Pd = $12.02\ g/cm^3$

Mass of PdNP = $6.54*10^{-21} * 12.02 = 7.86*10^{-20}$ g

Mass of PdNPs@GNF = 0.005 g

Mass of Pd in PdNPs@GNF (1 wt%) = 0.00005 g

Number of PdNPs = $0.00005/7.86*10^{-20} = 6.36 *10^{15}$

Atomic surface area of a PdNP = $4*(22/7)*(2.32/2)^2 = 16.9\ nm^2 = 1.69 *10^{-17}\ m^2$

Total surface area of all PdNPs = $6.36*10^{15} * 1.69*10^{-17} = 0.107\ m^2$
Active surface area (74 % of surface atoms are active, calculated using crystal structure) = $0.107 * 0.74 = 0.08\ m^2$

Number of active Pd sites in PdNPs@GNF used in the reaction =
Active surface area of all PdNPs / Surface area of a Pd atom

$0.08/2.36*10^{-19} = 3.40*10^{17}$

TON = Number of molecules of substrate consumed / Number of true active sites

$= 3.37*10^{19} / 3.4*10^{17} = 99.1$

TOF = TON/TIME = $99.1/24 = 4.13\ h^{-1}$

7. Bibliography

[1] I.Maluenda and O. Navarro, *Molecules*, 2015, **20** (5), 7528-7557.
[2] P. Schäfer, *Nat. Commun.*, 2017, **8** (1), DOI: 10.1038/ncomms15762.
[3] R.Martin and S.L. Buckwald *Acc. Chem. Res.*, 2008, **41** (11), 1461–1473.
[4] S.S Gujral *et al*. *Indo Global J. of Pharm. Sci.*, 2012, **2**, 351-367.
[5] C. Len, *Catalysts*, 2017, **7** (5), DOI: 10.3390/catal7050146.
[6] S. R. Chemler *et al. Angew. Chem., Int. Ed.*, 2001, **40** (24), 4544-4568
[7] V. Calo, A. Nacci, A. Monopoli and F. Montingelli, *J. Org.Chem*., 2005, **70**, 6040-6044.
[8] R. Martin and S. L. Buchwald, *Acc. Chem. Res.*, 2008, **41**, 1461.
[9] A. Jordan *et al*. *Chem. Rev.*,2022, **122** (6), DOI: 10.1021/acs.chemrev.1c00672
[10] C. Li, G. Xiao, Q. Zhao, H. Liu, T. Wang and W. Tang, *Org. Chem. Front.*, 2014, **1**, 225–229.
[11] M. J. Jin and D. H. Lee, *Angew. Chem., Int. Ed.*, 2010, **49**, 1119–1122.
[12] Q. Zhang, Z. Mao, K. Wang, N. T. S. Phan and F. Zhang, *Green Chem.*, 2020, **22**, 3239–3247.
[13] P. Priecel and J. A. Lopez-Sanchez, *ACS Sustainable Chem. Eng.*, 2019, **7** (1), 3-21.
[14] M. Hartings, *Nat. Chem.*, 2012, **4**, 764–764.
[15] Mining Technology, https://www.mining-technology.com/analysis/five- most-expensive-metals-and-where-they-are-mined/, (accessed May 2022)
[16] Statista, https://www.statista.com/statistics/693767/palladium-global-consumption-by-industry/, (accessed May 2022)
[17] Y. Rangraz, F. Nemati, A. Elhampour, *J. Phys. Chem. Solids*, 2020, **138**, 109251
[18] M. Lamblin, L. Nassar-Hardy, J.-C. Hierso, E. Fouquet and F.-X. Felpin, *Adv. Synth. & Catal.*, 2010, **352**, 33–79.
[19] E. Farnetti, R. Di Monte and J. Kašpar, in *Inorganic and Bio-Inorganic Chemistry Vol II*, ed. I.Bertini, EOLSS Publications, 2009, ch.2, 50-87.
[20] J. Cookson, *Platinum Met. Rev.*, 2012, **56**, 83–98.
[21] J. Guerra and M. A. Herrero, *Nanoscale*, 2010, **2**, 1390–1400.
[22] Y. Zhu, L. P. Stubbs, F. Ho, R. Liu, C. P. Ship, J. A. Maguire and N. S. Hosmane, *ChemCatChem*, 2010, **2**, 365–374.
[23] J. Zhu, T. Zhao, I. Kvande, D. Chen, X. Zhou and W. Yuan, *Chin. J. Catal.*, 2008, **29**, 1145–1151.
[24] K. Hong, M. Sajjadi, J. M. Suh, K. Zhang, M. Nasrollahzadeh, H. W. Jang, R. S. Varma and M. Shokouhimehr, *ACS Appl. Nano Mater.*, 2020, **3**, 2070–2103.
[25] Serp P, Corrias M, Kalck P. *Appl. Catal. A.*, 2003, **253**, 337-358
[26] M. Melchionna, S. Marchesan, M. Prato and P. Fornasiero, *Catal. Sci. Technol.*, 2015, **5**, 3859–3875.
[27] R. Rauti, M. Musto, S. Bosi, M. Prato and L. Ballerini, *Carbon*, 2019, **143**, 430–446.
[28] L. Boumia, M. Zidour, A. Benzair and A. Tounsi, *Phys. E (Amsterdam, Neth.)*, 2014, **59**, 186–191.
[29] A. L. Hemasa, N. Naumovski, W. A. Maher and A. Ghanem, *Nanomaterials*, 2017, **186**, DOI:10.3390/NANO7070186.

[30] D. Hedman *et al.*, *Sci. Rep.*, 2015, **5**, DOI: 10.1038/srep16850
[31] A. R. Siamaki, Y. Lin, K. Woodberry, J. W. Connell and B. F. Gupton, *J. Mater. Chem. A*, 2013, **1**, 12909–12918.
[32] I. U. Din *et al.*, *Ceram. Int*., 2020, **46** (11), 18446-18452.
[33] W. A. Solomonsz, G. A. Rance, B. J. Harris and A. N. Khlobystov, *Nanoscale*, 2013, **5**, 12200–12205.
[34] N. Agasti, M. A. Astle, G. A. Rance, J. Alves Fernandes, J. Dupont and A. N. Khlobystov, *Nano. Lett.*, 2020, **20**, 1161.
[35] M. A. Astle, A. Weilhard, G. A. Rance, T. M. Lemercier, C. T. Stoppiello, L. T. Norman, J. A. Fernandes and A. N. Khlobystov, *ACS Appl. Nano. Mater.*, 2022, **5**, 2075–2086.
[36] M.Aygün, PhD thesis, University of Nottingham, 2017.
[37] F. Kettemann, M. Wuithschick, G. Caputo, R. Kraehnert, N. Pinna, K. Rademann and J. Polte, *CrystEngComm*, 2015, **17**, 1865–1870.
[38] F. Kettemann, M. Wuithschick, G. Caputo, R. Kraehnert, N. Pinna, K. Rademann and J. Polte, *CrystEngComm*, 2015, **17**, 1865–1870.
[39] J. Cookson, *Platin. Met. Rev.*, 2012, **56**, 83–98.
[40] M. S. Arvelos, A. C. Silva, A. L. F. de Souza, C. A. Achete, T. L. Vasconcelos, E. Robertis, B. S. Archanjo, L. C. S. Aguiar, L. F. B. Malta and J. D. Senra, *ChemistrySelect*, 2018, **3**, 9725–9730.
[41] E. O. Pentsak, A. S. Kashin, M. v. Polynski, K. O. Kvashnina, P. Glatzel and V. P. Ananikov, *Chem. Sci.*, 2015, **6**, 3302–3313.
[42] K. Titov *et al.*, *ACS Sustainable Chem. Eng.*, 2019, **7** (6), 5875-5885.
[43] D. N. Leonard and S. Franzen, *J. Phys. Chem. C*, 2009, **113** (29), 12706-127144.
[44] S. S. Zalesskiy and V. P. Ananikov, *Organometallics*, 2012, **31**, 2302–2309.
[45] M. Cong, Y. Fan, J. M. Raimundo, J. Tang and L. Peng, *Org. Lett.*, 2014, **16**, 4074–4077.
[46] R. Narayanan and M. A. El-Sayed, *Top. Catal.*, 2008, **47**, 15–21.
[47] Z. Zhang, J. Lu, B. Zhang, W. Shi, Y. Guo and F. Cui, *Environ. Sci.: Nano*, 2020, **7**, 2117–2129.
[48] R. Chutia *et al.*, *Results Chem.*, 2021, **3,** 100225.
[49] B. P. Isaacoff and K. A. Brown, *Nano Lett.*, 2017, **17**, 6508–6510.
[50] I. Khan *et al*., *Arabian J. Chem*., 2019, **12** (7), 908-931.
[51] N. Abid *et al*., *Adv. Colloid Interface Sci*., 2021, **300** (15), DOI: 10.1016/j.cis.2021.102597
[52] V. R. Manikam, K. Y. Cheong and K. A. Razak, *J. Mater. Sci. Eng. B*, 2011, **176**, 187–203.
[53] R. Kumar and P. Kamakshi, *Nanostruct. Zinc Oxide*, 2021, 23-56.
[54] R. Cai, P. R. Ellis, J. Yin, J. Liu, C. M. Brown, R. Griffin, G. Chang, D. Yang, J. Ren, K. Cooke, P. T. Bishop, W. Theis and R. E. Palmer, *Small*, 2018, **14**, 1703734.
[55] L. Calabria, J. A. Fernandes, P. Migowski, F. Bernardi, D. L. Baptista, R. Leal, T. Grehl and J. Dupont, *Nanoscale*, 2017, **9**, 18753–18758.
[56] S. Liu, M. Wang, X. Yang, Q. Shi, Z. Qiao, M. Lucero, Q. Ma, K. L. More, D. A. Cullen, Z. Feng and G. Wu, *Angew. Chem. Int. Ed. Engl.*, 2020, **59**, 21698–21705.
[57] E. C. Kohlrausch, H. Andrade Centurion, R. W. Lodge, Xuanli Luo, Thomas Slater, M. J. L. Santos, Sanliang Ling, V. R. Mastelaro, M. J. Cliffe, R. Vitalino Goncalves and J. A. Fernandes, *J. Mater. Chem. A*, 2021,

9, 26676–26679.
[58] I. Cano, A. Weilhard, C. Martin, J. Pinto, R. W. Lodge, A. R. Santos, G.A. Rance, E. H. Åhlgren, E. Jónsson, J. Yuan, Z. Y. Li, P. Licence, A. N. Khlobystov and J. Alves Fernandes, *Nat. Commun.*, 2021, **12**, 1–6.
[59] M. S. Muralidhar *et al*., *IOP Conf. Ser.: Mater. Sci. Eng*., 2016, **149** (1), DOI: 10.1088/1757-899X/149/1/012071
[60] J. Liang, Q. Liu, T. Li, Y. Luo, S. Lu, X. Shi, F. Zhang, A. M. Asiri and X. Sun, *Green Chem.*, 2021, **23**, 2834–2867.
[61] H. Ur Rashid, K. Yu, M. Naveed Umar, M. Naveed Anjum, K. Khan, N. Ahmad and M. Tariq Jan, *Rev. Adv. Mater. Sci.*, 2015, **40**, 235–248.
[62] D. He *et al*., R. Soc. *Open Sci.*, 2018**, 5**, 172364.
[63] C. Liang, W. Xia, H. Soltani-Ahmadi, O. Schlüter, R. A. Fischer and M. Muhler, *Chem. Commun.*, 2005, 282–284.
[64] V. Cominos and A. Gavriilidis, *Appl. Catal., A*, 2001, **210**, 381–390.
[65] H. Veisi, A. Nikseresht, N. Ahmadi, K. Khosravi and F. Saeidifar, *Polyhedron*, 2019, **162**, 240–244.
[66] R. Li, P. Zhang, Y. Huang, P. Zhang, H. Zhong and Q. Chen, *J. Mater. Chem.*, 2012, **22**, 22750–22755.
[67] A. Stopin, F. Pineux, R. Marega and D. Bonifazi, *Chem. Eur. J.*, 2015, **21**, 9288–9301.
[68] Q. Guo, R. Ghadiri, T. Weigel, A. Aumann, E. L. Gurevich, C. Esen, O. Medenbach, W. Cheng, B. Chichkov and A. Ostendorf, *Polymers*, 2014, **6**, 2037–2050.
[69] F. Pineux, S. Federico, K. N. Klotz, S. Kachler, C. Michiels, M. Sturlese, M. Prato, G. Spalluto, S. Moro and D. Bonifazi, *ChemMedChem*, 2020, **15**, 1909–1920.
[70] F. Pineux, R. Marega, A. Stopin, A. La Torre, Y. Garcia, E. Devlin, C. Michiels, A. N. Khlobystov, D.
Bonifazi, *Nanoscale*, 2015, **7**, 20474– 20488.
[71] I. Cano, C. Martin, J. A. Fernandes, R. W. Lodge, J. Dupont, F. A. Casado-Carmona, R. Lucena, S. Cardenas, V. Sans and I. de Pedro, *Appl. Catal. B*, 2019, **260**, 118110.
[72] M. Melchionna, A. Beltram, A. Stopin, T. Montini, R. W. Lodge, A. N. Khlobystov, D. Bonifazi, M. Prato and P. Fornasiero, *Appl. Catal. B*, 2018, **227**, 356–365.
[73] M. Aygün, T. W. Chamberlain, M. del C. Gimenez-Lopez and A. N. Khlobystov, *Adv. Funct.Mater.*, 2018, **28** (34), DOI:10.1002/ADFM.201802869
[74] P. D. Stevens, G. Li, J. Fan, M. Yen and Y. Gao, *Chem. Commun.*, 2005, 4435.
[75] L. Ye, X. Liu and Y. Lu, *J. Catal*., 2021, **397**, 36–43.
[76] R. Chutia, B. Chetia and R. Hazarika, *Results Chem.*, 2021, **3**, 100225.
[77] D. G. Brown. *J. Med. Chem.*, 2016, **59** (10), 4443-4458.
[78] A.J.Reay, PhD Thesis, University of York, 2016.
[79] Y. Zare, *Composites, Part A*, 2016, **84**, 158-164.
[80] A. Kocjan *et al*., *Sci. Rep.*, 2017, **7**, DOI: 10.1038/s41598-017-02760-7
[81] D. R. Anton and R. H. Crabtree, *Organometallics*, 1983, **2**, 855–859.
[82] A. Singh and P. R. Sharp, *Organometallics*, 2006, **25** (3), 678-683.
[83] G. Vanti and M. Kurjogi, *Advance in Nano-Fertilizers and Nano-Pesticides in Agriculture*, ed. S. Jogaiah *et al.*, Woodhead Publishing, Cambridge, 2021, ch. 21, pp. 505-534.

[84] Z. Luo *et al*., *Appl. Catal., A*, 2018, **554**, 54-63.
[85] K. Santosh *et al., Org. Lett.,* 2014, **16** (4), 1264-1267.
[86] Y. Chen and L. Feng, *J. Photochem. Photobiol., B*, 2020, **205,** 111807.
[87] H. Sawada, *Mater. Res. Bull.*, 1994, **29**, 239–245.
[88] R. Lodge *et al*., *Nanoscale*, 2018, **10**, 19046-19051.

8. Appendices

Appendix A: ^{1}HNMR graphs for PdNPs@GNF-1

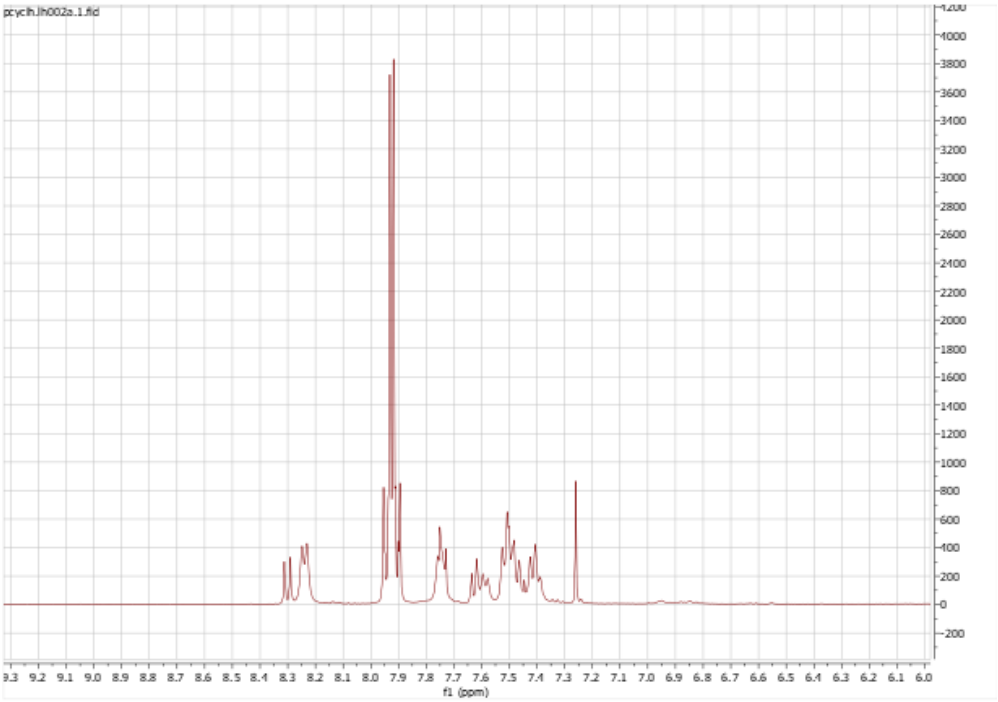

Appendix A-1: ^{1}HNMR graph for PdNPs@GNF-1 – Cycle 1

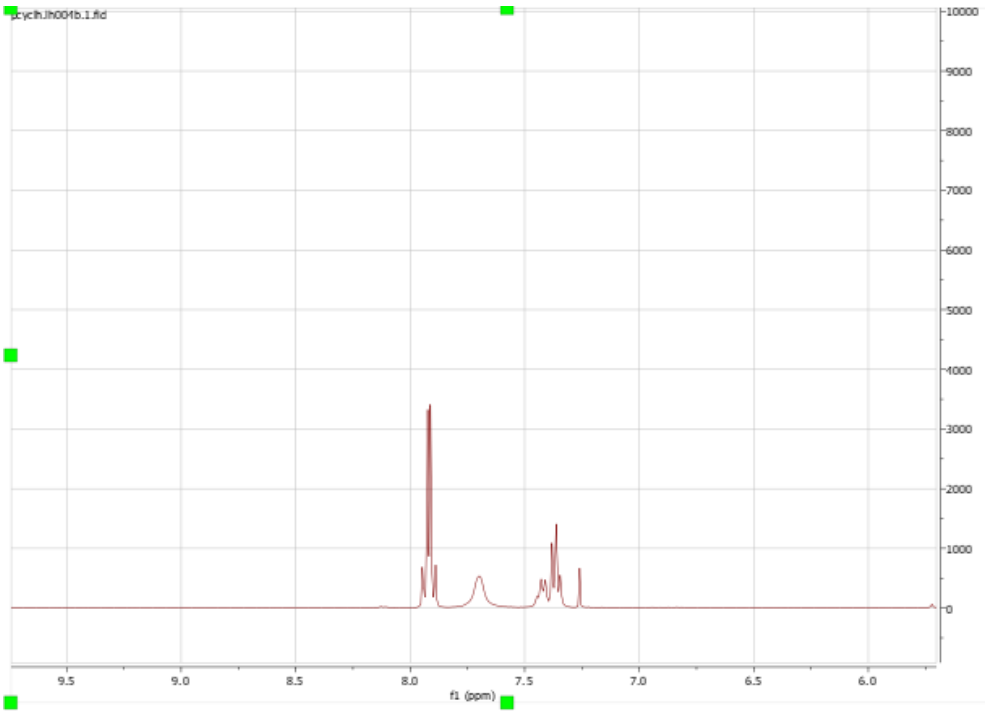

Appendix A-2: ^{1}HNMR graph for PdNPs@GNF-1 – Cycle 2

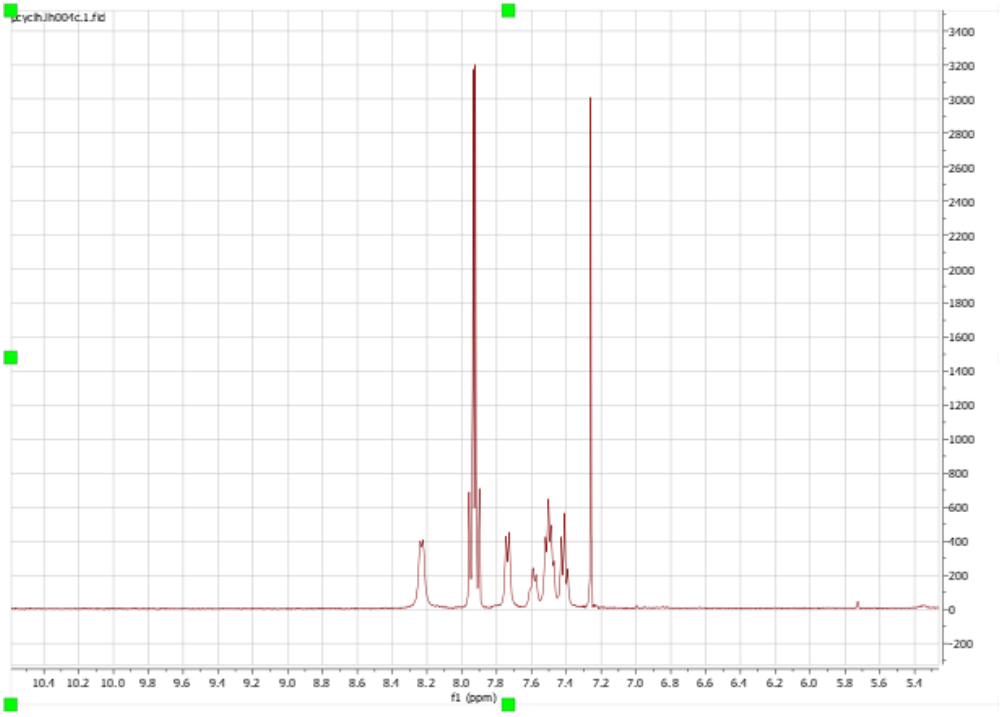

Appendix A-3: ^{1}HNMR graph for PdNPs@GNF-1 – Cycle 3

Appendix B: ^{1}HNMR graphs for PdNPs@GNF-2

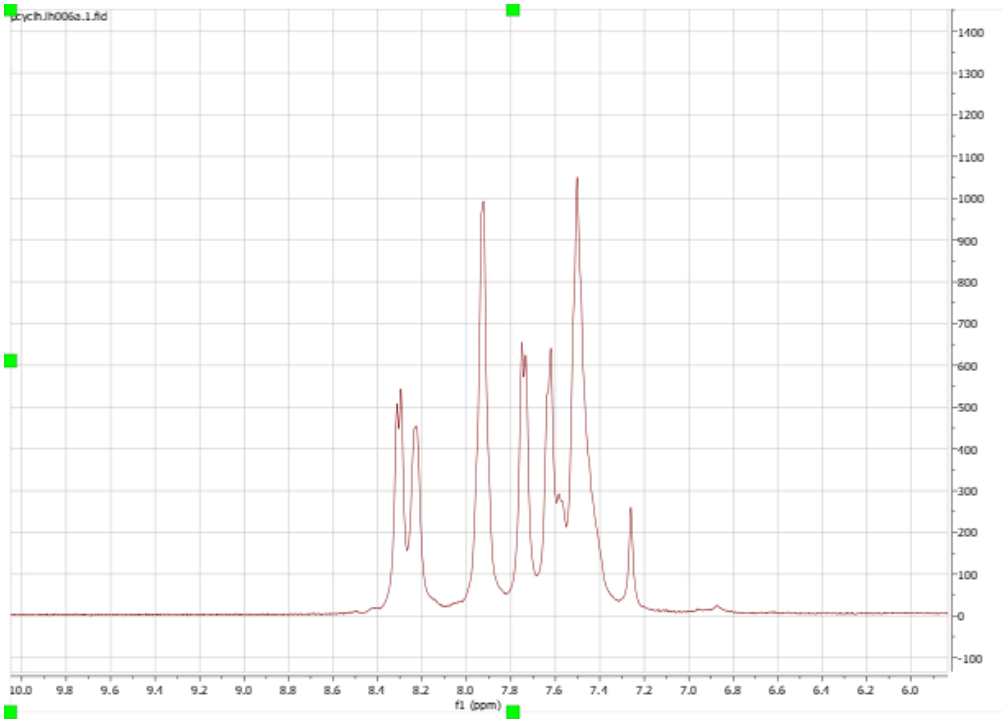

Appendix B-1: ^{1}HNMR graph for PdNPs@GNF-2 – Cycle 1

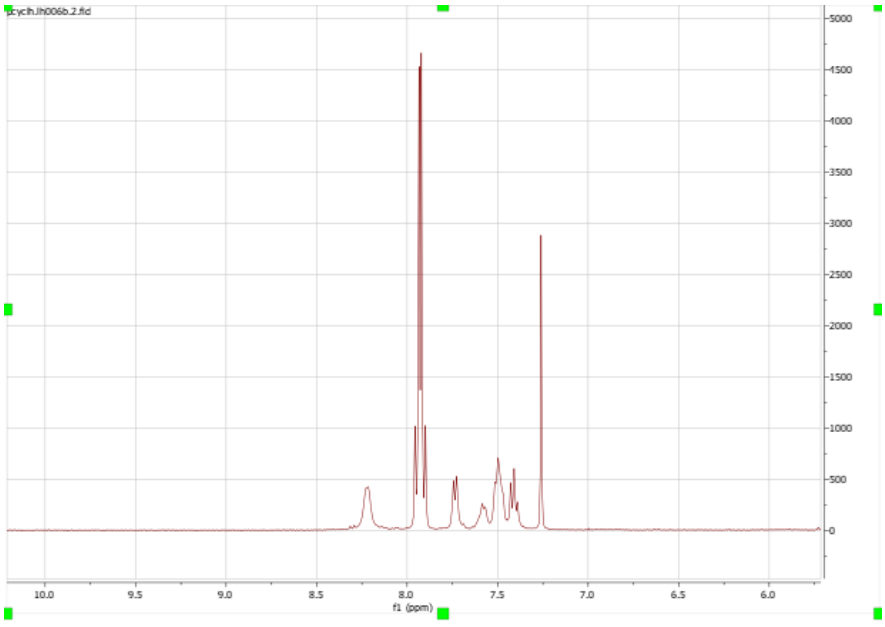

Appendix B-2: ^{1}HNMR graph for PdNPs@GNF-2 – Cycle 2

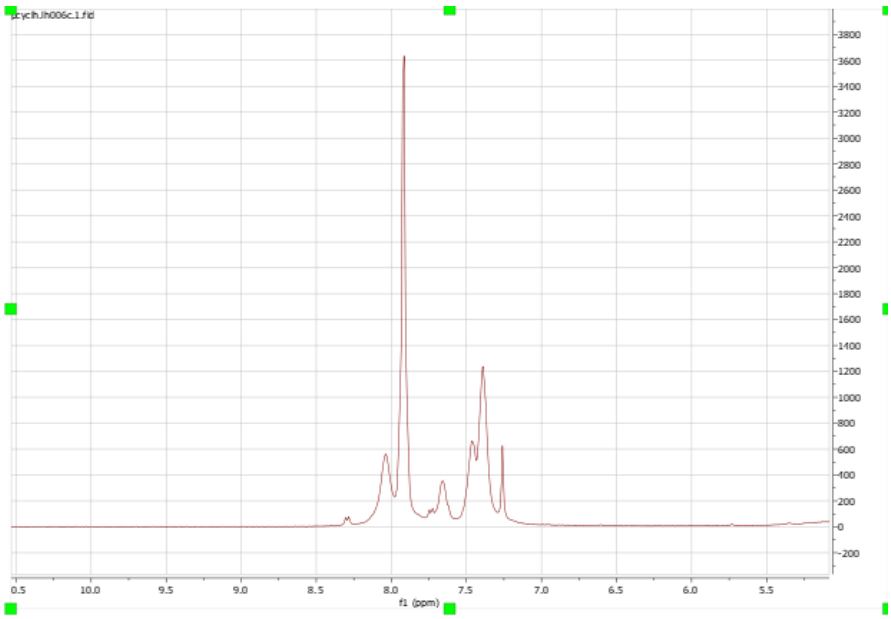

Appendix B-3: ^{1}HNMR graph for PdNPs@GNF-2 – Cycle 3

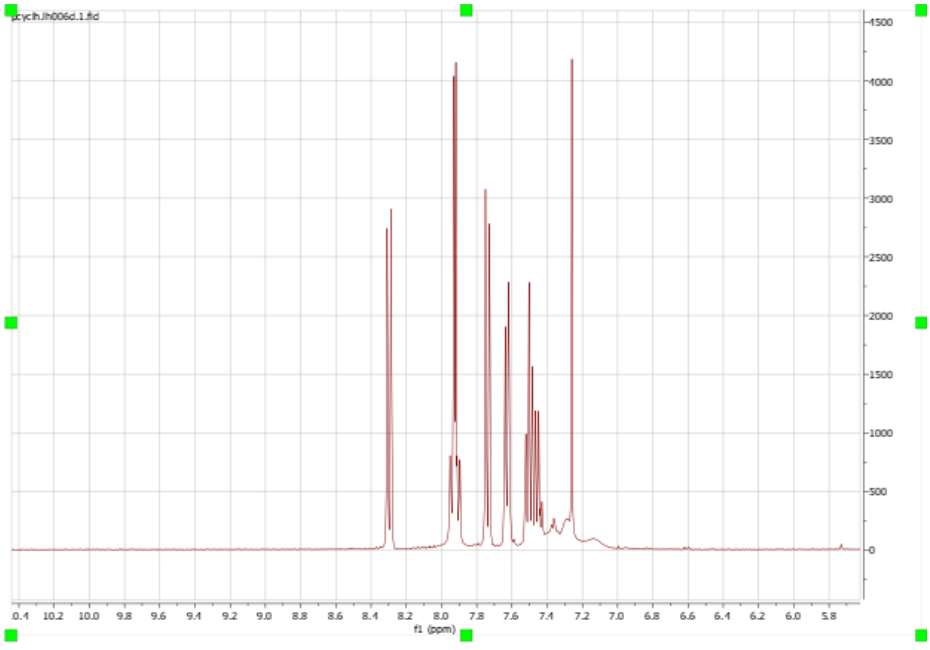

Appendix B-4: ^{1}HNMR graph for PdNPs@GNF-2 – Cycle 4

Appendix C: ^{1}HNMR graphs for FeCn/PdNPs@GNF-1

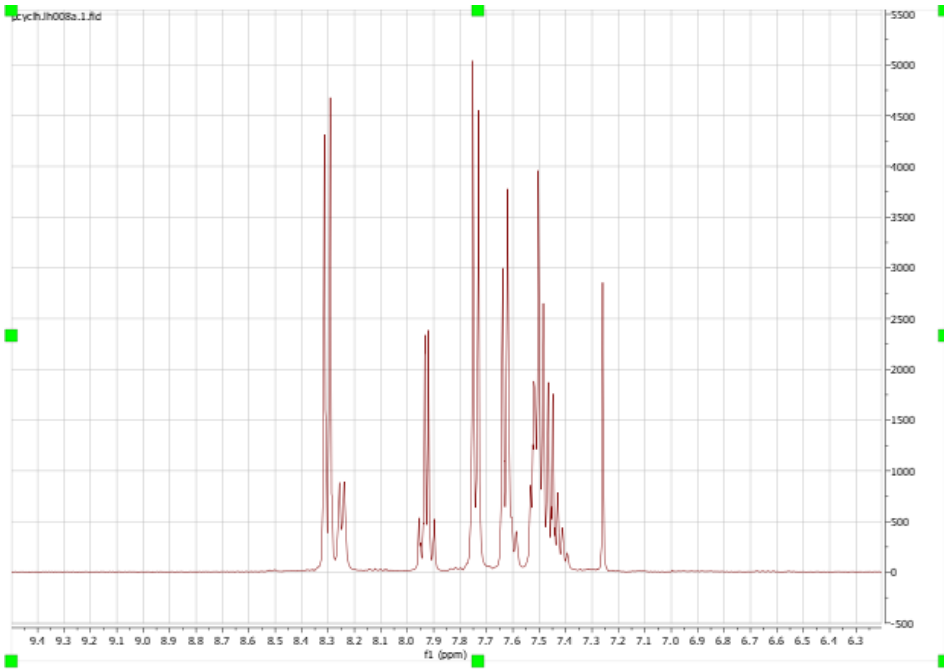

Appendix C-1: ^{1}HNMR graph for FeCn/PdNPs@GNF-1 – Cycle 1

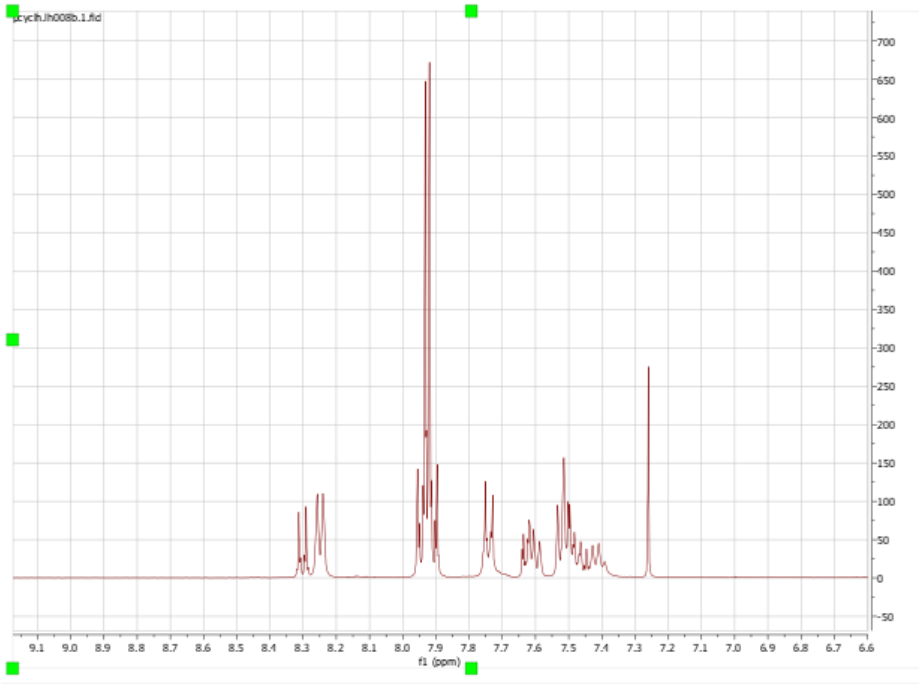

Appendix C-2: ^{1}HNMR graph for FeCn/PdNPs@GNF-1 – Cycle 2

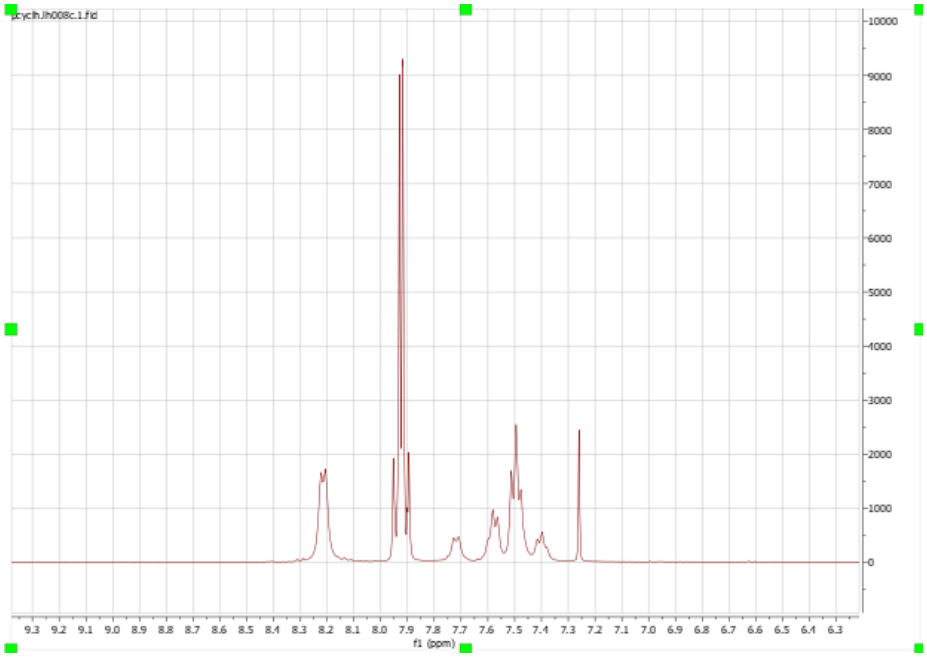

Appendix C-3: ^{1}HNMR graph for FeCn/PdNPs@GNF-1 – Cycle 3

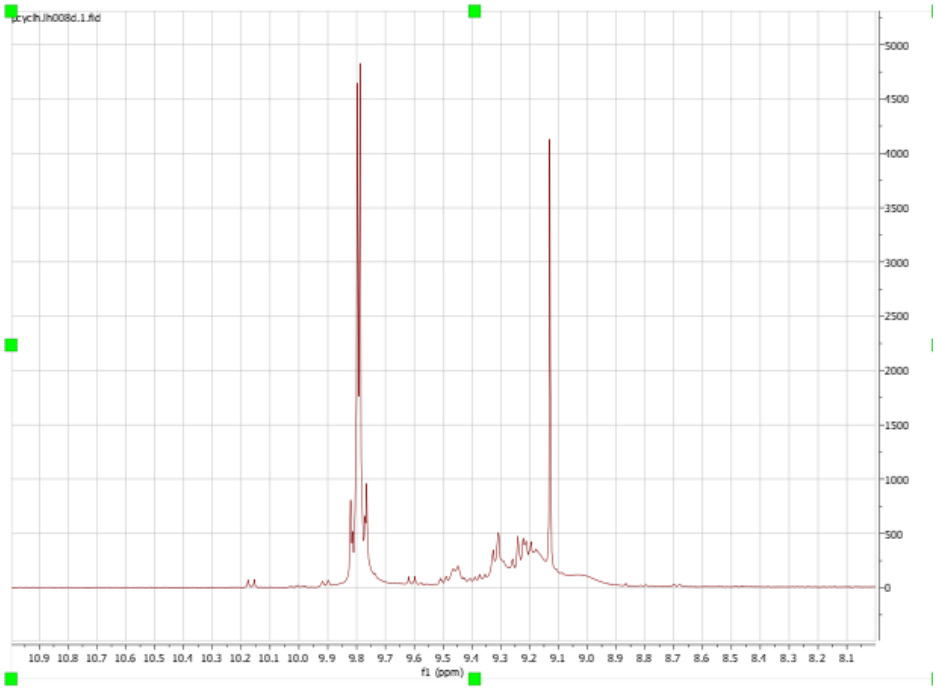

Appendix C-4: ^{1}HNMR graph for FeCn/PdNPs@GNF-1 – Cycle 4

Appendix D: ^{1}HNMR graphs for PdNPs/GNF-3

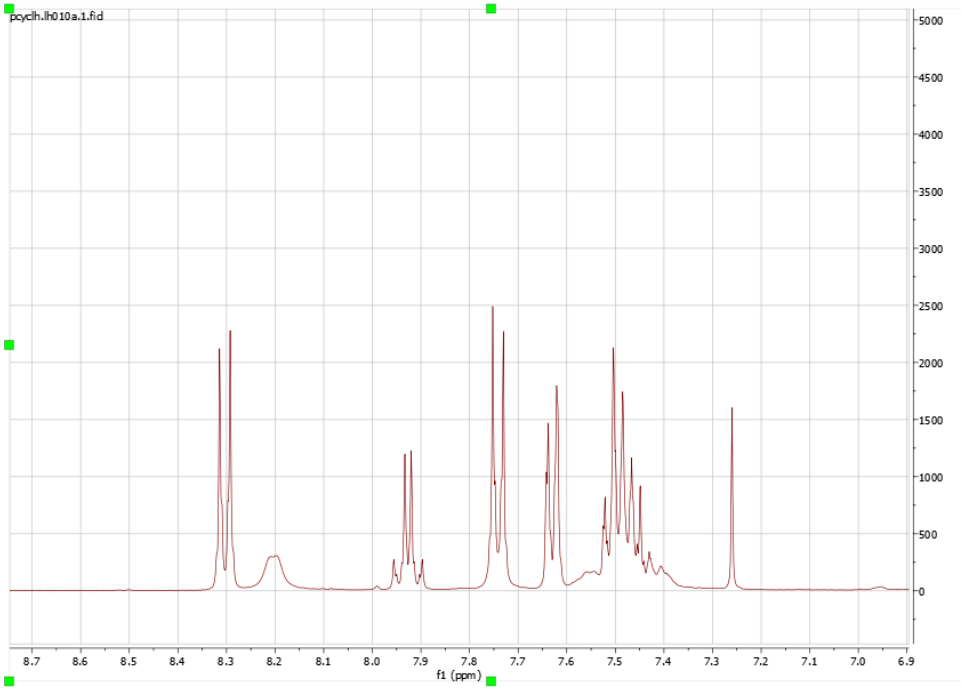

Appendix D-1: ^{1}HNMR graph for PdNPs/GNF-3 – Cycle 1

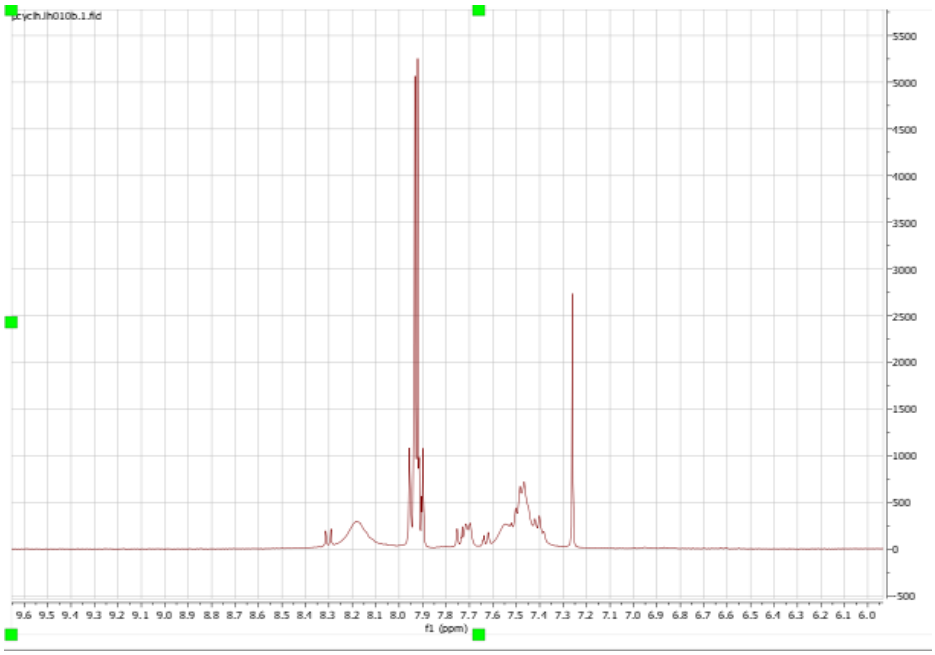

Appendix D-2: ^{1}HNMR graph for PdNPs/GNF-3 – Cycle 2

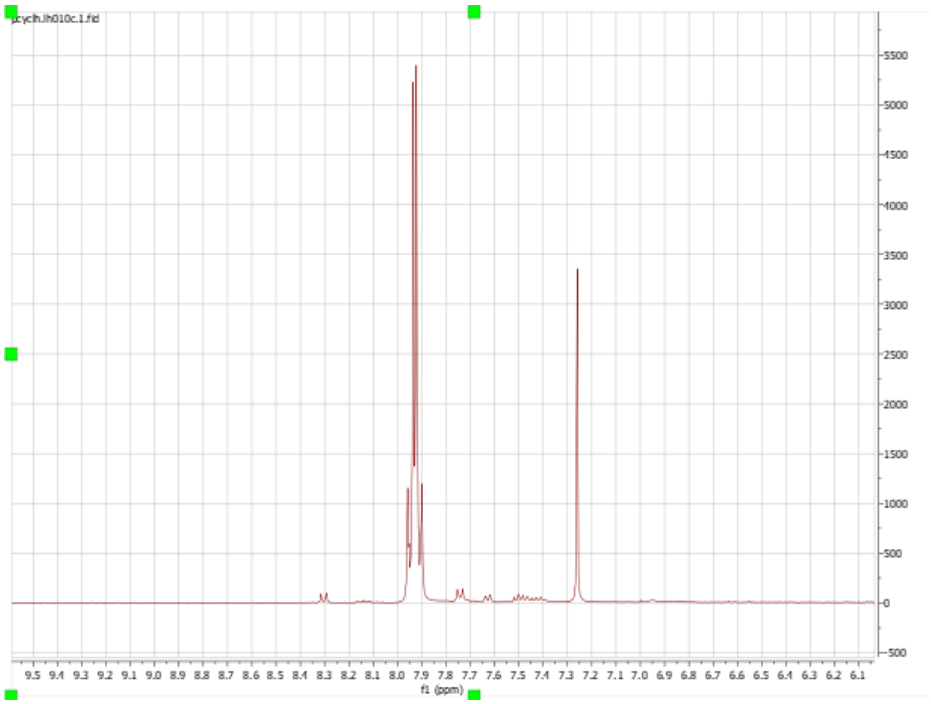

Appendix D-3: ^{1}HNMR graph for PdNPs/GNF-3 – Cycle 3

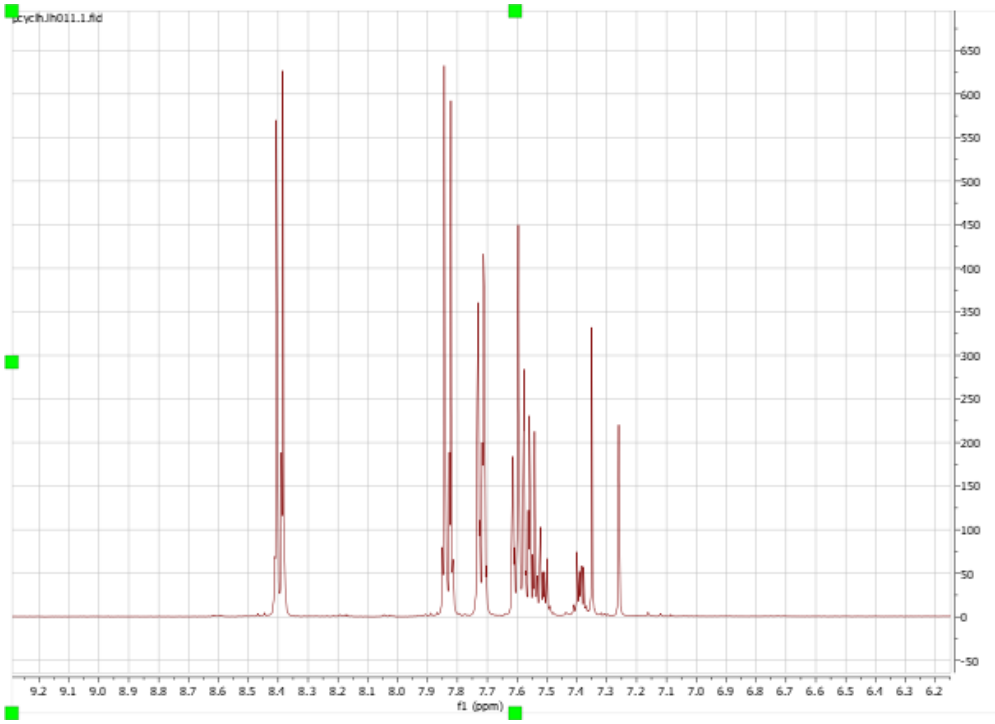

Appendix E: DCT test

Appendix F: ^{1}HNMR graphs for PdNPs@GNF-4

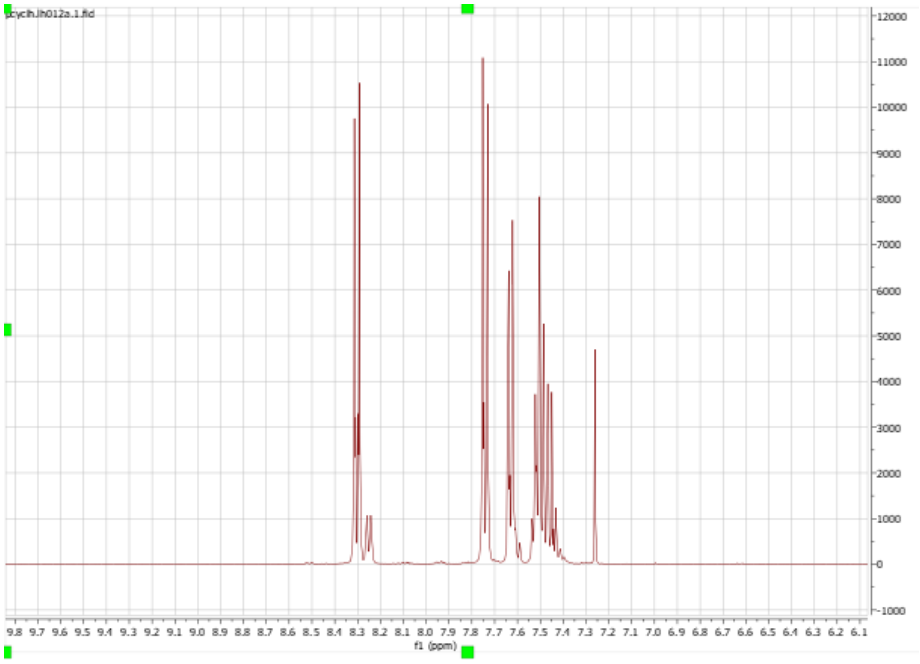

Appendix F-1: ^{1}HNMR graph for PdNPs@GNF-4 – Cycle 1

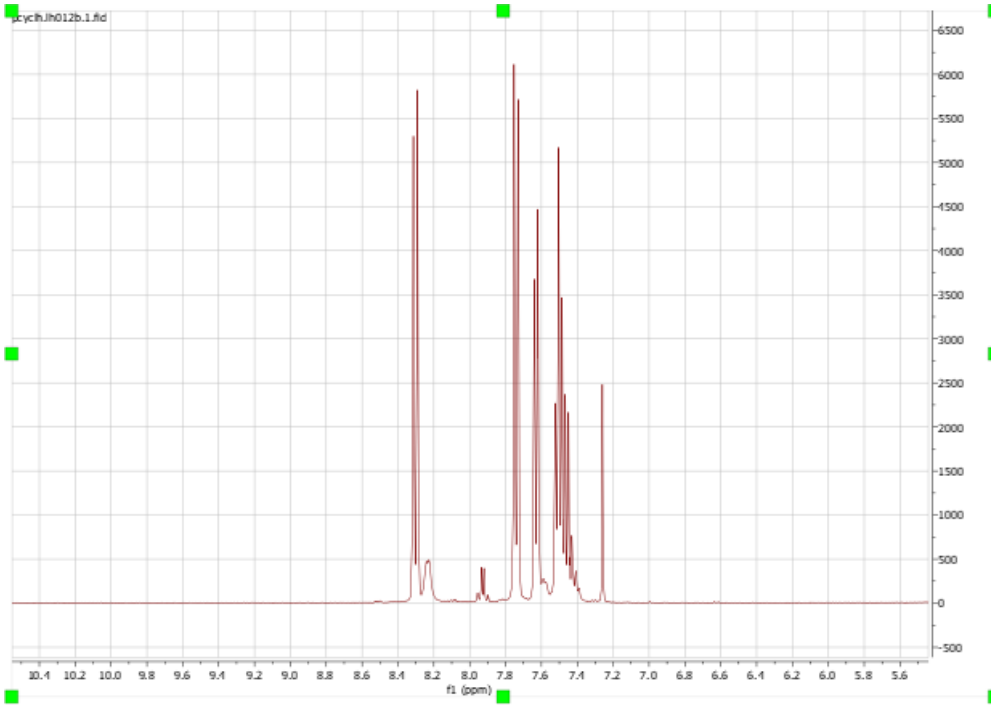

Appendix F-2: ^{1}HNMR graph for PdNPs@GNF-4 – Cycle 2

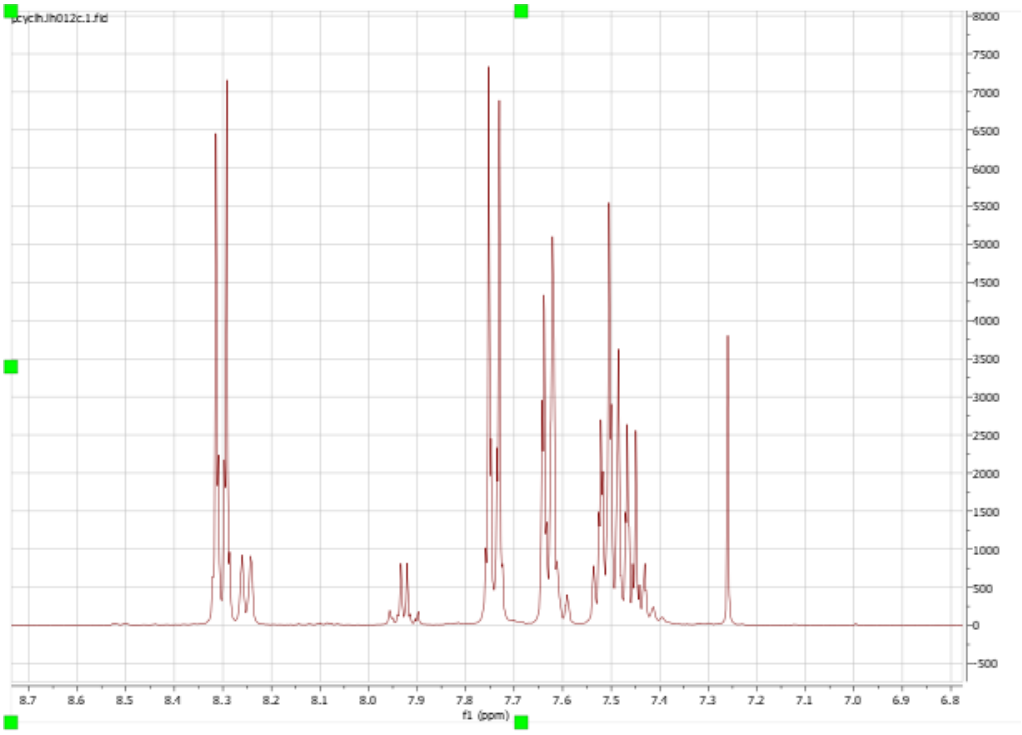

Appendix F-3: ^{1}HNMR graph for PdNPs@GNF-4 – Cycle 3

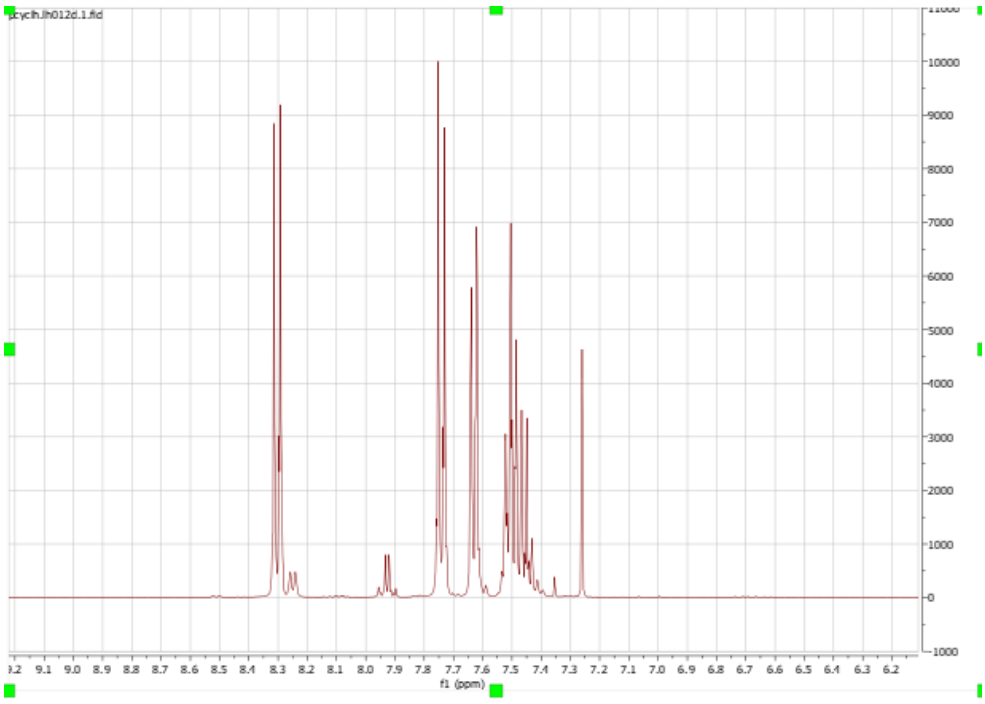

Appendix F-4: ^{1}HNMR graph for PdNPs@GNF-4 – Cycle 4

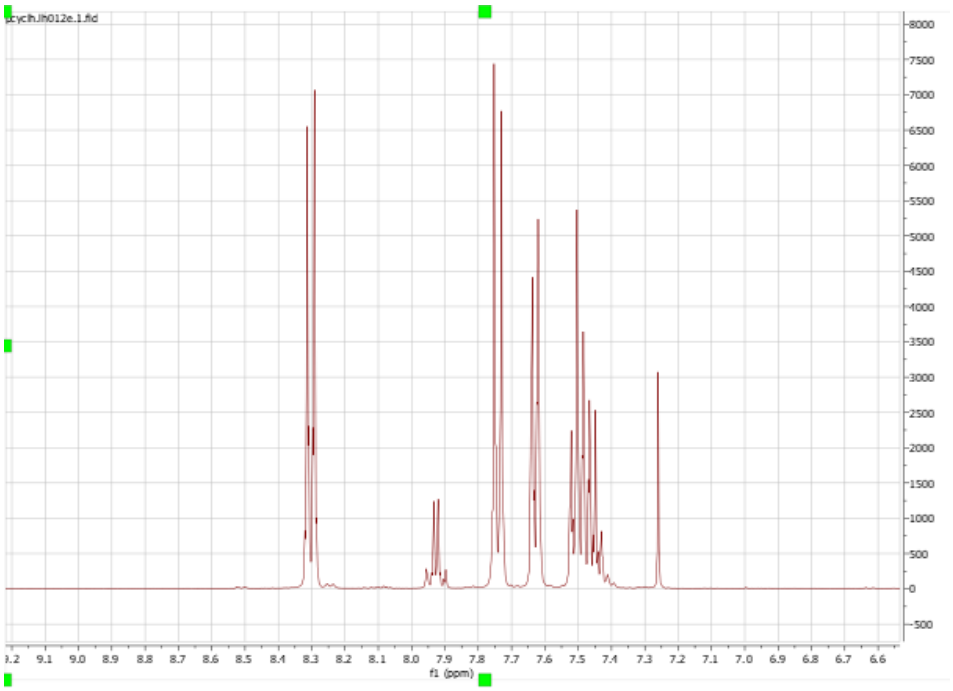

Appendix F-5: ^{1}HNMR graph for PdNPs@GNF-4 – Cycle 5

Appendix G: ^{1}HNMR graphs for PdNPs@GNF-4 repeat

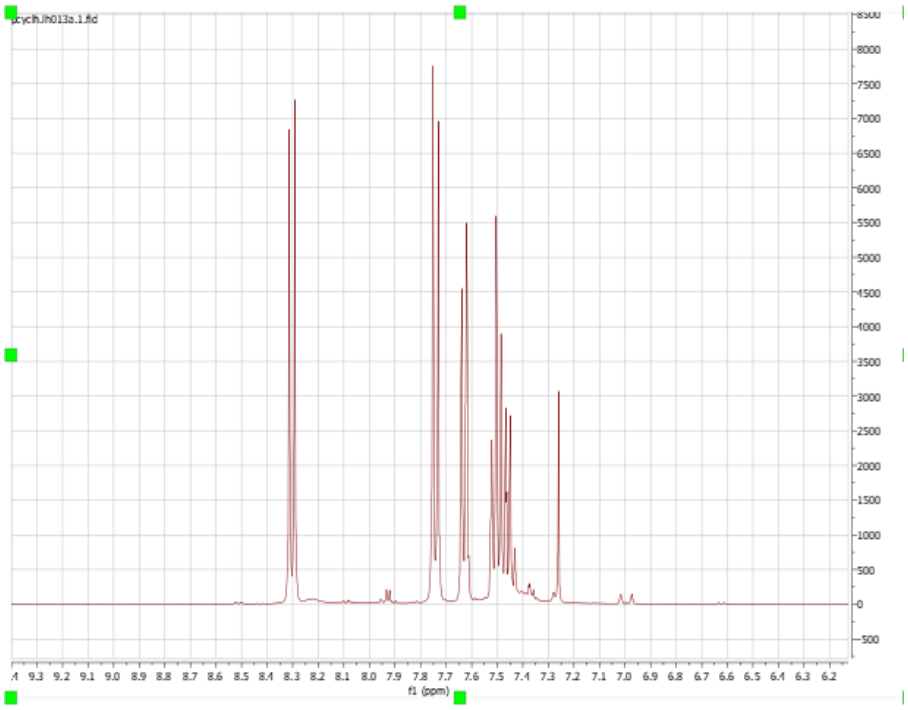

Appendix G-1: ^{1}HNMR graph for PdNPs@GNF-4 repeat – Cycle 1

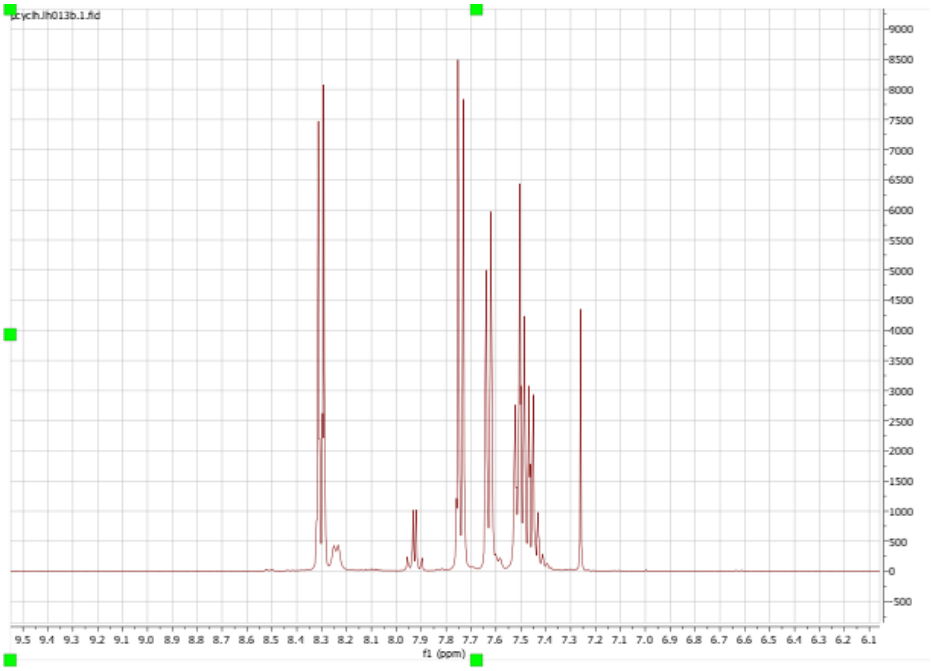

Appendix G-2: ^{1}HNMR graph for PdNPs@GNF-4 repeat – Cycle 2

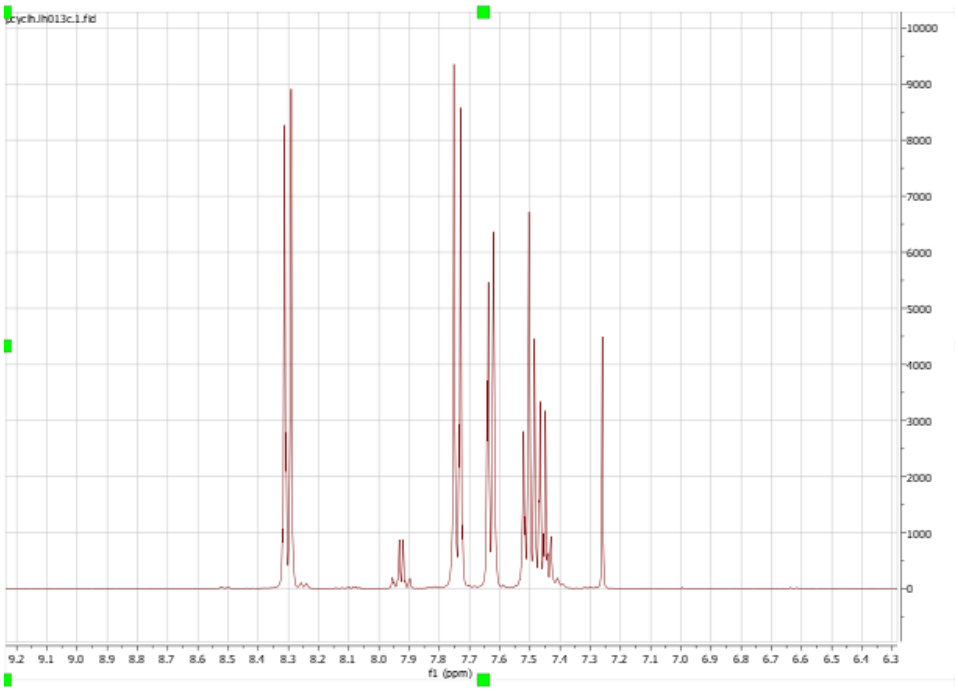

Appendix G-3: ^{1}HNMR graph for PdNPs@GNF-4 repeat – Cycle 3

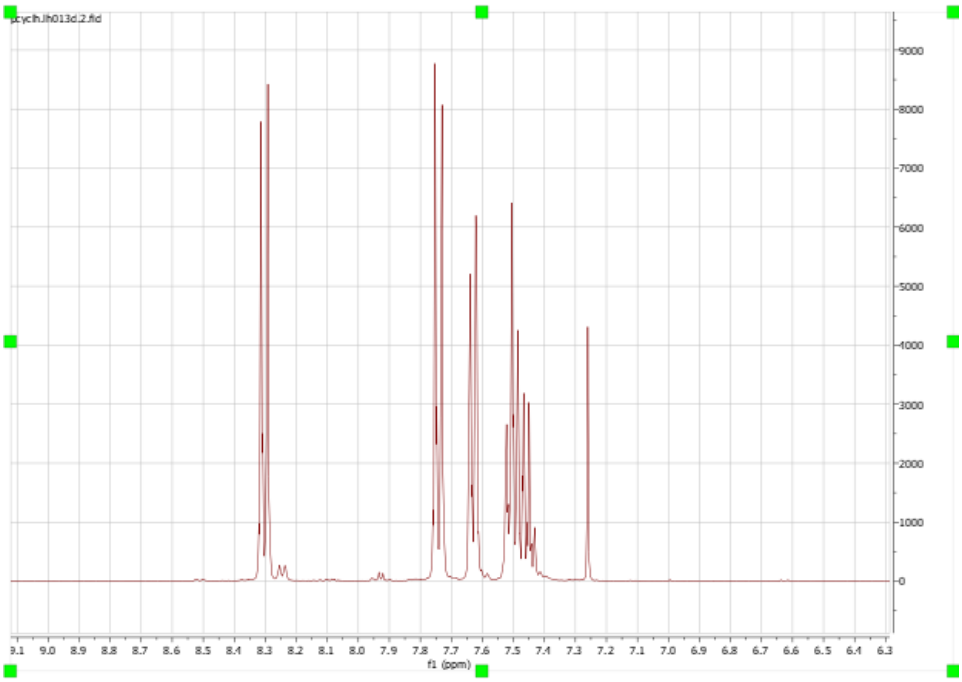

Appendix G-4: ^{1}HNMR graph for PdNPs@GNF-4 repeat – Cycle 4

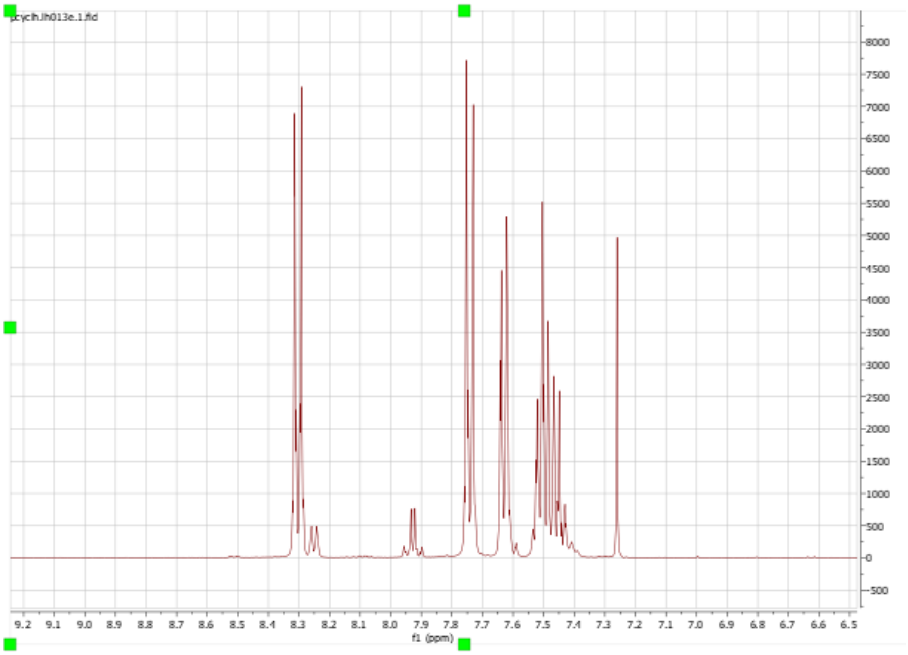

Appendix G-5: ^{1}HNMR graph for PdNPs@GNF-4 repeat – Cycle 5

Appendix H: ^{1}HNMR graphs for PdNPs/GNF-5

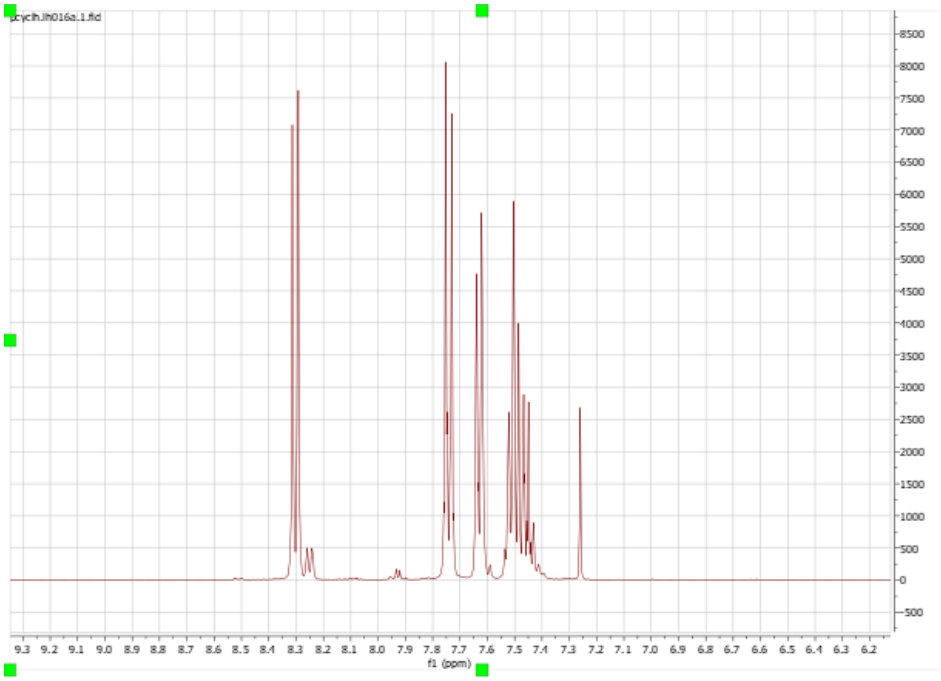

Appendix H-1: ^{1}HNMR graph for PdNPs/GNF-5 – Cycle 1

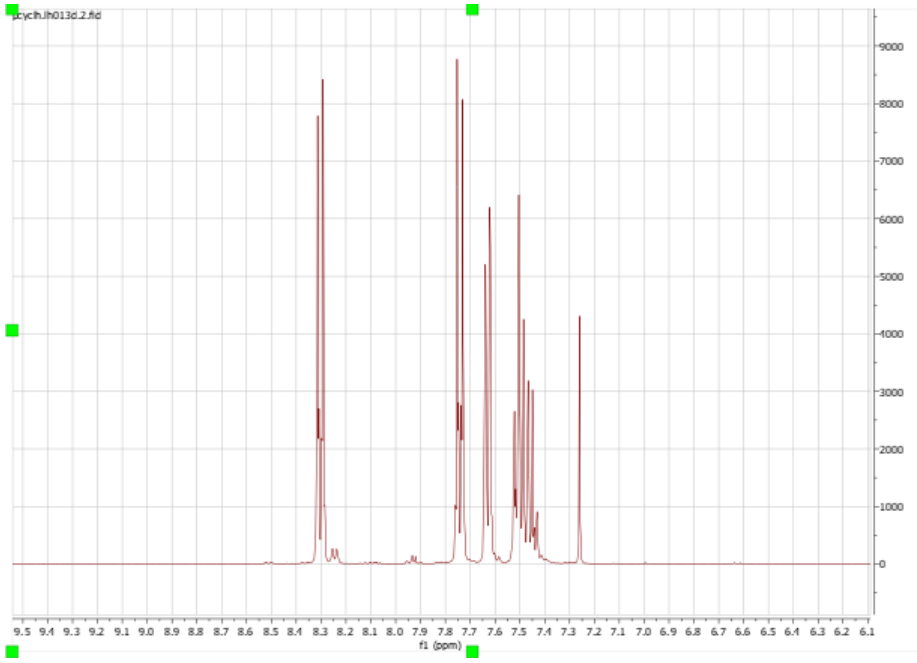

Appendix H-2: ^{1}HNMR graph for PdNPs/GNF-5 – Cycle 2

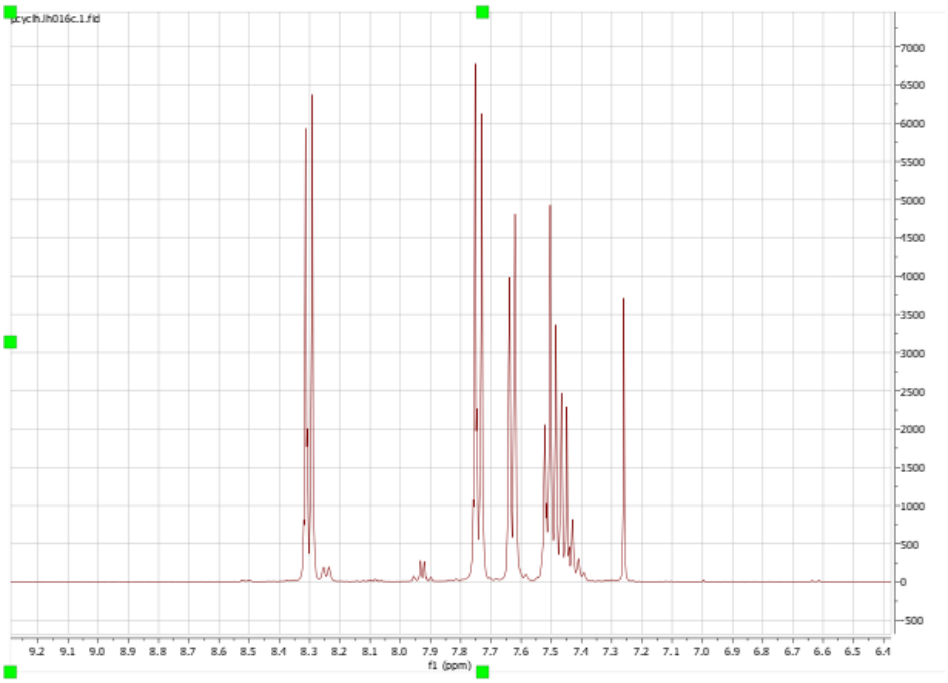

Appendix H-3: ^{1}HNMR graph for PdNPs/GNF-5 – Cycle 3

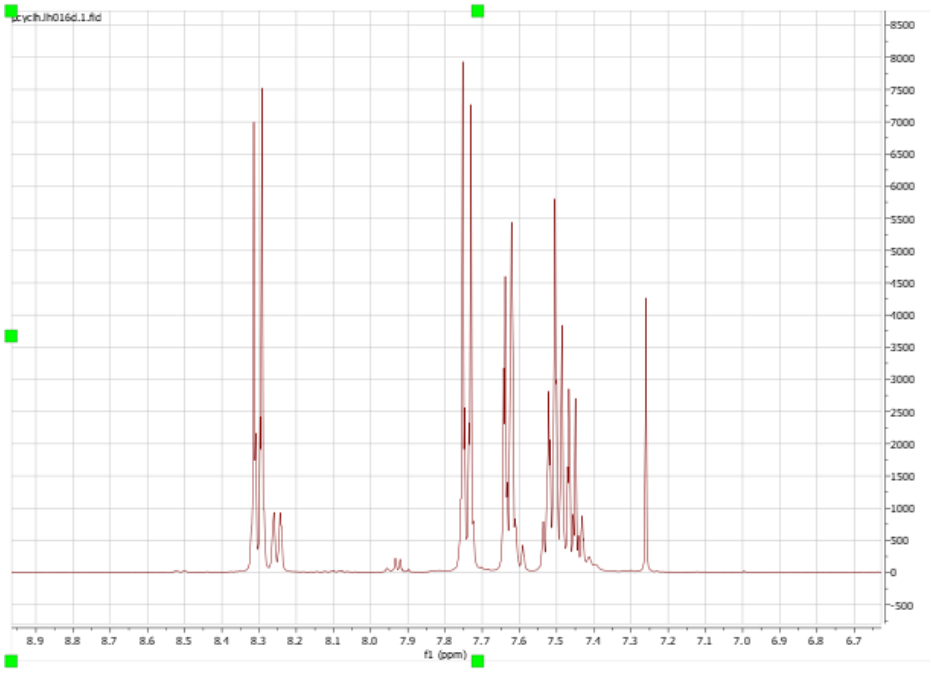

Appendix H-4: ^{1}HNMR graph for PdNPs/GNF-5 – Cycle 4

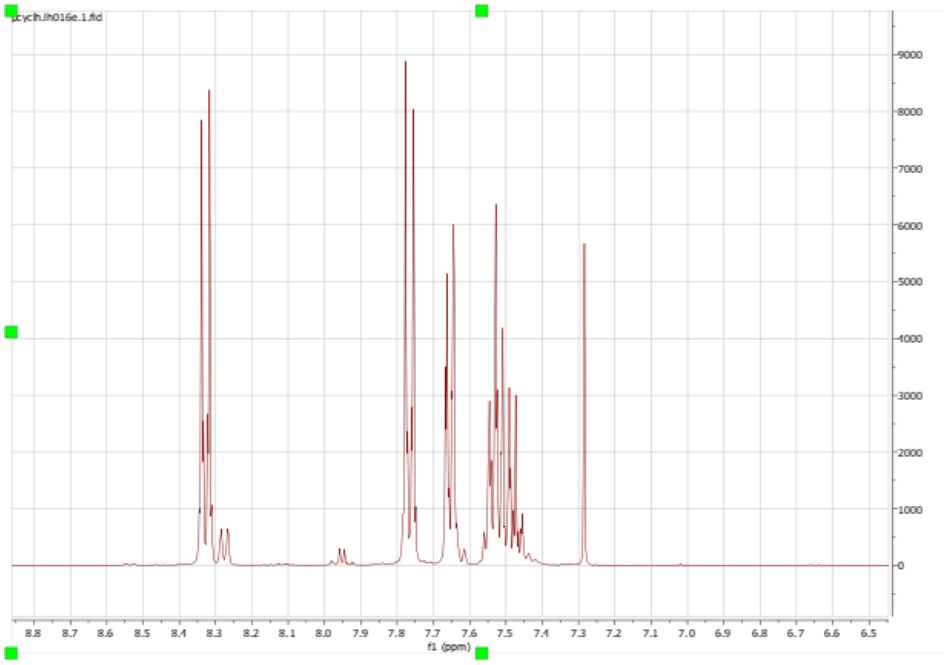

Appendix H-5: ^{1}HNMR graph for PdNPs/GNF-5 – Cycle 5

Appendix I: ^{1}HNMR graphs for PdNPs@GNF-6

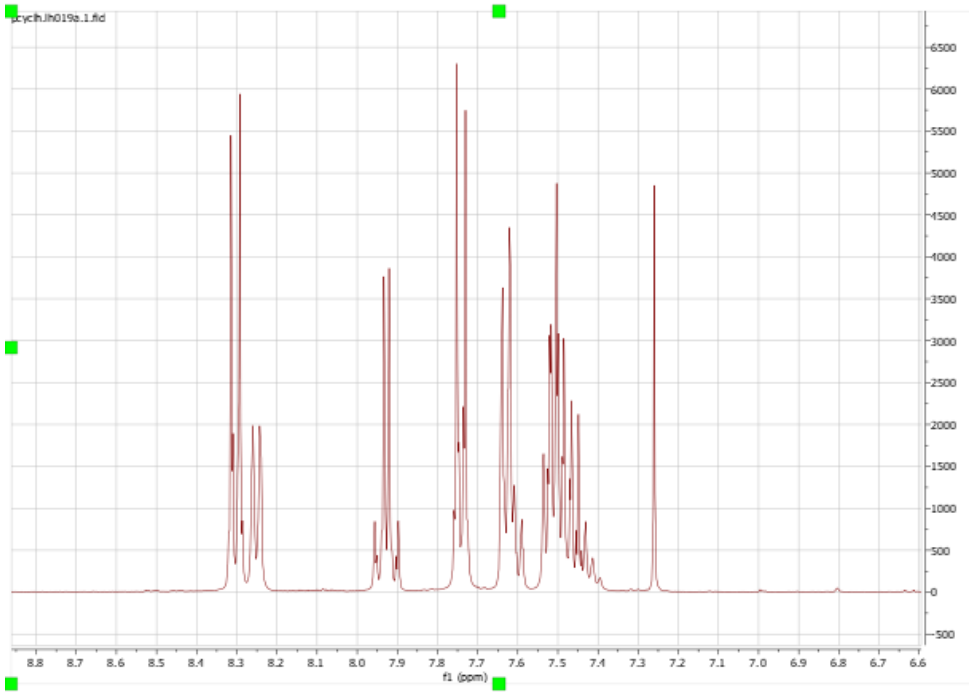

Appendix I-1: ^{1}HNMR graph for PdNPs@GNF-6 – Cycle 1

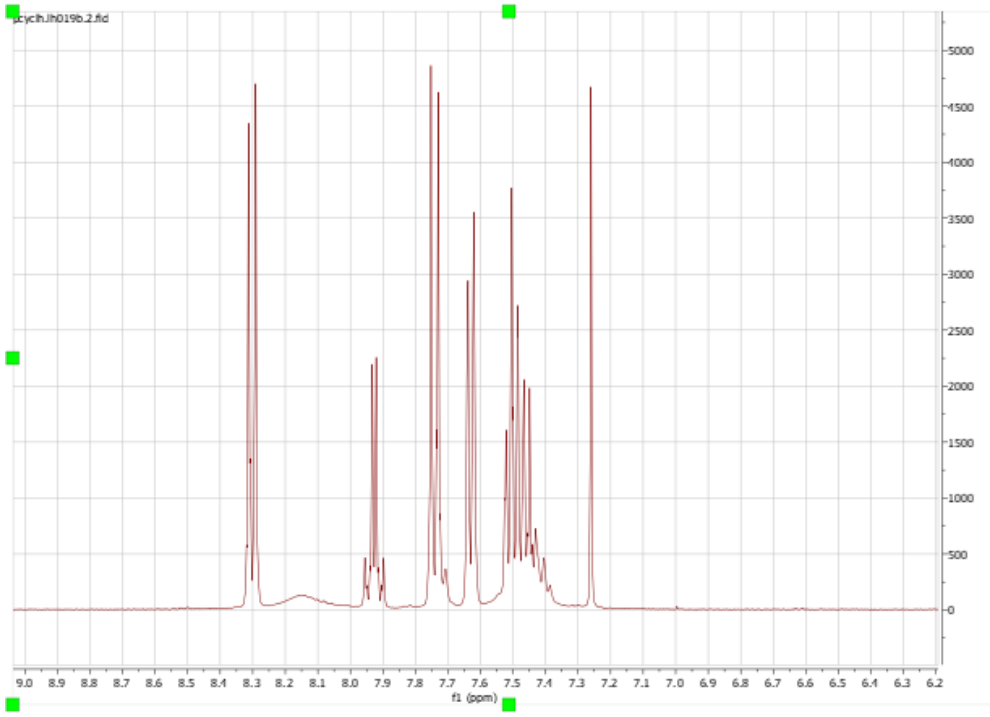

Appendix I-2: ^{1}HNMR graph for PdNPs@GNF-6 – Cycle 2

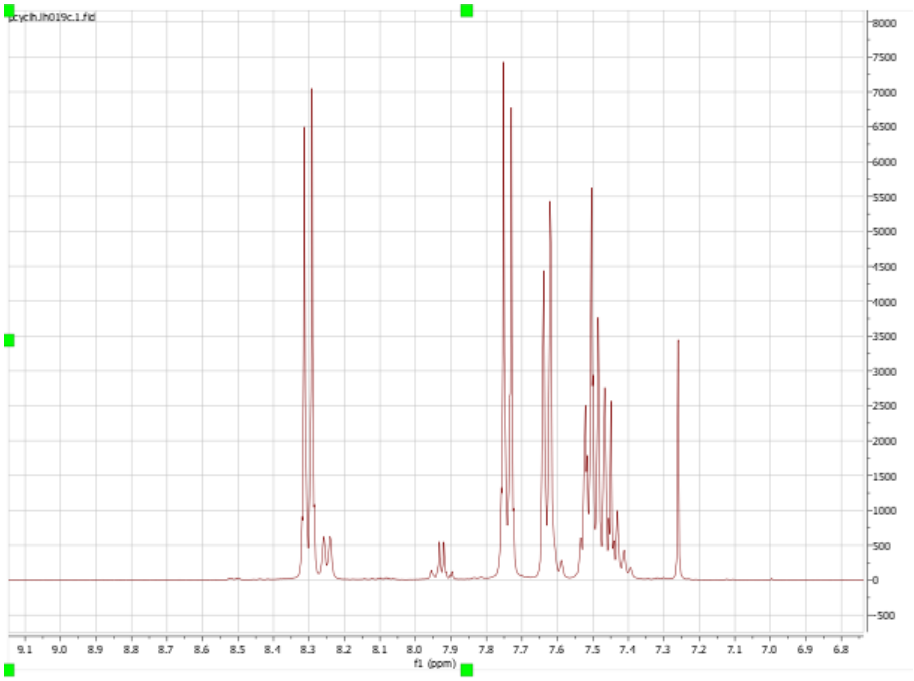

Appendix I-3: ^{1}HNMR graph for PdNPs@GNF-6 – Cycle 3

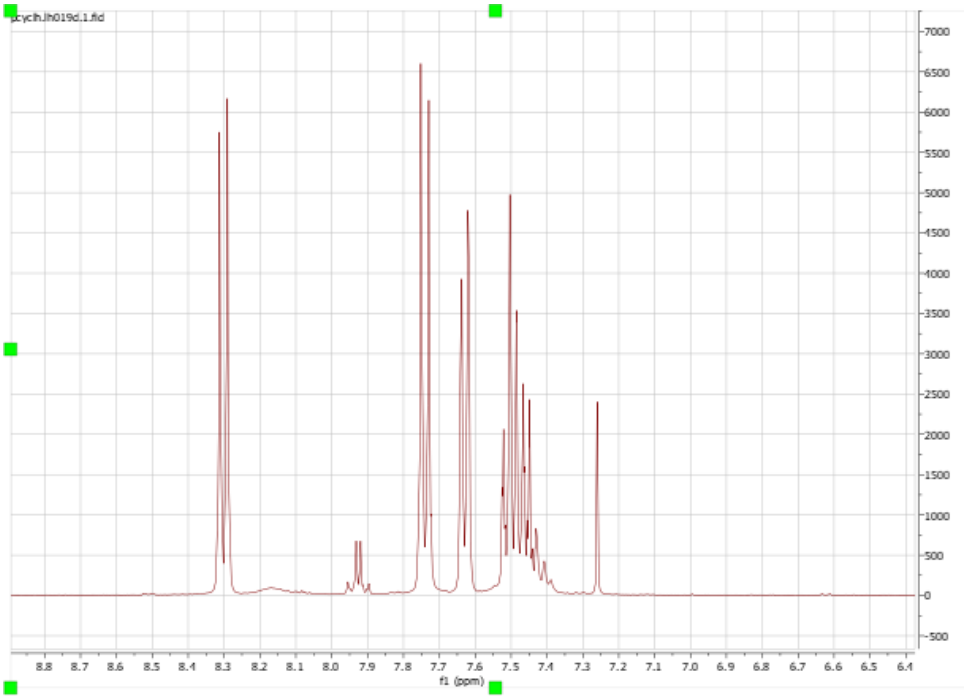

Appendix I-4: ^{1}HNMR graph for PdNPs@GNF-6 – Cycle 4

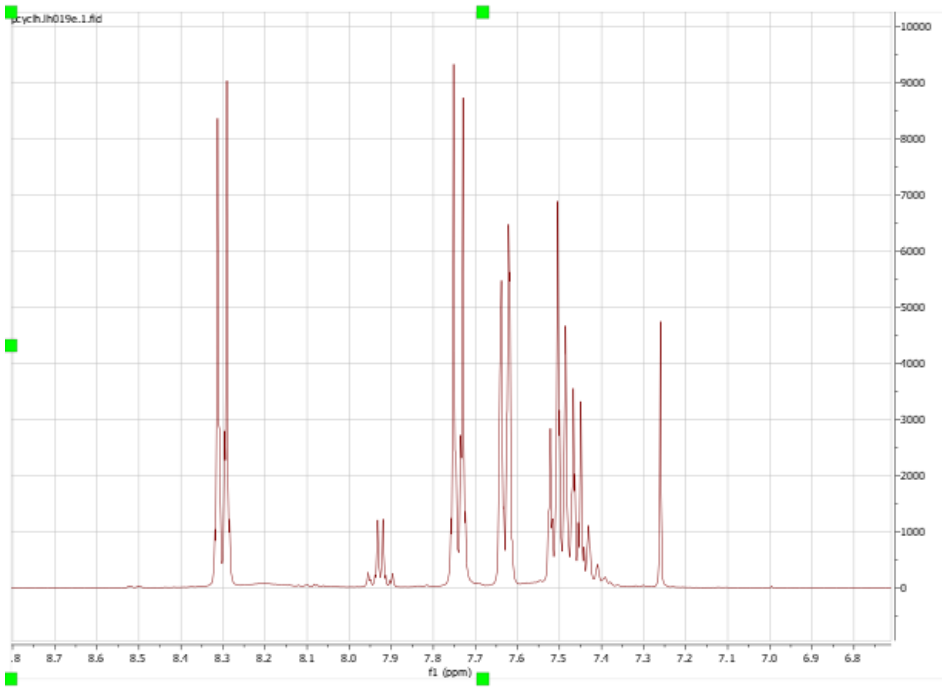

Appendix I-5: ^{1}HNMR graph for PdNPs@GNF-6 – Cycle 5

Appendix J: ^{1}HNMR graphs for FeCn/PdNPs@GNF-2

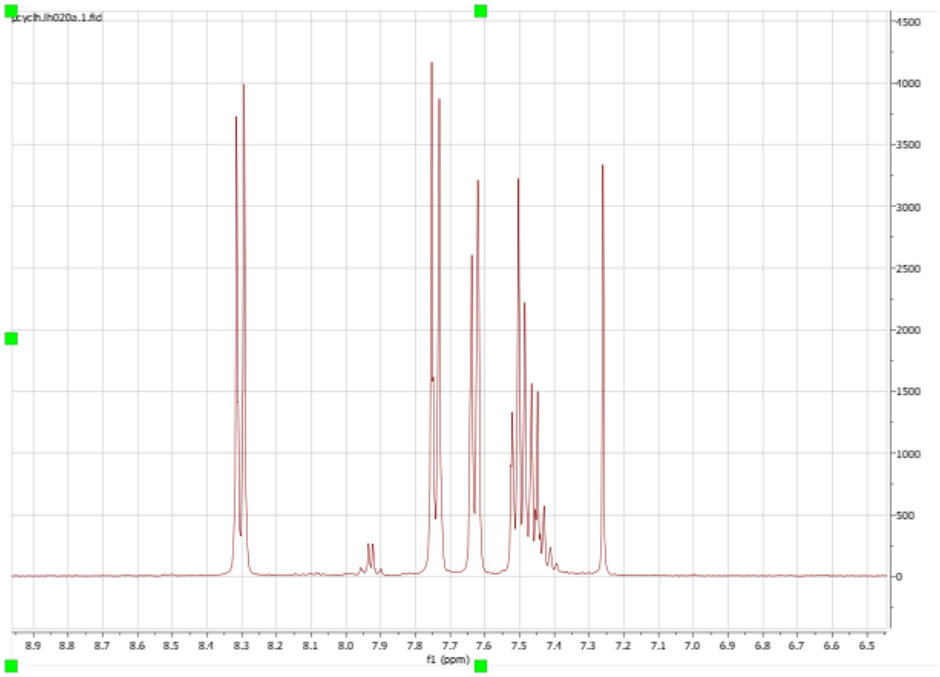

Appendix J-1: ^{1}HNMR graph for FeCn/PdNPs@GNF-2 – Cycle 1

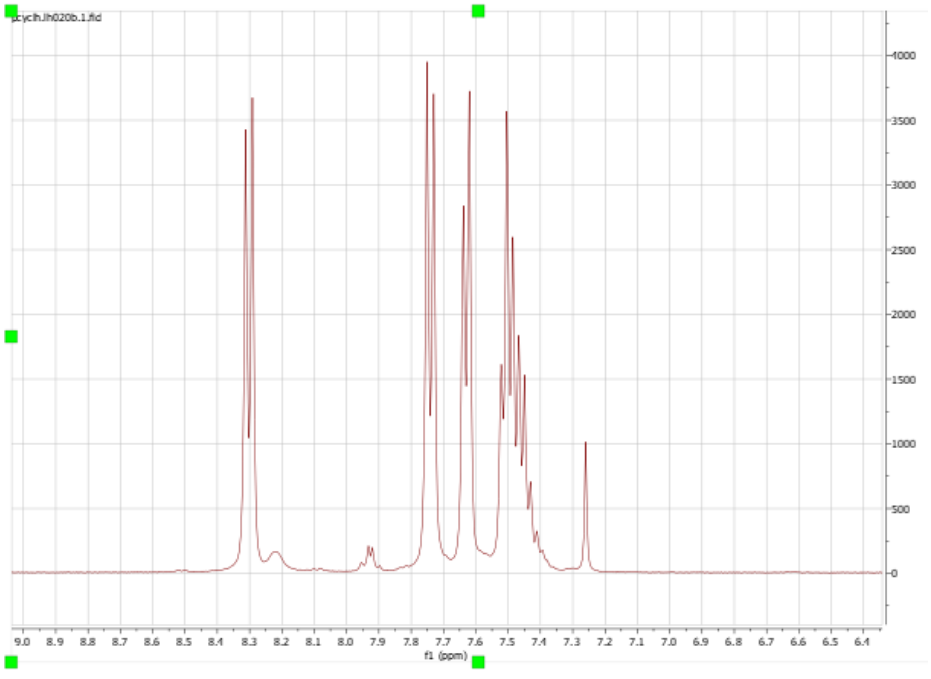

Appendix J-2: ^{1}HNMR graph for FeCn/PdNPs@GNF-2 – Cycle 2

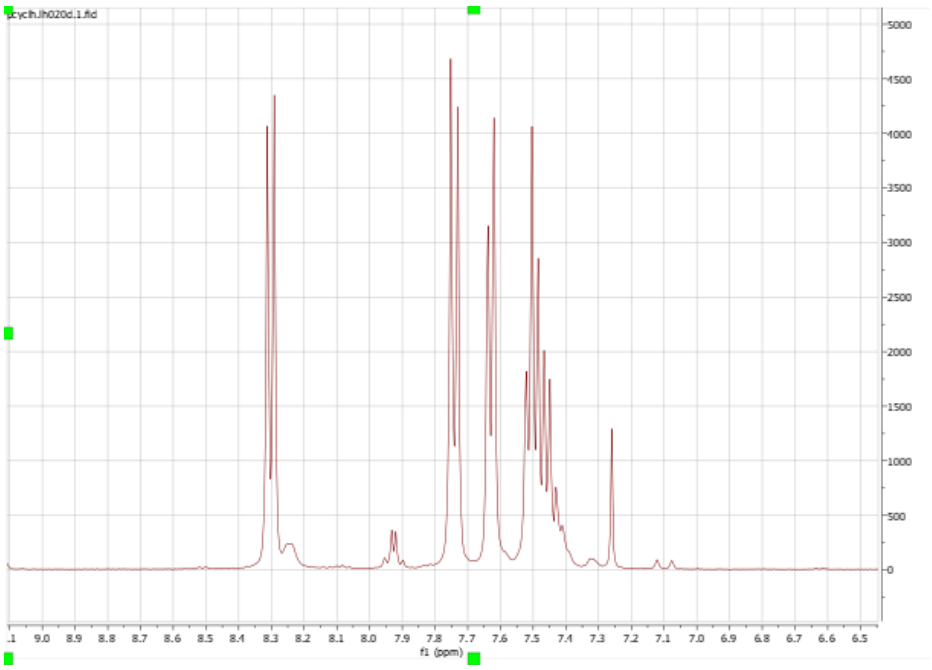

Appendix J-3: ^{1}HNMR graph for FeCn/PdNPs@GNF-2 – Cycle 3

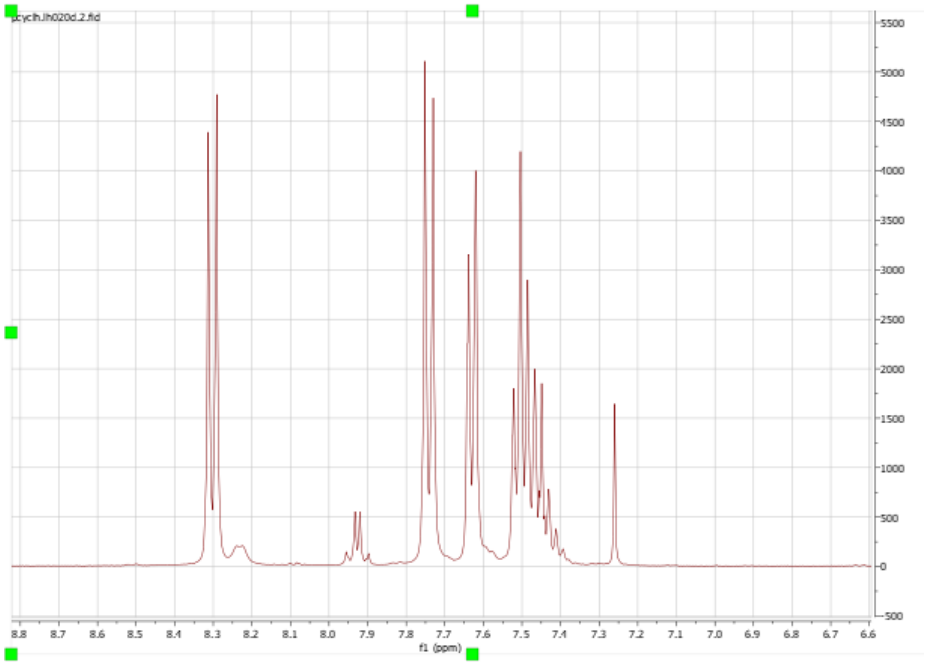

Appendix J-4: ^{1}HNMR graph for FeCn/PdNPs@GNF-2 – Cycle 4

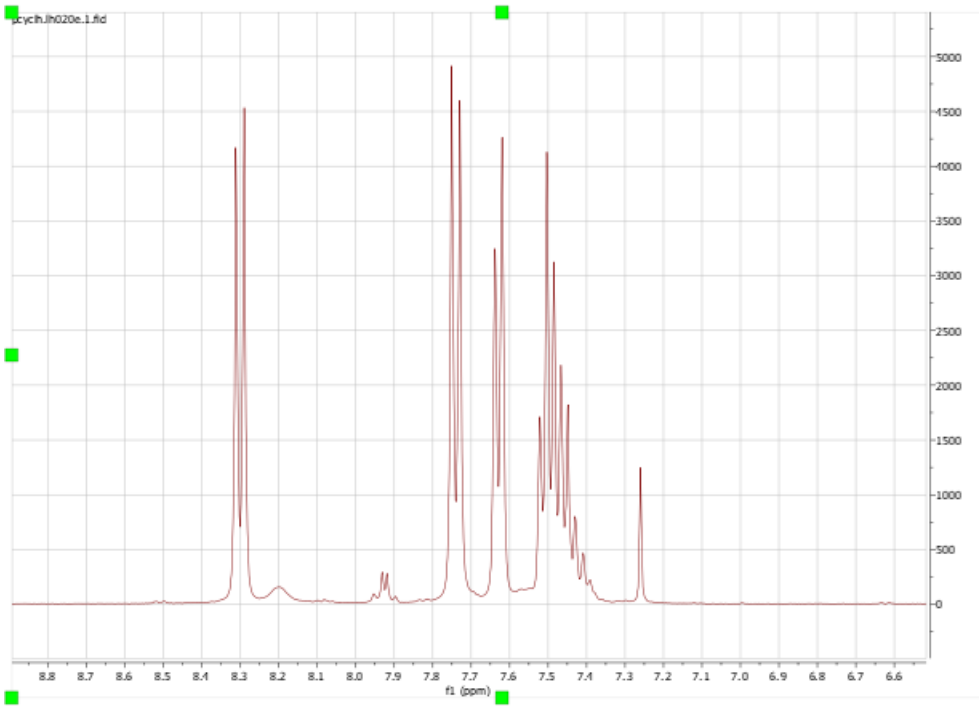

Appendix J-5: ^{1}HNMR graph for FeCn/PdNPs@GNF-2 – Cycle 5

Appendix K: ^{1}HNMR graphs for PdNPs/GNF-7

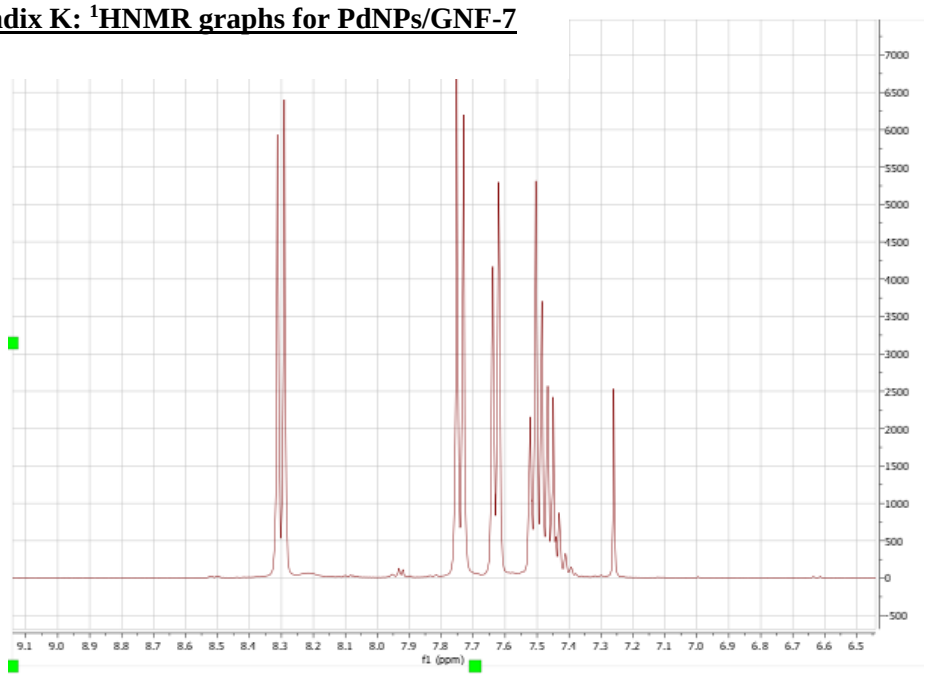

Appendix K-1: ^{1}HNMR graph for PdNPs/GNF-7 – Cycle 1

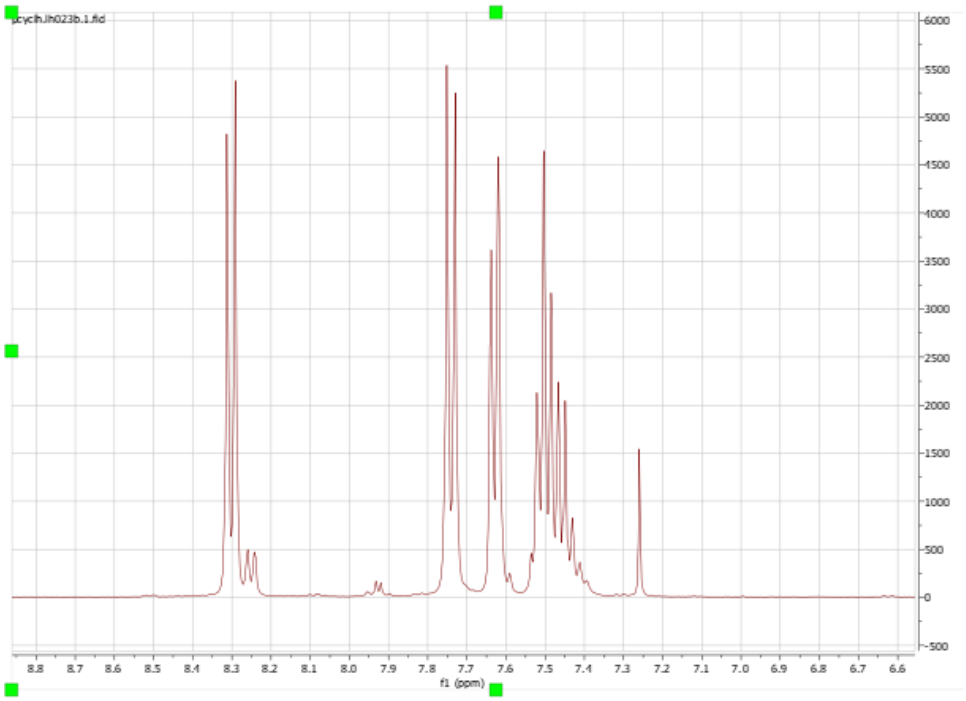

Appendix K-2: ^{1}HNMR graph for PdNPs/GNF-7 – Cycle 2

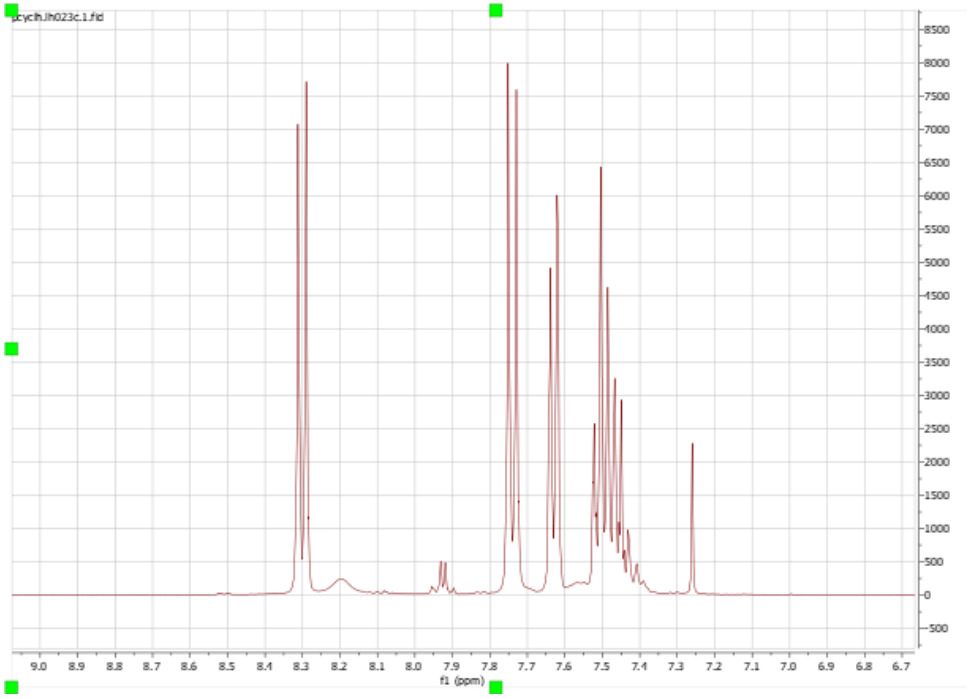

Appendix K-3: ^{1}HNMR graph for PdNPs/GNF-7 – Cycle 3

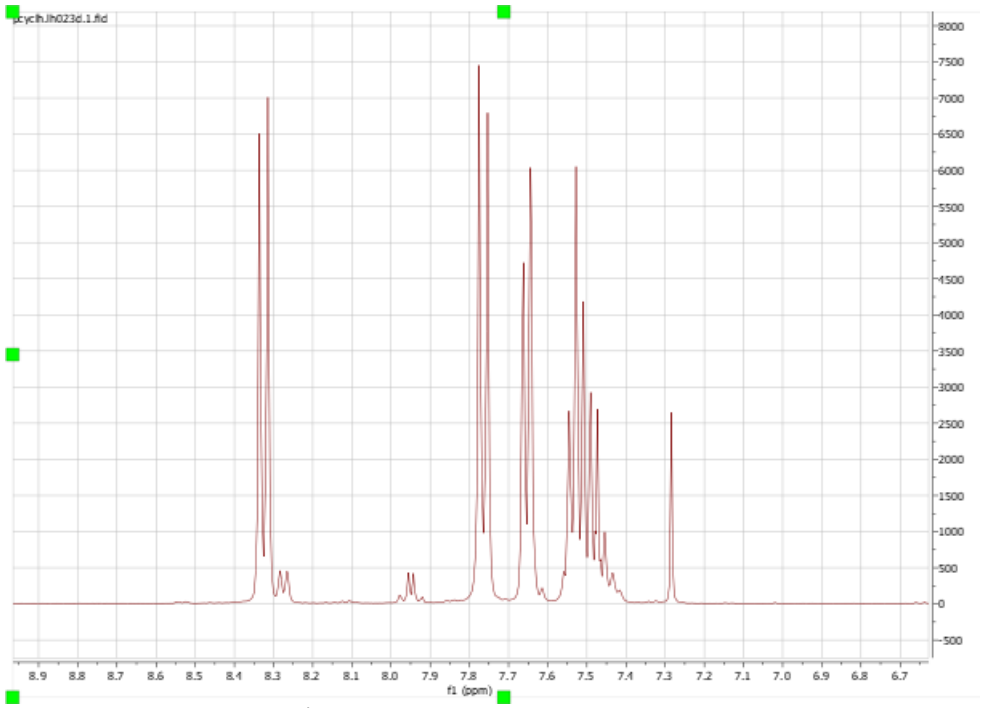

Appendix K-4: ^{1}HNMR graph for PdNPs/GNF-7 – Cycle 4

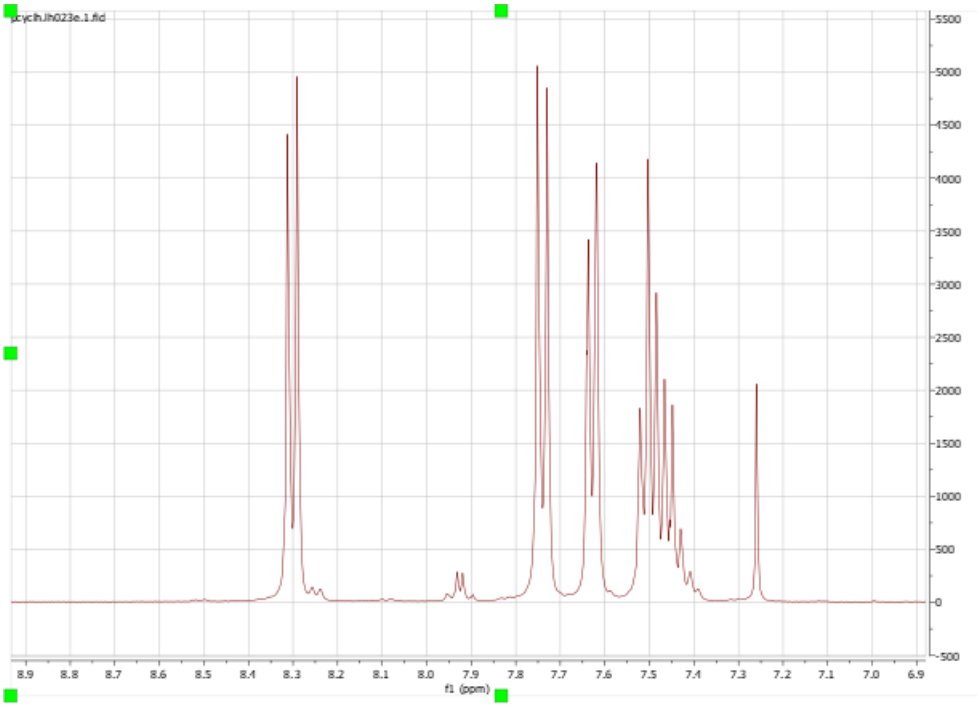

Appendix K-5: ^{1}HNMR graph for PdNPs/GNF-7 – Cycle 5

Appendix L: ^{1}HNMR graphs for PdNPs/GNF-8

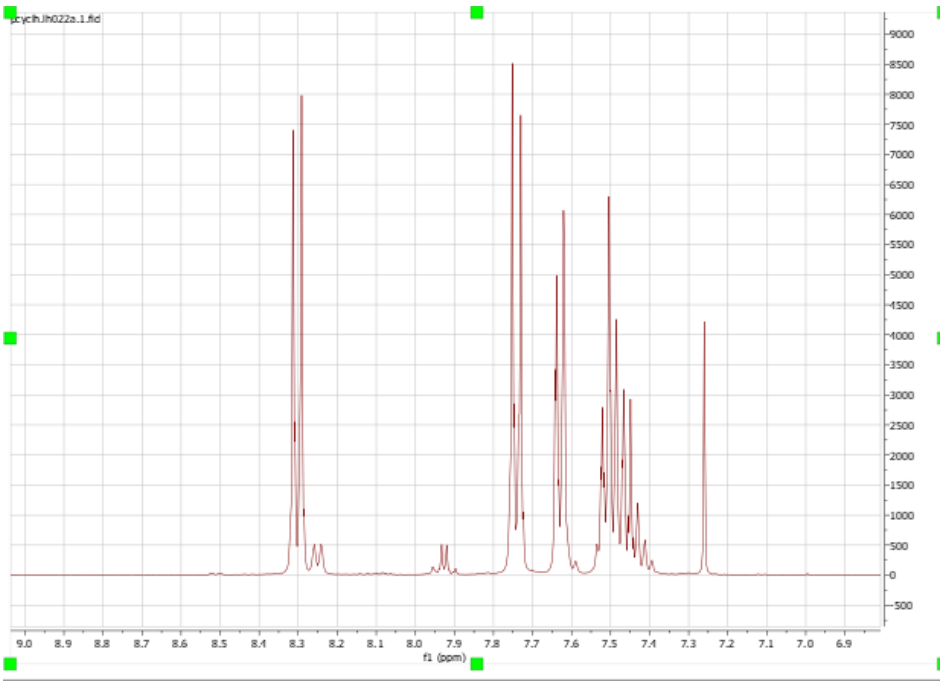

Appendix L-1: ^{1}HNMR graph for PdNPs/GNF-8 – Cycle 1

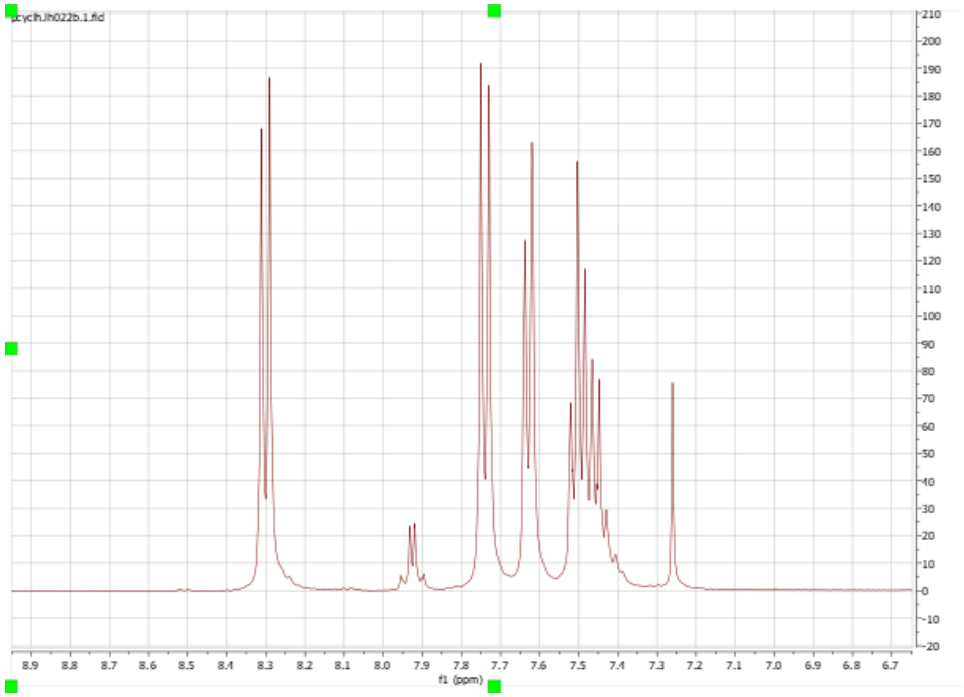

Appendix L-2: ^{1}HNMR graph for PdNPs/GNF-8 – Cycle 2

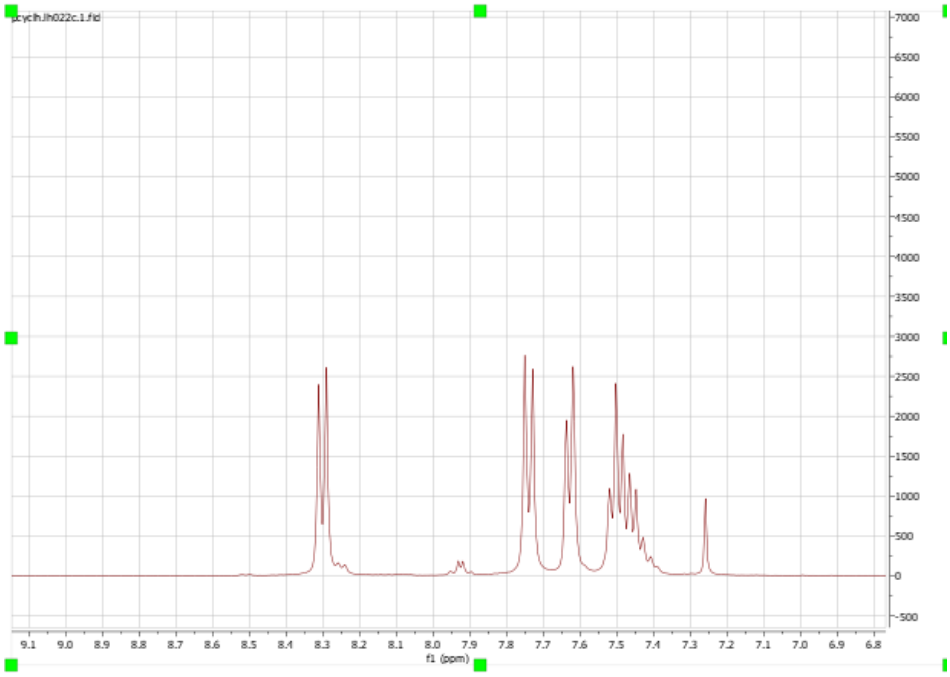

Appendix L-3: ^{1}HNMR graph for PdNPs/GNF-8 – Cycle 3

Appendix M: TGA graphs for PdNPs@GNF catalysts

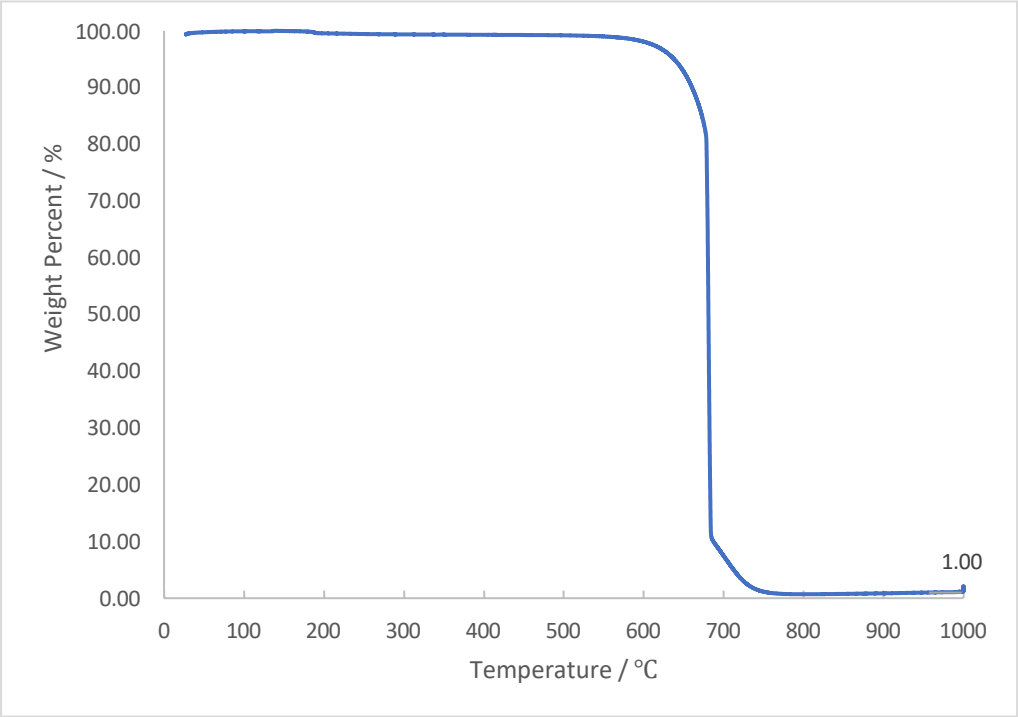

Appendix M-1: TGA graph of PdNPs@GNF-2 showing 1 % loading of Pd

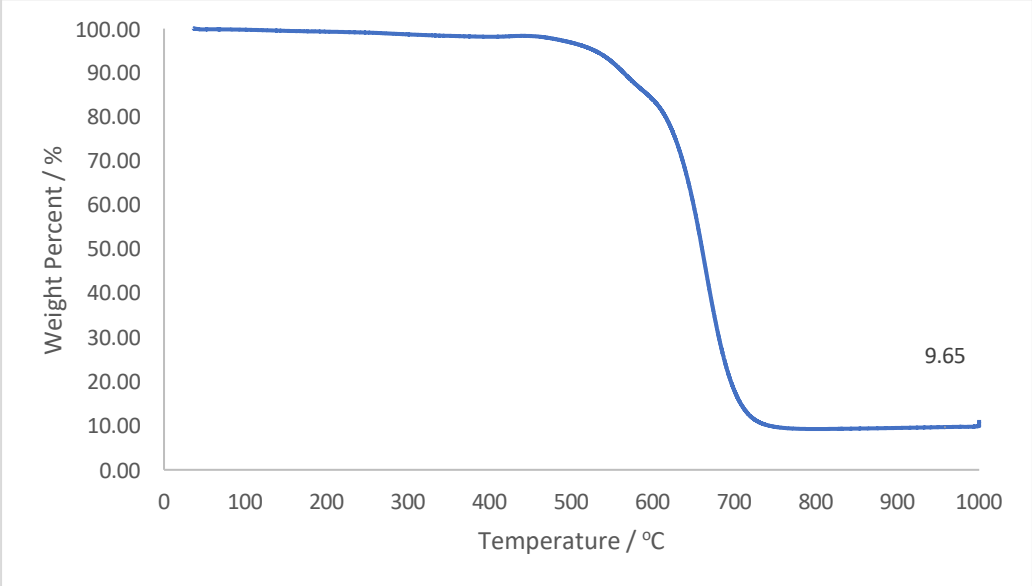

Appendix M-2: TGA graph of FeC_n/PdNPs@GNF-1 showing 1 % loading of Pd

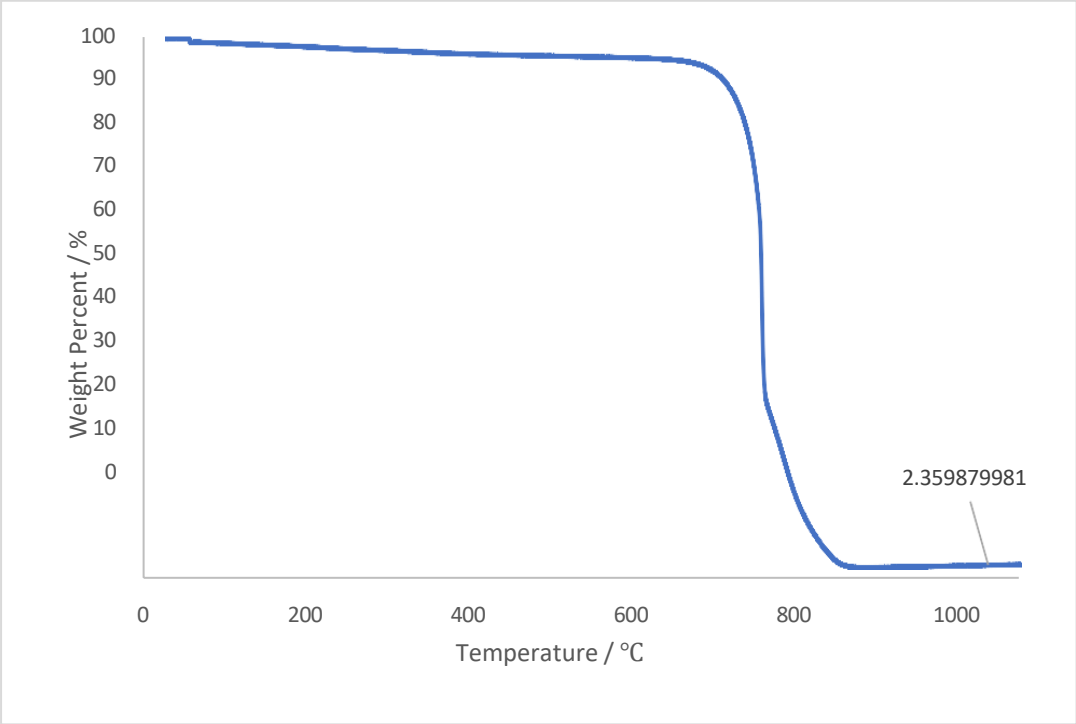

Appendix M-3: TGA graph of PdNPs@GNF-4 showing 2.36 % loading of Pd

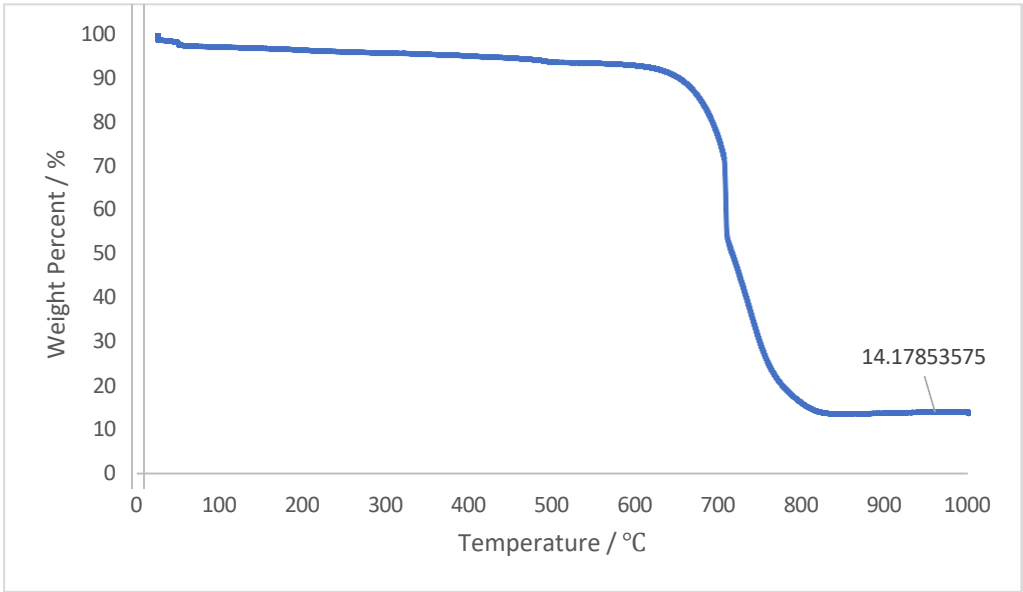

Appendix M-4: TGA graph of PdNPs/GNF- 5 showing 14 % loading of Pd

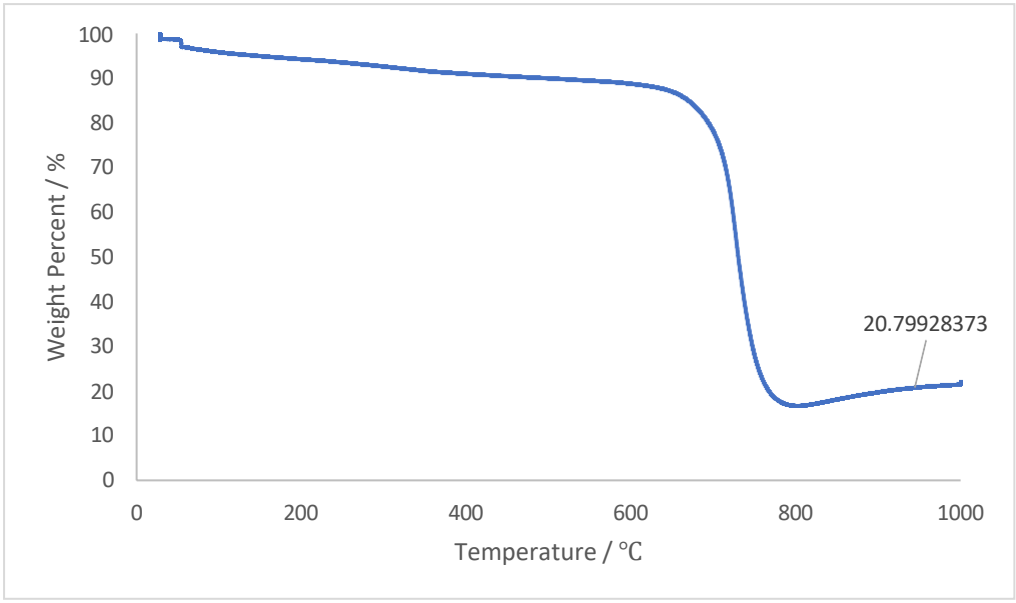

Appendix M-5: TGA graph of PdNPs@GNF-6 showing metal 21 % loading

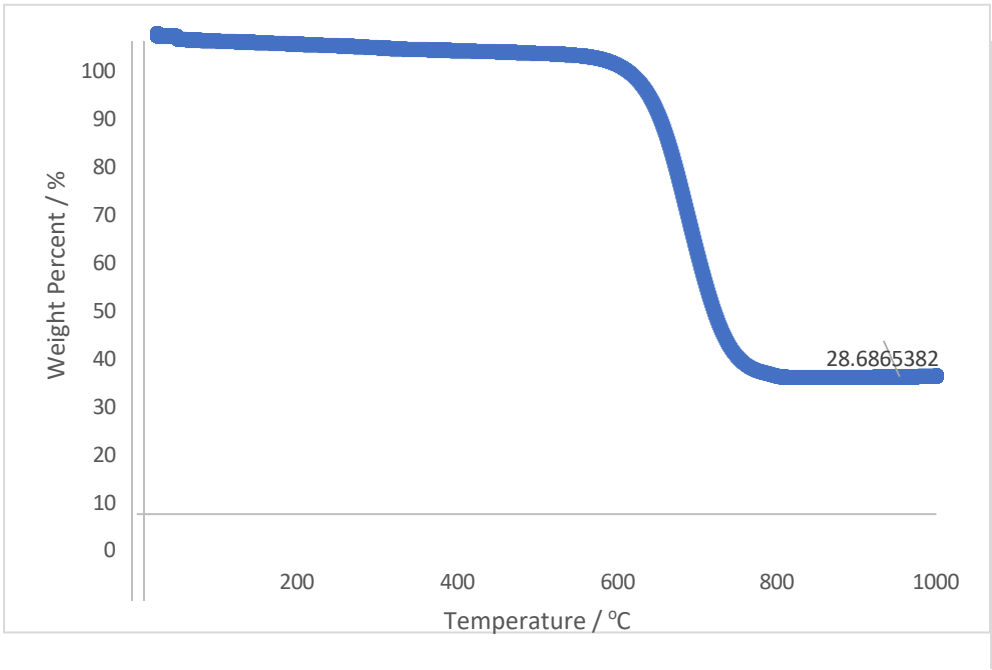

Appendix M-6: TGA graph of PdNPs/GNF-7 showing 29 % loading of Pd

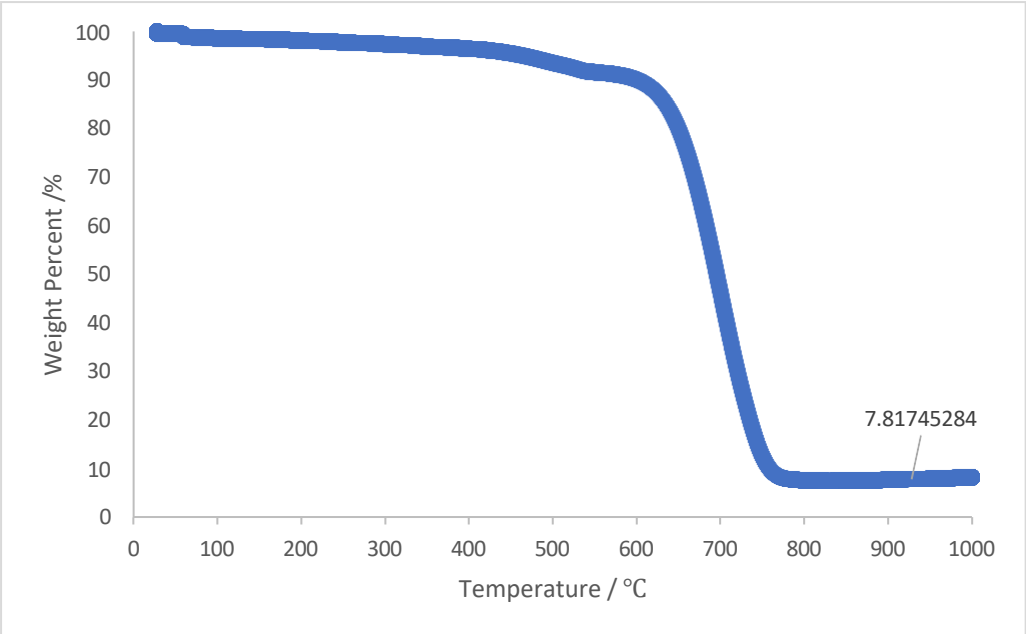

Appendix M-7: TGA graph of PdNPs/GNF-8 showing 7.8 % metal loading

Appendix N: EDX graphs of the cataylsts

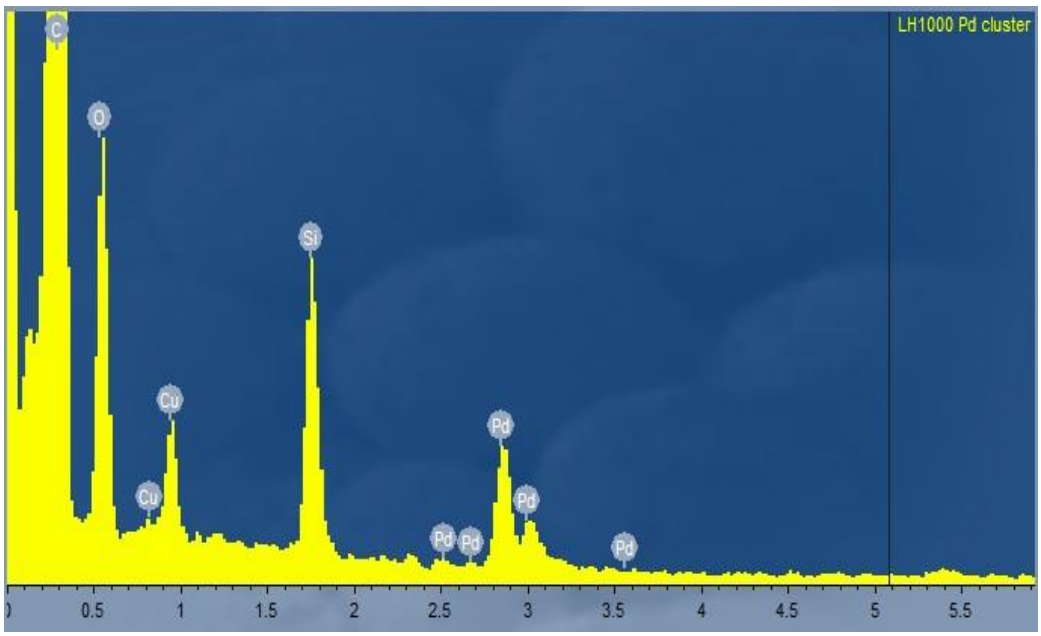

Appendix N-1: EDX capture of PdNPs/GNF-5 pre-Suzuki reactions showing elemental composition

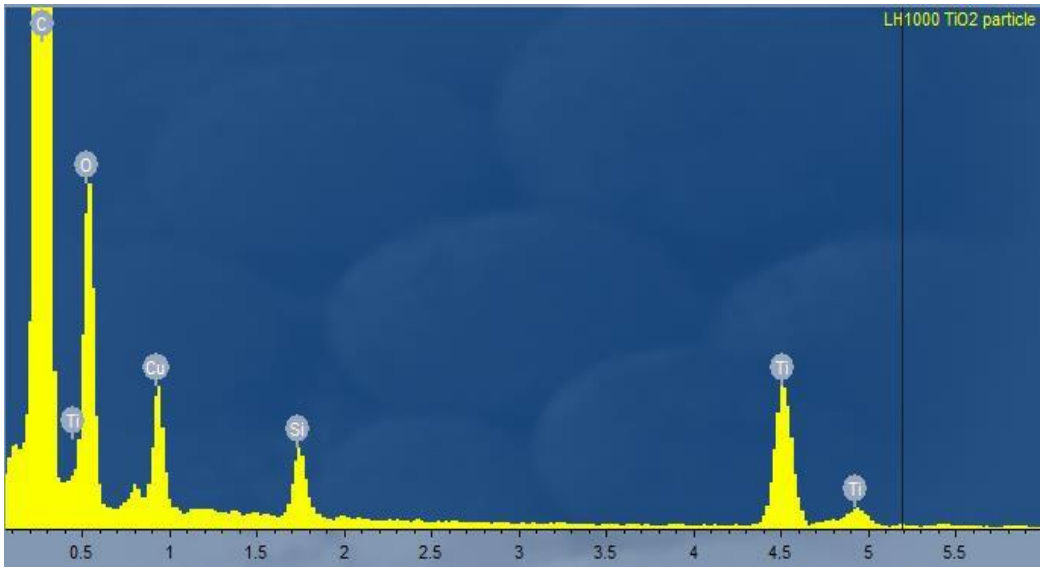

Appendix N-2: EDX capture focussed on TiO_2 NP on PdNPs/GNF-5 pre-Suzuki reactions

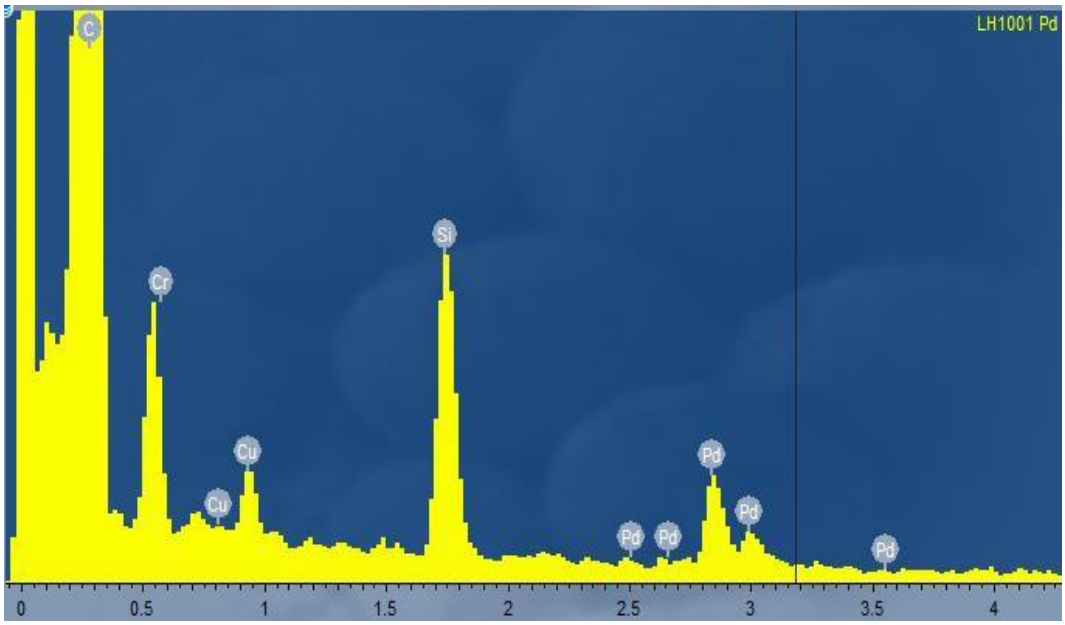

Appendix N-3: EDX capture of PdNPs/GNF-5 post Suzuki reactions showing elemental composition

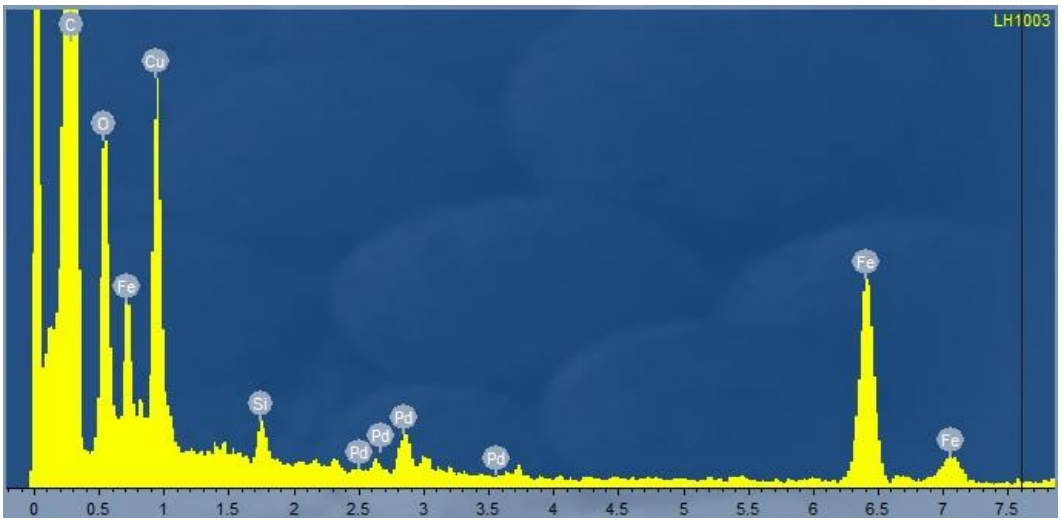

Appendix N-4: EDX capture of FeC_n@PdNPs/GNF-2 pre-Suzuki reactions

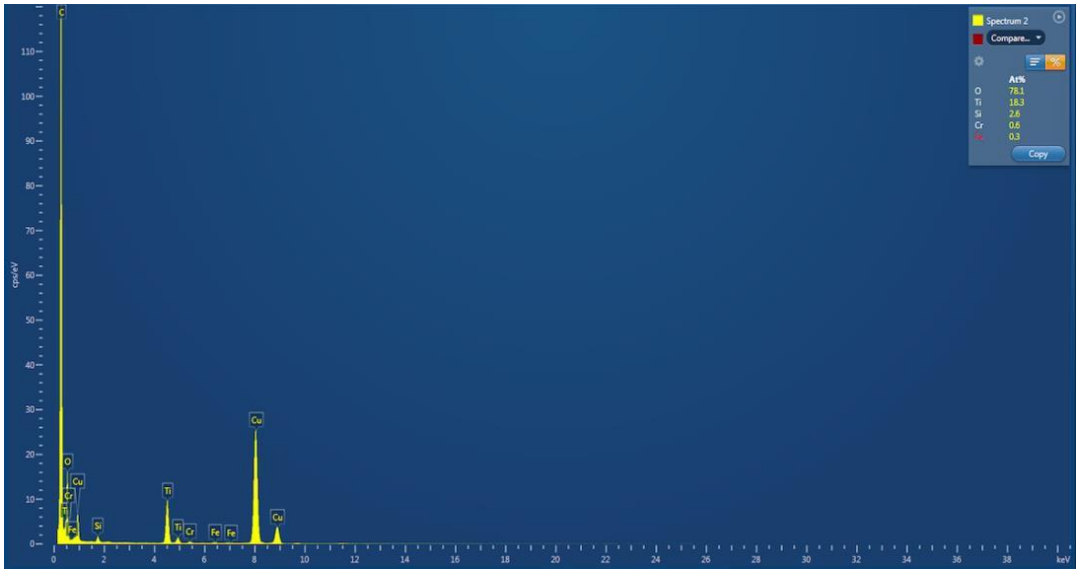

Appendix N-5: EDX capture of PdNPs/GNF-7 post-Suzuki reactions

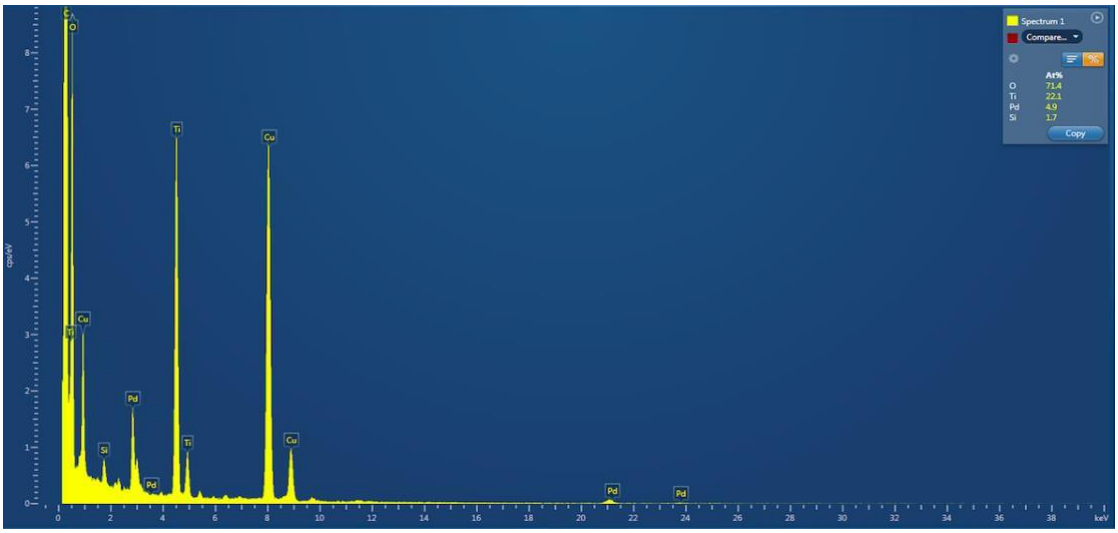

Appendix N-6: EDX capture of PdNPs/GNF-7 post Suzuki reactions

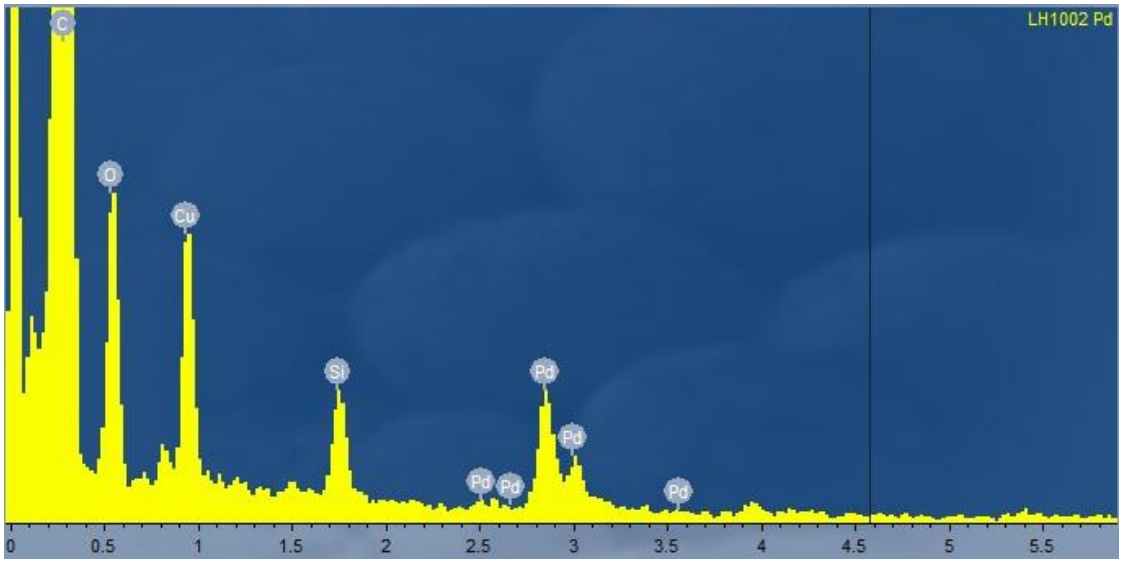

Appendix N-7: EDX capture of PdNPs/GNF-6 post Suzuki reactions

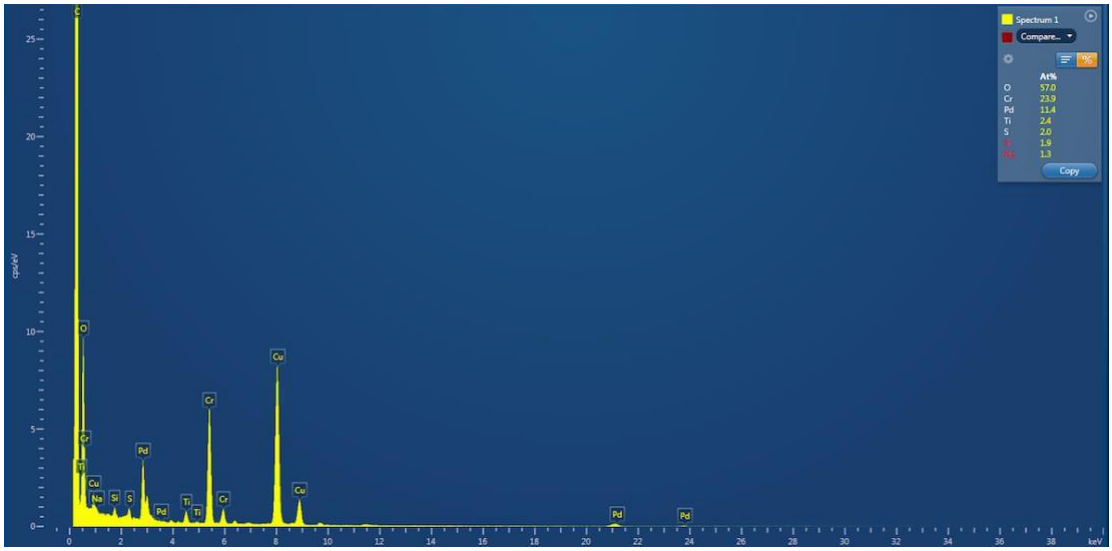

Appendix N-8: EDX capture of PdNPs/GNF-8 post-Suzuki reactions